# Porous textile composites (PTCs) for the removal and the decomposition of chemical warfare agents (CWAs) – A review

Nelly Couzon, Jérémy Dhainaut, Christine Campagne, Sébastien Royer, Thierry Loiseau, Christophe Volkringer

Coordination Chemistry Reviews xxx (xxxx) xxx

Contents lists available at ScienceDirect

Coordination Chemistry Reviews

journal homepage: www.elsevier.com/locate/ccr

Review

# Porous textile composites (PTCs) for the removal and the decomposition of chemical warfare agents (CWAs) – A review

Nelly Couzon [a], Jérémy Dhainaut [a], Christine Campagne [b], Sébastien Royer [a], Thierry Loiseau [a], Christophe Volkringer [a,c,*]

[a] Univ. Lille, CNRS, Centrale Lille, Univ. Artois, UMR 8181 - UCCS - Unité de Catalyse et Chimie du Solide, F-59000 Lille, France
[b] Univ. Lille, GEMTEX – Laboratoire de génie Matériaux Textiles, F-59000 Lille, France
[c] Institut Universitaire de France, 1 rue Descartes, 75231 Paris Cedex 05, France

ARTICLE INFO

*Article history:*
Received 31 January 2022
Accepted 29 April 2022
Available online xxxx

*Keywords:*
Chemical warfare agents
Porous solids
Textiles
Detoxification

ABSTRACT

Since the first use of a chemical warfare agent (CWA), specific methods of protection have been developed to protect human body from such lethal compounds. The first protection systems rely on impermeable clothing or the capture of the toxics species by an adsorbent such as activated carbon. However, both present important limitations, i.e. heat stress for impermeable protection and a risk of saturation or release of toxic compounds for the adsorbent. The optimal protection should therefore be active, i.e. be able to both capture and detoxify CWAs. In this optic, this review describes active porous textiles composites (PTC) used as protective garments against CWAs. To this day, a large variety of porous compounds such as zeolites, metal organic frameworks (MOFs) or aerogels have shown catalytic degradation of CWAs. The integration of these active solids to textile fibers is then detailed, highlighting the importance of the electrospinning technique or the pre-functionalization of fibers. Concerning the detoxification process, MOFs have focused a large part of the PTC research due to their exceptional properties (high surface area and tunable porosity combined to a catalytic activity). More particularly, Zr-based MOFs exhibit exceptional results in terms of CWA detoxification and are currently highly studied. Besides, this present state of art includes other active PTCs (functionalized activated carbon fibers ACFs or zeolite composites) rarely discussed in reviews, to give a full overview of the existing PTC used against CWA.



**Contents**



* Corresponding author at: Univ. Lille, CNRS, Centrale Lille, Univ. Artois, UMR 8181 - UCCS - Unité de Catalyse et Chimie du Solide, F-59000 Lille, France
*E-mail address:* christophe.volkringer@centralelille.fr (C. Volkringer).

https://doi.org/10.1016/j.ccr.2022.214598
0010-8545/

## 1. Introduction

Chemical warfare agents (CWAs) are one of the most toxic man-made compounds with incapacitating or lethal effects on humans. Natural poisonous extracts, from plants or animals, were used since Middle Ages but the use of synthetic chemical agents in battle fields were only developed at large scale since the 19th century [1]. Their first massive deployment was during World War I (WWI) with chlorine, phosgene and mustard gases [2]. Since then, the utilization of nerve agents was reported in recent wars (Iran-Irak in 1988, Syria in 2013) or by terrorist groups (Tokyo subway in 1995) [3]. Assassinations were also planned recently using CWAs, with the use of VX in 2017 at Kuala Lumpur (Malaysia) or with a Novichok nerve agent in 2018 in UK [4]. These examples, combining with the fact that CWAs are relatively easy and inexpensive to synthesize, evince the importance to provide protective methods for military and civilians. Furthermore, the variety of CWAs (vesicants, nerve agents, blood agents, chokings agents, ...) highlights the necessity for full protection against various ways of attack (inhalation, penetration by the skin, ...). The first reported personal protection equipment (PPE) was developed during WWI with the combination of a gas mask containing active carbons and an impermeable clothing to isolate the body from any contact with the CWAs [5]. Although being efficient, problems of heat stress with the impermeable clothing motivated the development of alternative solutions.

Chemical protective clothing relies on two possible and complementary processes, the adsorption and/or the decontamination (i.e. chemical neutralization or physical sequestration) of CWAs. The most efficient materials nowadays for the adsorption of toxic species are solid porous compounds such as activated carbons (or derivatives), which are currently used in armies worldwide [6]. The adsorbent acts as a filter to avoid the contact between the skin and CWAs while allowing the moisture vapor diffusion. Nevertheless, as toxic species are only captured in the porous media, several drawbacks remain such as the saturation of the adsorbent, as well as the handling and the disposal of the contaminated materials. Whereas decontamination solutions for Personal Protective Equipment (PPE) after exposure exist, their efficiency is limited to some toxic compounds [7]. The detoxification of CWAs by a catalytic adsorbent compound is an attractive alternative. Indeed, since decades a library of materials have been tested for CWA decontamination, from aqueous NaOH to catalyst materials like metallic or metal oxide nanoparticles, polyoxometalates or metal–organic frameworks (MOFs) [3,8,9].

Among the compounds adapted to PPE for the adsorption and decontamination of CWAs, active carbons and MOFs are the most studied nowadays. Active carbons, and more especially Active Carbon Fibers (ACFs), have proven excellent in terms of adsorption due their high specific surfaces (up to 2500 $m^2/g$) and accessible microporosity [10]. On the other side, MOFs also possess large surface areas generally comprised between 1000 and 3000 $m^2/g$ with tunable pore sizes. Furthermore, Zr-based MOFs such as UiO-66, MOF-808 or NU-1000 show adequate porosity and good catalytic activity due to numerous accessible Lewis acid $Zr_6$ clusters [11,12]. This double capacity, i.e. adsorption with porous properties and decontamination with catalytic properties, have made MOFs an obvious candidate for the capture and the decomposition of CWAs [9,12-14]. In this review, we extend this knowledge to porous textile composite (PTC) against these toxic agents.

## 2. Detoxification of chemical warfare agents (CWAs) and their simulants

The regulation and destruction of chemical weapons began in 1993, with the writing of the Convention on the prohibition of the development, production, stockpiling and use of chemical weapons and on their destruction (shortly named the chemical weapons convention) [15]. This document is nowadays ratified by 193 countries and is managed by the Organization for the Prohibition of Chemical Weapons (OPCW). The latter defined a chemical weapon as "a chemical used to cause intentional death or harm through its toxic properties. Munitions, devices and other equipment specifically designed to weaponise toxic chemicals also fall under the definition of chemical weapons" [16]. Depending on their toxicities and their utilizations for authorized applications (*e.g.* research or agriculture), toxic chemicals have been classified from schedule 1 to 3. Schedule 1 includes the most toxic compounds and their precursors such as Sarin, VX, Sulfur Mustard or Lewisite. These latter are commonly classified as Chemical Warfare Agent (CWA). Other toxic compounds such as Amiton and arsenic trichloride (Schedule 2), or HCN and phosgene (Schedule 3) will not be further discussed here as this review is devoted to CWAs.

Among the toxic chemicals in Schedule 1, the majority of the current research about detoxification focuses on five specific CWAs: sulfur mustard, Tabun, Sarin, Soman and VX, as well as their

regular simulants, presented in Fig. 1. Details about these CWAs will be discussed in the next sections.

### 2.1. Sulfur mustard and simulants

Sulfur mustard, also called mustard gas, Yperite or HD (H for the munition grade and D for distilled), is a blistering agent (vesicant) with a bis(2-chloroethyl) sulfide structure (Fig. 1). It is one of the most used CWAs during military conflicts, recognizable by its garlic or mustard smell. HD is highly toxic as vapor or liquid and is persistent (see Table 1). Its high reactivity leads to the irreversible alkylation of guanine nucleotides composing the DNA and the rapid cells death [11,17]. Until now, it still does not possess a known antidote [18].

Four methods of degradation of HD exist (Fig. 2). Dehydrohalogenation (or elimination) process is a nucleophilic substitution ($S_N1$ mechanism), forming the non-toxic products Vinyl HD (VHD) and Divinyl HD (DVHD or DVS), and releasing HCl [19]. The degradation, or recombination path, is a radical reaction with the cleavage of S-C bond and the formation of ethyl sulfide radicals, which recombine into non-toxic but malodorous diethyl disulfide (DEDS) [20]. Hydrolysis mechanism relies on the formation of a sulfonium ion to produce hemi sulfur mustard and thiodiglycol (TDG), but is limited due to the hydrophobicity of HD [21]. The last method for HD degradation corresponds to its partial oxidation to nontoxic sulfoxide [19]. However, the oxidation of HD could lead to sulfone, a known harsh blistering agent. A 100 % selective reaction to sulfoxide demands mild oxidant agents such as photosensitizers or hydrogen peroxide [22-24].

The selection of a simulant considers several parameters such as structural similarity, electronegativity of the functional groups, chemical stability or size [9]. The most usual simulant of HD is chloroethyl ethyl sulfide (CEES or 2-CEES) (see Fig. 1). It possesses an analogous structure to HD with C-S and C-Cl bonds, same size (5.9 Å for HD vs 5.8 Å for CEES) [25], and close sorption/desorption behavior [21,26,27]. However, the toxicity of CEES remains high and precautions are still needed. Few others simulants, having less similarities with HD, are also reported in the literature such as diethyl sulfide (EES or DES) or 2-chloroethyl methyl sulfide (CEMS). The detoxification paths of CEES, as well as other sulfide mustard simulants, are similar to those reported for HD.

### 2.2. Nerve agents and simulants

Nerve agents are organophosphorus derivatives that can be fatal by any route of exposure at sufficient concentrations. Indeed, they act on the chemical communications of the nervous system by forming irreversible phosphonate esters bonds with the neuroenzyme acetylcholinesterase. An accumulation of the neurotransmitter acetylcholine leads to a constant neuron stimulation, causing muscle contraction, exhaustion, paralysis and death [4,18]. Contrary to HD, antidotes for nerve agents exist, like atropine sulfate or pralidoxime chloride [28].

Nerve agents are usually classified in two mains classes. The G series, named G because Germans scientists first synthesized them in the 1930–1940s, gathers three notorious species: tabun (GA), sarin (GB), and soman (GD). GA possesses a cyanide group connected through phosphorous via a P-CN bond, while GB and GD

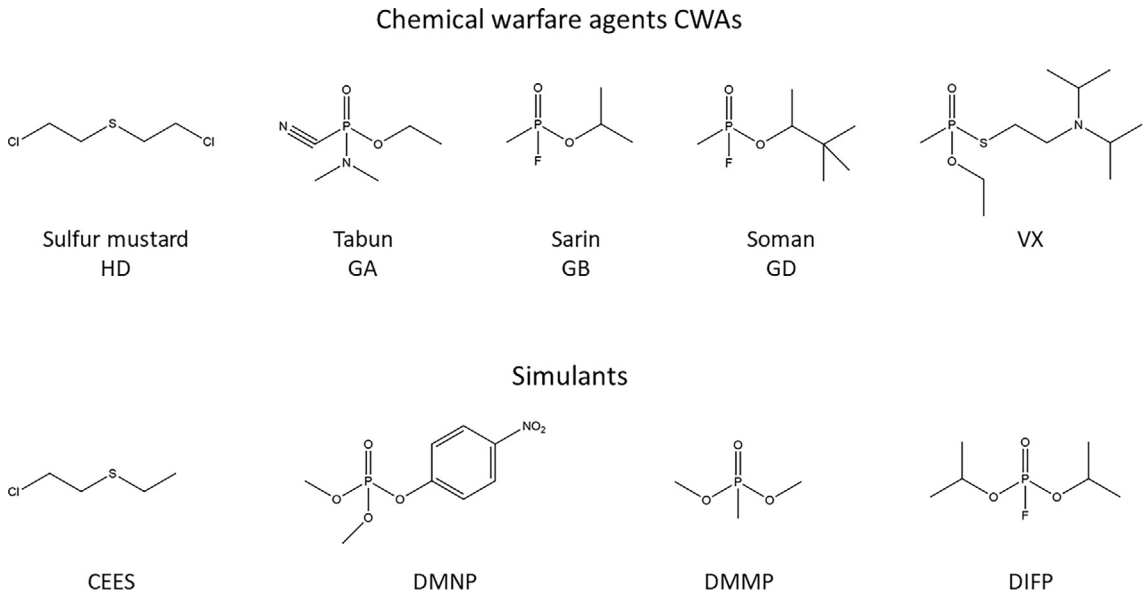


**Fig. 1.** Most common CWAs (Schedule 1) and their simulants.

**Table 1**
Characteristics of common CWAs (HD and nerve agents) [3,21,25,29].

| | HD | Tabun GA | Sarin GB | Soman GD | VX |
|---|---|---|---|---|---|
| Chemical formula | $C_4H_8Cl_2S$ | $C_5H_{11}N_2O_2P$ | $C_4H_{10}FO_2P$ | $C_7H_{16}FO_2P$ | $C_{11}H_{26}NO_2PS$ |
| Size (Å) | 5.9 | ~ 6–6.5 | ~ 6 – 6.5 | 6.7 | 7.6 |
| Vapor pressure (mmHg 20 or 25 °C) | 0.11 | 0.037 at 20 °C | 2.10 at 20 °C | 0.40 at 25 °C | 0.0007 |
| Volatility (mg/m$^3$) at 25 °C | 920 | 610 | 22,000 | 3900 | 10.5 |
| Water solubility (g/L) at 25 °C | 0.92 | 98 | Miscible | 21 | 30 |
| Persistence | 30.5–51.2 h at 25 °C | 24–36 h | 2–24 h at 2–25 °C | Relatively persistent | 2–6 days |
| Allowed exposure for 30 min (mg/m$^3$) | 0.7 | 0.1 | 0.1 | 0.05 | 0.003 |

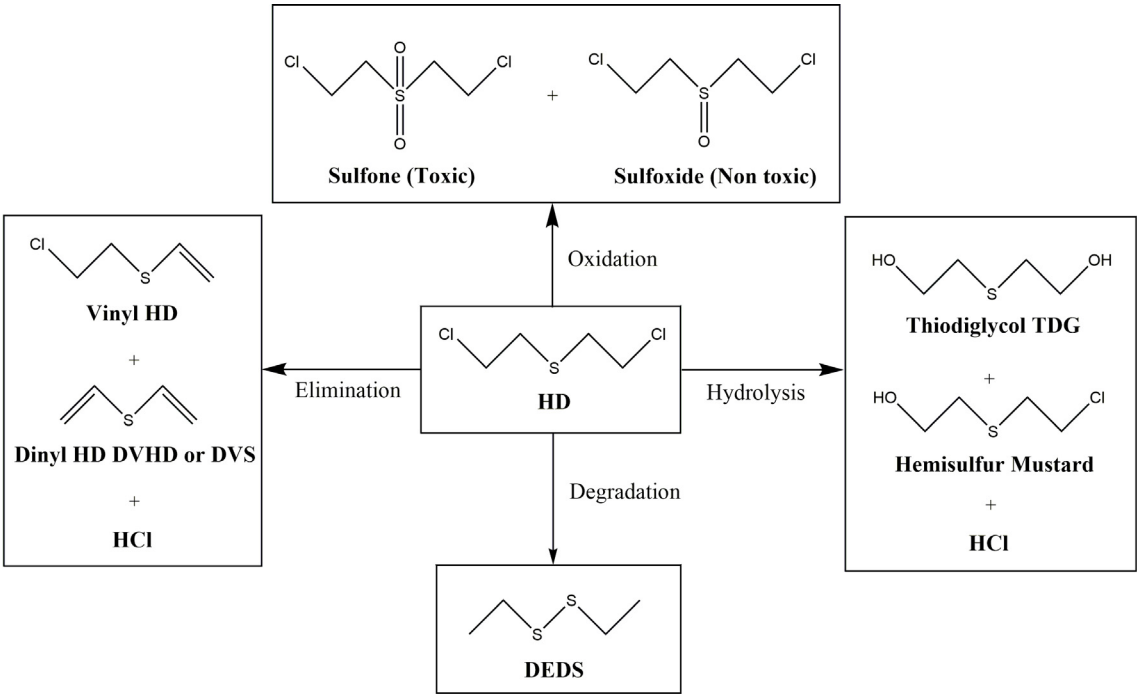


**Fig. 2.** The four decomposition pathways of HD.

have a fluorine substituent group (Fig. 1). Thanks to their relative high volatility and/or water solubility (Table 1), these colorless liquids diffuse very quickly in the human body by skin contact and inhalation [3,21]. The V series (V stands for Venomous) was discovered after the second World War in Great Britain and contains the extremely toxic VX agent, known as more deadly than sarin [3]. This thiophosphonate compound is odorless, less volatile than G agents and is a persistent liquid on surfaces (Table 1) [21].

The main route to detoxify nerve agents is based on hydrolysis, which induces nucleophile substitution around the phosphorus atom (Fig. 3). Therefore, the hydrolysis of organophosphorus nerve agents generates different intermediates, mainly depending on the pH occurring during the reaction. For example, GD and GB, which possess a similar structure, react both with water. The phosphorus $S_N2$ nucleophilic attack (hydrolysis) produces hydrofluoric acid and nontoxic isopropyl methylphosphonic acid IMPA for sarin (GB) and pinacolyl methylphosphonic acid (PMPA) for soman (GD), respectively. This reaction can continue to form methylphosphonic acid (MPA) [3].

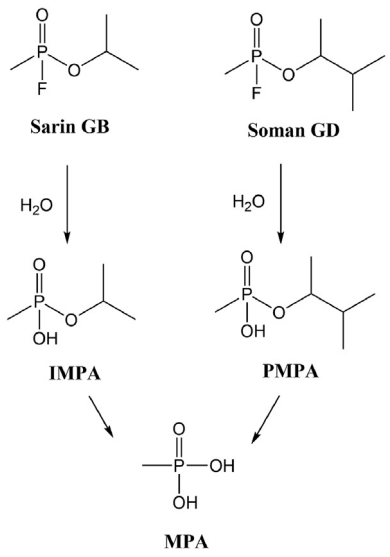


**Fig. 3.** Hydrolysis path for the decomposition of sarin (GB) and soman (GD) into methylphosphonic acid (MPA).

Simulants of nerve agents are numerous due to the rich library of toxic organophosphorus derivatives. To evaluate their analogy to nerve agents, classifications have been proposed considering their properties or using simulation methods [26,27,30]. Generally, surrogates still include the P═O bond, whereas P-C≡N (for GA), P-F (for GB and GD) or P-S (for VX) bonds are scarcer. Indeed, even if these functions are generally involved in the hydrolysis reaction of nerve agents, the simulants containing these chemical groups remain too toxic for a safe use in academic research. For Tabun, diethylcyanophosphonate (abbreviated as DCNP or DECP) is a suitable simulant, thanks to a very similar structure and a lower toxicity [4,31]. Other simulants such as diethyl ester phosphonic acid (DEHP) or diethyl ethyl phosphonate (DEEP) have also been proposed, but they do not contain the P-C≡N bond [26]. Simulants for Sarin (GB) and Soman (GD) are usually identical, due to their very close structures. According to DFT calculations, dimethyl 4-nitrophenyl phosphate (DMNP, also called methyl-paraoxon) was shown to possess similar adsorption to Soman on porous MOF solids while dimethyl methyl phosphonate (DMMP) is closer to Sarin behavior [30]. The use of di-isopropyl fluorophosphate (DFP or DIFP) also proved to be a promising option as it owns a P-F bond. Aside from these usual simulants, others can be also considered for GB and GD such as di-isopropyl methyl phosphonate or dimetyl chlorophosphate [26,27]. For VX, there is no convincing simulant which can mimic the -S-$(CH_2)_2$-N(i-Pr)$_2$ chain occurring in this CWA [4]. It is admitted that amiton (VG), which conserves P = O and P-S bonds could be a good simulant for VX. However, this agent is listed in the schedule 2 substances, due to its high toxicity. Others simulants less toxic, such as malathion, parathion or DEMP

(O,S-diethyl methylphosphonothioate), are therefore preferred [26,27,32].

## 3. Precursors of PTC: Porous materials and textiles

### 3.1. Current equipment of protection

To isolate the skin and the respiratory tracks from any contact with CWAs, the first personal protective equipment (PPE) used during WWI, was impermeable. It consisted of butyl rubber clothing with gloves, boots and respiratory masks to cover the entire body. This kind of resistant protection ensures a complete barrier to liquids, vapors and aerosols (see Fig. 4). Nevertheless, it showed a severe disadvantage, as the diffusion of moisture vapor is blocked. The heat stress created limits its use to short periods of times [33,34]. Therefore, for decades researches have been focused on optimizing the quality of protective clothes, by considering the comfort of people [35].

Contrary to impermeable protection, permeable clothing usually allows a good moisture vapor transport rate (MVTR), limiting heat stress. The protection against CWAs is provided by adsorption and/or detoxification processes, filtering the toxic chemicals. Various levels of permeability can be reached such as semi-permeable, air-permeable or selectively permeable membranes (SPM) (Fig. 4). Semi permeable and air permeable clothing are similar, as they both rely on a multilayers composite with at least a layer made of a sorbent material (*e.g.* activated carbons). Air and moisture vapor can cross the garment, while liquid is generally blocked by the outer repellent layer. The difference between air and semi-permeable membranes relies on their reaction toward aerosol, as the first one allows its diffusion when the second blocks it [6,33].

The composition of an air-permeable garment generally consists in a combination of three layers. The inner layer, in contact with the skin, acts as a support to avoid the direct contact between the skin and the sorbent. The in-between layer containing a sorbent absorbs the toxic vapors due to their adapted porosity. Finally, the outer layer (*e.g.* plastic membrane) protects from liquid and aerosol, while being permeable to vapor [36]. Examples of air-permeable protection are the Joint Service Lightweight Integrated Suit Technology (JSLIST) overgarment used by the US military or the FELIN combat clothing developed by the French army. They consist in an outer layer of nylon/cotton with a water-repellent coating and an inner layer with activated carbon to adsorb a wide library of toxic agents [34]. This equipment is supposed to offer a protection against CWAs for at least 24 h.

The last protective textile is a SPM which allows the moisture vapor evacuation, while blocking the penetration of organic molecules [6,33]. They are composed of multilayer composite polymers such as poly(vinyl alcohol), cellulose acetate, cellulosic cotton or poly(allylamine) [37]. The lightweight, thinness and durability of SPM-based clothes made them also attractive for commercialization [38].

The permeable protections presented above have become the reference garments for long-term use [33]. However, as the toxic gases are only physisorbed (weak interaction), the handling and disposal of these protective cloths are an important issue, as desorption and further human contamination remains possible [13,35,39]. Furthermore, the absorbents can reach saturation overtime, which makes the protection ineffective. This saturation rate is usually measured and designed as the breakthrough time ($t_B$), which corresponds to the permeation rate of the toxic compound reaching 0.1 μg/(min/cm$^2$) (according to norms European EN 16523–1 or American ASTM F739-20). To solve these problems, a recent strategy of research is dedicated to active protection textiles, able to both adsorb and decontaminate CWAs. Among the possibilities, porous catalysts appear as the privileged solution for active protective textiles [9].

### 3.2. Porous catalysts against chemical warfare agents (CWAs)

Thanks to their high internal surface area, porous adsorbents are well adapted for the capture of large amounts of toxic species. Due to the small size of CWAs (*e.g.* 5.9 Å for HD or 7.6 for VX), their immobilization is usually optimized with small pore diameters, i.e. around 20 Å [20,25]. Microporous ($\varnothing_{pore}$ < 20 Å) and mesoporous solids (20 Å <$\varnothing_{pore}$ < 500 Å) are therefore the most suitable to retain CWAs within their network. In this family, solids like MOFs [11] or zeolites [40] contain reactive metal sites which can induce the catalytic decomposition of CWAs into less toxic species. On the other hand, when the porous solid is inert against CWAs, functionalization or addition of a catalyst is required, like metallic and metal oxides nanoparticles (NPs). These species can be stabilized within porous solids, while keeping their catalytic activity for the degradation of CWAs [33,41].

The porous materials detailed in the next sections focus on those already used for the capture and/or detoxification of CWAs

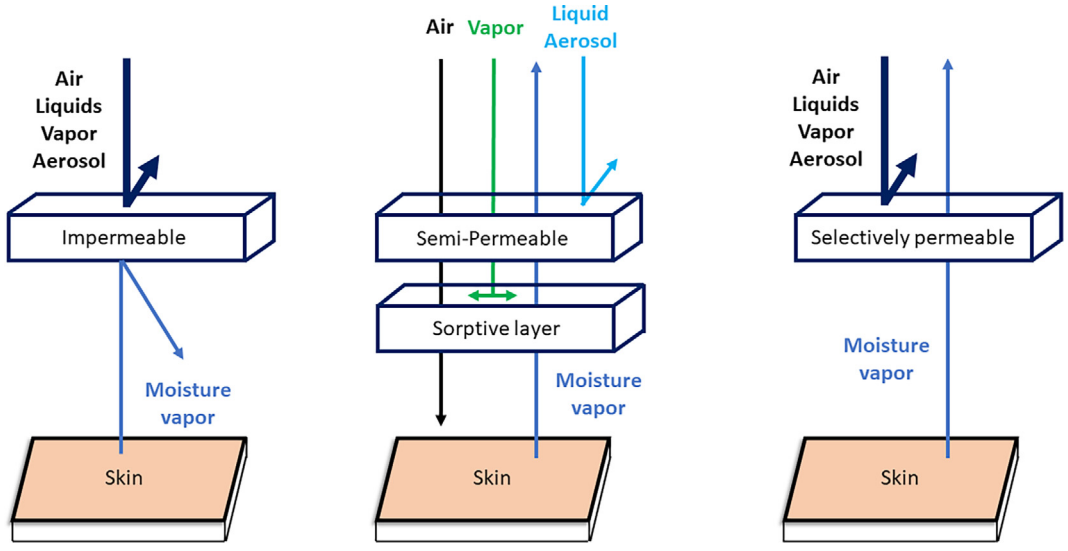


**Fig. 4.** Impermeable, semi-permeable and selectively permeable membranes (SPMs) of protective garments (inspired from Truong and Wilusz) [6].

(Fig. 5). Although all have not already been used for an active protective garment (clay or aerogel for example), their presentation allows to give an overview of the existing materials for CWAs deactivation.

### 3.2.1. Zeolite and clay

Zeolites and clays are mainly aluminosilicate materials with open structures [42], usually possessing surface areas of several hundreds of $m^2/g$. Their natural occurrence and their good adsorptive properties make them attractive for the production of low-cost sorbents. Clays, such as montmorillonite, vermiculite or saponite, are 2D structures of tetrahedrally coordinated silicate and octahedrally coordinated aluminate layers, encapsulating cations and/or $H_2O$ molecules [43]. In comparison, zeolites possess a crystalline 3D structure constructed from the connection of only $AlO_4$ and $SiO_4$ tetrahedral units. They possess a well-defined structure with a uniform distribution of micropores and channels/cavities, as well as relatively high specific surface area (<1000 $m^2/g$) [44]. In addition, zeolites exhibit high thermal stability and possess strong acidic centers. They are also known for their excellent cation exchange properties ($H^+$, $Na^+$, $K^+$, $Ca^{2+}$, $Cu^+$ or $Mg^{2+}$ for example). However, the diffusion and the transport of species can be limited through its channels due to their small pores size (usually 1–10 Å). The main applications of zeolites concern the petrochemistry, oil refining and wastewater treatment using their catalytic, ion exchange and adsorption properties [45,46].

The adsorption and retention capacity of clays, linked to their structures and properties, have made them interesting candidates as solid decontaminants of CWAs [47-49]. To enhance the degradation capacity of clays, several functionalizations have been tested [50]. The addition of oximes ($R^1C(=NOH)NR^2R^3$), known for their ester hydrolysis capacity and nucleophily, has been used for the

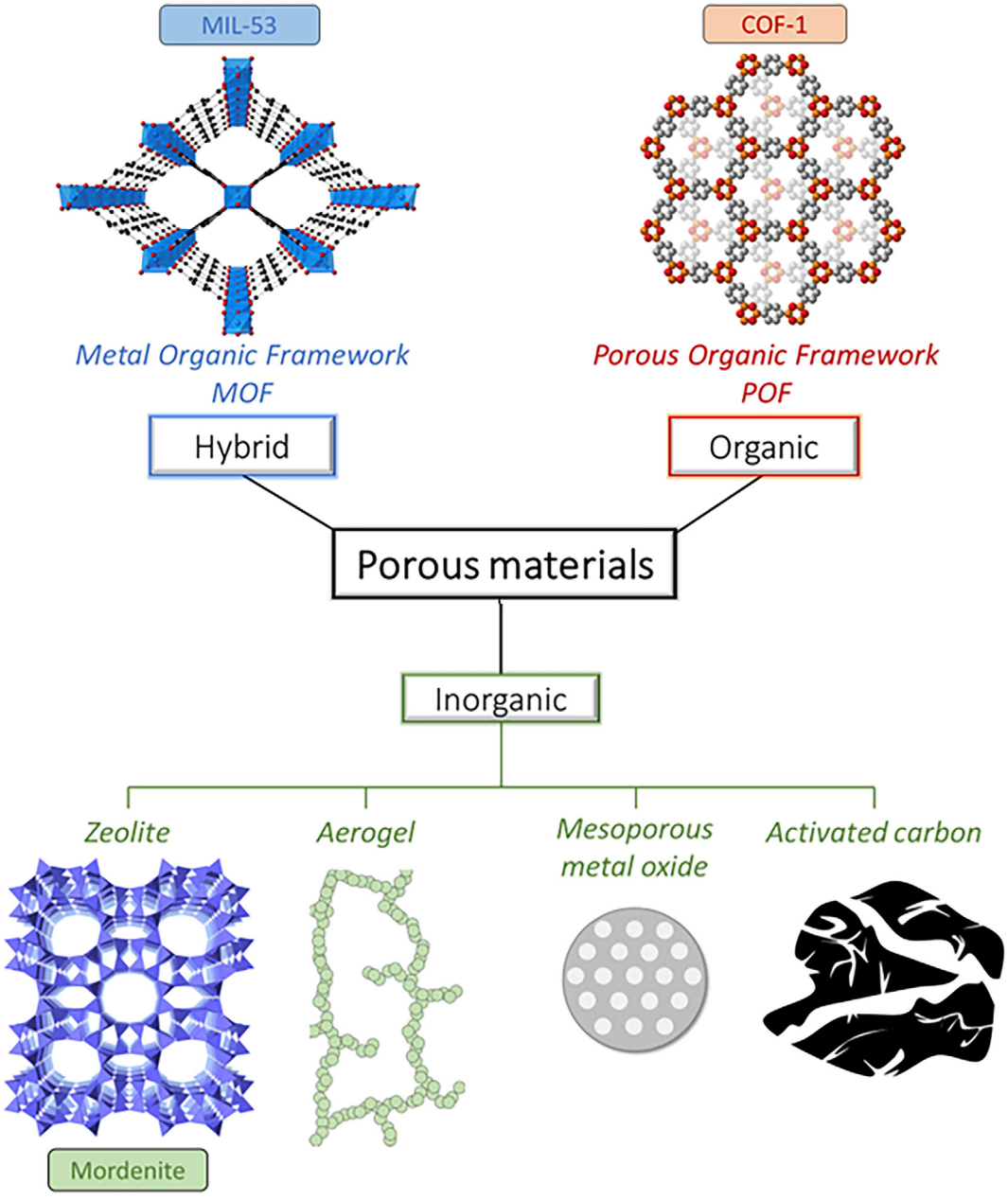


**Fig. 5.** Illustration of porous materials used for the capture and/or decontamination of CWAs, with illustrations of structures for zeolite (mordenite), MOF (MIL-53) and POF (COF-1).

degradation of nerve agents or simulants [51]. So far, the shortest half-life for GB decomposition was obtained with a montmorillonite-oxime composite (0.3 h) [52]. Modified Montmorillonite (MT) and vermiculite were also tested for chemical (HD) and biological (bacterial strains) warfare agents absorption [53]. Yperite breakthrough time was higher with MT (1180 min vs 448 min for vermiculite) due to an easier penetration (and therefore retention) of the organic species into its interlamellar porosity. Metal doped clays have also been tested for the degradation of HD or its simulant CEES [41,43,47,54]. $Ag_2O$ NPs supported on MT gave excellent results, with a full decontamination of HD within 2 h, while others ($Fe_2O_3$, ZnO, $CeO_2$, MgO, ...) required at least 16 h [41].

Despite small pore diameters (1–10 Å), limiting the diffusion of the largest CWAs agents [55,56], some zeolites showed good efficiency for the decontamination of several toxic agents [57-65]. A pioneer study was made in 1994 about the interaction of gaseous HD within zeolite 13X [57]. The dried zeolite showed a high absorption capacity up to 1.4 mmol of S-mustard per gram of zeolite. Furthermore, degradation products were detected using $^1H$ and $^{13}C$ NMR, but not certainly assigned. In the late 90 s, Wagner and Bartram studied the reactivity of doped-zeolites against CWAs and simulants [58]. They showed that AgY was efficient for HD decontamination while NaY was more active towards VX by P-S bond cleavage. Typically, the good results obtained with Ag-doped clays and zeolites are attributed to the affinity of silver for the complexation of sulfur-containing compounds [41,55,58,60,61]. In addition to these works, zeolites have also been used as sensors for CWAs (or simulants), evaluating their properties using ionic conductivity measurements or a quartz crystal microbalance [56,62].

### 3.2.2. Activated carbons (ACs) and activated carbon fibers (ACFs)

Activated carbons (ACs) or activated charcoals, are naturally available materials, produced from multiple natural or synthetic precursors (*e.g.* wood, bamboo, coconut shells, petroleum pitch or synthetic macromolecular system) [66,67]. They can be shaped under various forms (powders, granules, fibers, etc.). Their structure is analogous to a disorganized graphite network, with a dominant microporous behavior. The porosity is directly associated to an activation step (physical or chemical treatment), which is needed to create and clear pores [10,68]. Thanks to their high specific surface (usually > 2000 $m^2/g$), activated carbons find a lot of applications involving adsorption process, such as air decontamination [69,70]. Since World War I and their use in protective mask [5], activated carbons have remained prototypical materials for the study of CWAs adsorption [22,71,72].

To further improve the protection filtration systems based on activated carbons, several derivatives of those materials have been developed, like activated carbon impregnation foam, activated carbon nanoparticles or activated carbon-based clothes (woven or non-woven). Among these, activated carbon fibers (ACFs) or cloths, developed from the 1960 s, exhibit a particular interest. Indeed, their micropores opening are directly connected to the external surface of the fibers, providing minimum resistance to mass transfer, minimizing pressure drops, while keeping high specific surface area (800–2500 $m^2/g$) [73]. They possess excellent adsorption capacities with fast adsorption/desorption rates, as well as an easy and rapid regeneration. Furthermore, these fibers are very flexible, allowing a large variety of shapes to be produced (i.e., cloths, papers, felts or monoliths) [73,74]. Compared to other porous compounds like zeolites or MOFs, activated carbon fibers possess the unique advantage of being woven, allowing cohesive and bendable fabrics. They are already commercially available (for example, Kynol®), and used in various domains, such as water purification [67,75-77], air purification [78-81], CWAs adsorption [20,25,82,83], gas sensing [84,85] or electrochemical capacitors [86-88].

### 3.2.3. Aerogels

Aerogels were discovered by Kistler in the 1930s with the formation of a silica-based ultralight material [89]. This class of materials can be defined as low density porous compound having a great surface area (up to 1200 $m^2/g$), usually obtained by supercritical drying. Their composition was extended to other metals (Ti, Al, ...), chalcogenides, polymers or carbons [90-92]. Their porosity, combined with a low density, and a low thermal conductivity made aerogels excellent candidates for various applications such as environmental clean-up (water and air) [92,93], thermal insulation [94,95] or in biomedical applications [96]. However, very few studies on the absorption and/or degradation of CWAs have been made with aerogels. The reactivity of MgO and $Al_2O_3$ aerogels have been studied, with a degree of conversion of sulphur mustard to non-toxic products up to 70 % after one hour for the aluminum oxide aerogel and 40% after 3 h for MgO aerogel [97,98]. The adsorption and the preconcentration of Sarin and a simulant (DMMP) were studied using a hierarchical porous graphene aerogel [99]. It showed excellent adsorption efficiency for Sarin and an equilibrium adsorption capacity for DMMP of 148 mg/g. Recently, $TiO_2$ mesoporous aerogels supporting Cu NPs were tested on the simulant DMMP, showing that the high concentration of OH surface groups at the Cu/$TiO_2$ junctions enhances the hydrolysis efficiency [100].

### 3.2.4. Mesoporous metal oxides

Mesoporous metal oxide materials are of particular interest for CWAs degradation due to the combination of large pores giving high specific surface areas (up to several hundreds of $m^2/g$) and the occurrence of catalytic metallic centers [101]. Mesoporous metal oxides are usually made according two ways of synthesis. The soft template method is based on the utilization of surfactants (either cationic, anionic, or nonionic) to form micelles, while the metal oxide forms by condensation in-between, allowing to form a porosity replicating the size and shape of the micelles after calcination. With the hard template method, typically mesoporous silica (MCM-41, SBA-15 for example) or carbon (CMK-1, CMK-3) serve as templates and are impregnated by the metal oxide precursors. The hard template is removed in a second step, by using NaOH or HF solution. A large variety of ordered mesoporous metal oxides have been made (Ti-, Mg-, Al-, or Mn-oxides), as well as solids mixing at least two metals [101]. Among the different mesoporous metal oxides studied for the degradation of mustard gas [102-114] and/or nerve agents [31,105,110,112-116], excellent results were obtained with nanosized mesoporous $MnO_2$ which degrades 95, 56 and 99% for HD, GD and VX, respectively into non-toxic products in 1 h [113]. High activity against HD and VX have been linked to the oxidizing character of $MnO_2$ while GD hydrolysis necessitates more surface hydroxyl groups. $SiO_2$ NPs also showed promising results due to the combination of physisorption and degradation functions, with half-life of 12 min for GB and under 3 min for HD when functionalized by trichloroisocyanuric acid [110].

### 3.2.5. Porous organic frameworks (POFs)

Porous Organic Frameworks (POFs) are porous materials generated from only organic building blocks. Depending on the crystallinity of the materials, one can distinguish two types of POFs [117]. Covalent Organic Frameworks (COFs) are multidimensional crystalline porous materials made of light elements (H, C, B, N, and O) connected to each other through stable covalent bonds [118,119]. They show a rigid structure with excellent thermal stability (up to 600 °C), low density, large pores diameter (up to 58 Å)

and high specific surface area (up to 5000 $m^2/g$) [120,121]. In contrast, Porous Organic Polymers (POPs) are crosslinked amorphous polymers usually integrating microporosity. They can be divided into several groups, such as Polymers of Intrinsic Microporosity (PIMs), Conjugated Microporous Polymers or Porous Aromatic Frameworks. The synthesis of POPs generally consists in a polymerization of highly connected and rigid monomers. They typically possess similar pores size analogous to COFs but lower surface area, ranging from 300 to 1100 $m^2/g$ [119,122-124].

Concerning the decontamination of CWAs, recent works have shown interesting results [123,125-131]. The breakdown rate of methyl paraoxon by methanolysis was studied with two porous organic polymers (POPs) functionalized by lanthanum or aluminum(porphyrin)-based compounds [123,125]. They highlighted the importance of pores accessibility for methyl paraoxon degradation, as the increase of pores size (from 9 to 27 Å) enhances the catalytic activity. Recently, an imine-based COF was used for the hydrolytic degradation of DIFP [131]. They showed that the presence of imine (i.e. pyrrolidine or N-methylpyrrolidine) could replace usual basic co-catalysts such as N-ethylmorpholine (NEM) for a heterogeneous decomposition of organophosphorus compounds. As we will see hereafter (section 5.2), the presence of a basic co-catalyst (carried by the porous composite or added to the medium during the degradation analysis), is necessary for the degradation of phosphorous agent. For the mustard gas simulant, selective photo-oxidation of CEES to 2-chloroethyl ethyl sulfoxide (CEESO) was achieved with a yield over 99 % after 1 h, by using carbazole-based conjugated microporous polymers as photosensitizers [126].

#### 3.2.6. Metal-Organic Frameworks (MOFs)

Crystalline porous metal organic frameworks consist of metal ions or clusters connected to each other by organic ligands. Developed for two decades, they attract an ever-increasing attention due to their very high porosity (up to 7000 $m^2/g$) [132], tunable pore opening and broad possibilities of chemical functionalization. Almost all cations (from alkaline to actinides) have been used to construct MOF structures. For the organic ligands, anionic or neutral multidentate ligands with N- or O- donor atoms are privileged, like carboxylates, phosphonates, polyamines, cyano or pyridyl groups [133]. A large variety of synthesis methods are also available such as hydrothermal, electrochemical, mechanochemical or microwave-assisted irradiation. The precise choice of the primary building units (PBUs, i.e the precursors), synthesis method and parameters (T°C, pH, etc.) allow therefore for a controllable size, shape and functionalization of MOFs pores [134]. Furthermore, depending on the target properties (luminescence, magnetism, catalytic, ...), a selection of the adequate precursors is possible, offering a wide range of potential applications. Among the most famous MOFs, one can cite the MIL-n series, HKUST-1, MOF-5 or UiO-n series [135-138], which are commercially available, for some of them [134].

The first example of MOFs utilization for CWAs capture was reported in 2010, when a Zn-based MOF was found to be efficient for the encapsulation of the nerve agent surrogate methylphosphonic acid (MPA), with an adsorption density of 3.42 mmol/g [139]. Researches involving CWAs degradation have therefore been developed with MOFs possessing unsaturated metal centers, showing a catalytic activity for the decomposition of toxic species [140-144]. Among them, highly stable Zr-based MOFs (i.e UiO-6n series, NU-1000 or MOF-808) have showed interesting results in the domain of CWAs decontamination [145,146]. Indeed, they possess high amounts of Zr(IV) sites which act as Lewis acid and promotes the degradation of CWAs [12]. Over the years, the increased knowledge has allowed to distinguish several important factors driving CWAs degradation. For organophosphorus compounds, the functionalization of ligands or the pores size control can modulate the degradation efficiency. Peterson *et al.* highlighted the increase of the degradation of DMNP when adding an amino $-NH_2$ moiety to the organic ligand, which acts as a Bronsted base and improves proton transfer for hydrolysis reactions [147]. Passing from UiO-66 to UiO-66-$NH_2$, half-life drops from 25 to 0.9 min. This study also showed that increasing pore size from 6 Å (UiO-66) to 8–11.5 Å (UiO-67) reduces DMNP half-life by a factor 7, due to an easier access to active sites and better diffusion [147]. Interestingly, combination of UiO-66 (functionalized by -H or $\_NH_2$ groups) and porous cellulose aerogel has also been developed, showing highly effective degradation of DMNP ($t_{1/2}$ < 10 min) [148,149]. For the degradation of HD and its simulant, recent studies showed that the photo-oxidation is an efficient way as it leads to the selective generation of non-toxic sulfoxide products [23,150]. A photosensitizer is generally required (*e.g.* porphyrin or pyrene), to generate under UV light singlet oxygen $^1O_2$, accelerating the degradation of HD or its simulant [151]. Thanks to this approach, half-life below 15 min for CEES can be reached [152,153].

### 3.3. Textiles fibers

Fibers can be defined as a unit of matter that is at least 100 times longer than its width or diameter. To be used into a yarn, this basic unit of textiles requires to meet specifications. It needs to have a length of at least 5 mm, be flexible, cohesive and to show sufficient strength. Furthermore, properties such as elasticity, uniformity, durability, comfort, fineness or lustering are also important for textiles. These features are directly linked to the nature of the fiber and the process used for the yarn manufacturing [154].

Fibers are generally divided into two categories: natural and man-made (or chemical) fibers (Fig. 6). The natural fibers designate those obtained by physical or mechanical transformation of a natural material, without any modification of its composition. One can find natural fibers from plants (*e.g.* cotton, linen), animals (*e.g.* silk, wool) or minerals sources (*e.g.* metal, asbestos). The man-made fibers mostly contain regenerated fibers, obtained by the modification of natural fibers, or synthetic fibers, i.e. from petrochemicals mainly [155].

Although single fibers do not present significant catalytic activity or porosity (except for ACFs), their nature is important for the anchoring of reactive species. Generally, natural fibers contain various surface functional groups (hydroxyl, carboxyl...) facilitating the deposition of active species whereas synthetic fibers surface are almost inert. The following discussion will describe fibers (natural or synthetic) usually used as supports for CWAs adsorption or detoxification.

#### 3.3.1. Natural fibers

**Cotton** are the most widespread natural fibers, used since 5000 BCE. Its main component is cellulose (between 88 and 96.5%) with few hemicellulose (~6%), which makes it one of the purest sources of cellulose known [156]. Cellulose is a polysaccharide consisting in linear chains of D-glucose linked by β-1,4-glycosidic bonds (single oxygen atoms bridging the C1 of one pyranose (6-membered ring) and the C4 of the next one (see Fig. 7)). Hydroxyl groups of the cellulose can link neighboring chains by hydrogen bond, giving to the cellulose its mechanical strength, chemical stability and insolubility in common solvents [157,158]. Cotton fabrics possess interesting properties such as high absorbency, softness, washability, breathability, flexibility and are relatively cheap [19,159].

To improve the properties of cotton, cellulose can be easily functionalized thanks to the presence of reactive hydroxyl groups. Mercerization is widely used as a finishing treatment of cellulose based-materials, improving its hygroscopic properties, mechanical durability and adsorption rate. This process consists in immersing

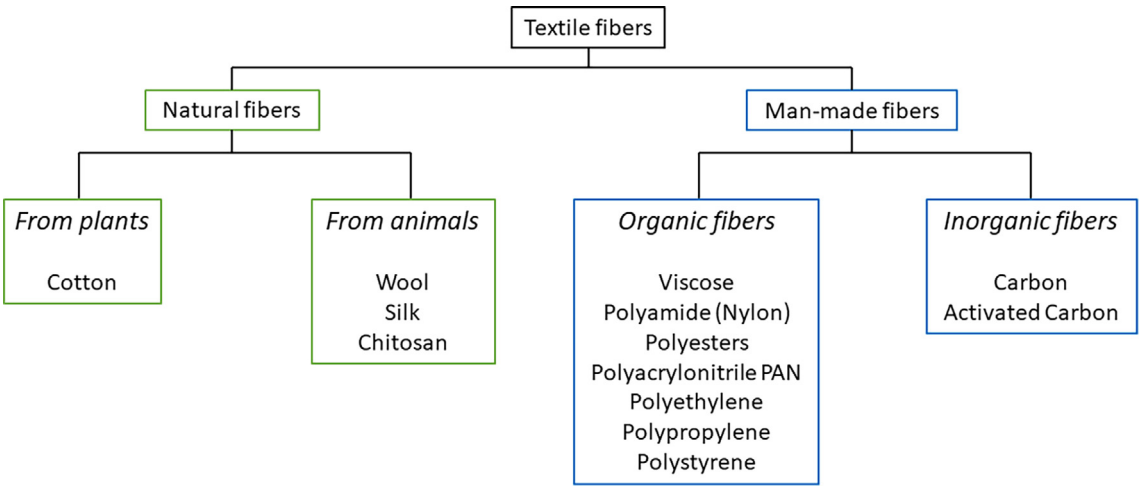


**Fig. 6.** Classification of the textile fibers used for porous textile composites (PTCs) against chemical warfare agents (CWAs).

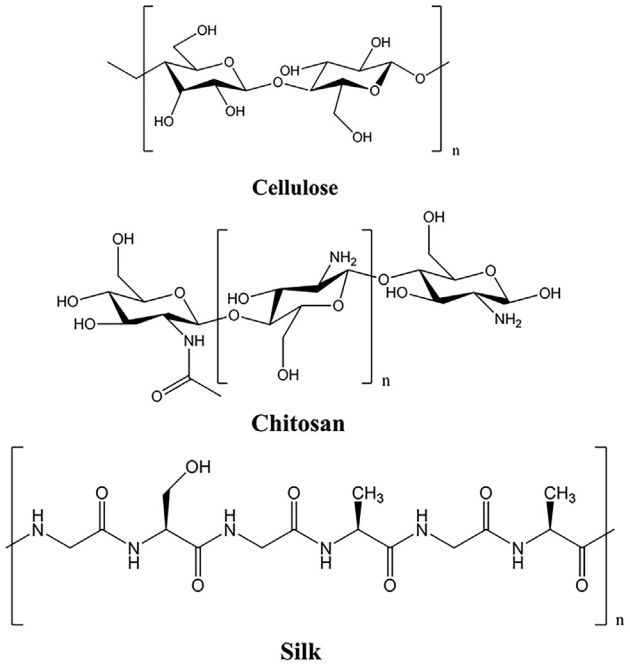


**Fig. 7.** Chemical structures of cellulose (main constituent of cotton), chitosan and silk.

the fibers in an alkaline solution (usually NaOH), which increases the content of free hydroxyl groups and facilitates the grafting of additional species (*e.g.* MOFs) [160]. Another common functionalization method is carboxymethylation, based on the creation of carboxylic functions at the surface of the fibers using chloroacetate salt and sodium hydroxide as catalysts [161,162]. Several other functionalization techniques exist for both natural and synthetic fibers, like the addition of a surface modification agent (dopamine, cyanuric chloride with cysteamine, . . .) or atomic layer deposition (ALD) [163-165].

**Chitosan** is a derived of chitin, a naturally abundant polysaccharide generally found in arthropod exoskeletons (*e.g.* marine crustaceans). It is the second most abundant biopolymer after cellulose. Chitosan is obtained from a N-deacetylation of chitin, and possesses linear polysaccharides of D-glucosamine (deacetylated unit) and N-acetyl D-glucosamine (acetylated unit), depending on the degree of N-deacetylation (from 50 to 90%). The polymer is semi-crystalline, with a direct link between the degree of crystallinity and the degree of deacetylation. The structural difference with cellulose lies in the replacement of the hydroxyl at the C2 position to an acetamide group, giving chitosan between 5 and 8 wt% of nitrogen. Chitosan is chemically active thanks to the occurrence of amine and hydroxyl groups on each deacetylated unit. It possesses biodegradable, bio-adhesive, bio-compatible, non-toxic and hemostatic properties along with a notable antibacterial activity, making it highly interesting for biomedical applications [166]. In terms of functionalization, carboxymethylation is one of the most used methods [157,167,168].

**Silk** is a commonly available natural biopolymer from various animal sources (*e.g.* spiders, scorpions, mites, bees and worms). Silk contains approximately 18 amino acids, the principal ones being the glycine, alanine and serine (see Fig. 7). They self-assemble into an anti-parallel β-sheet structure through intra and inter molecular forces (H-bonding, Van der Waals and hydrophobic interactions), giving to silk fibers their mechanical properties (*e.g.* strength and elasticity) [169]. Physical and chemical functionalizations are commonly employed, which is facilitated by abundant available groups (carboxyl, hydroxyl and amino) associated to amino acids of silk fibroins. The easy accessibility of their chemical groups and controllable biodegradability makes them interesting for water treatment and silk is already used in tissue engineering and biomedical applications [170,171].

### 3.3.2. Man-made fibers

This section will focus on carbonaceous fibers and polymeric fibers from petrochemicals. Regenerated fibers like Lyocell or viscose rayon, obtained from regenerated cellulose [156], were not applied to CWAs decontamination, so far. They are not be discussed in this review.

*3.3.2.1. Carbonaceous fibers:* **Carbon fibers** (CFs) were first synthesized in 1883, by the pyrolysis of cellulose fibers. It commonly leads to fibers containing at least 92 wt% of carbon, being a mixture of amorphous carbon and crystalline graphite. The proportion of graphite in the fiber can vary from 0 up to 100 %, the latter materials being called graphite fibers. The most used precursors nowadays for carbon fibers are polyacrylonitrile (PAN) and pitch [172]. Carbon fibers are light and possess high mechanical strength (1.7 GPa) and tensile modulus (400 GPa), good electrical and thermal conductivity, as well as a good stability to high temperature, chem-

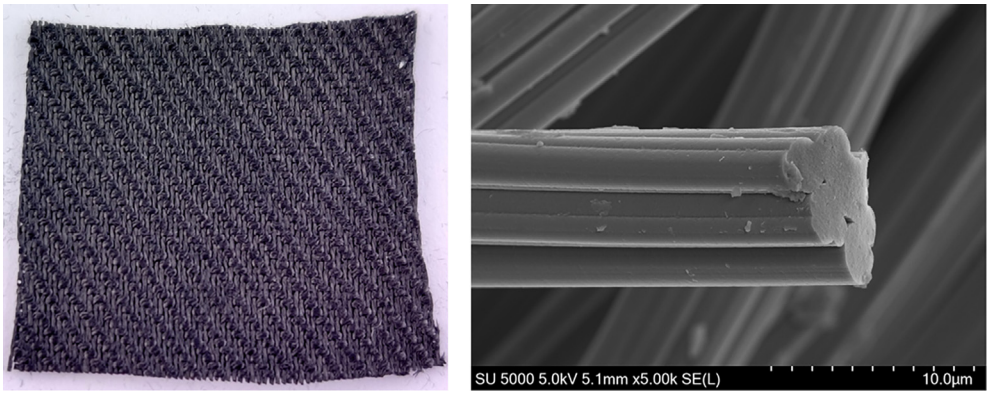


**Fig. 8.** Photograph and SEM image of an activated carbon fibers (ACFs) fabric.

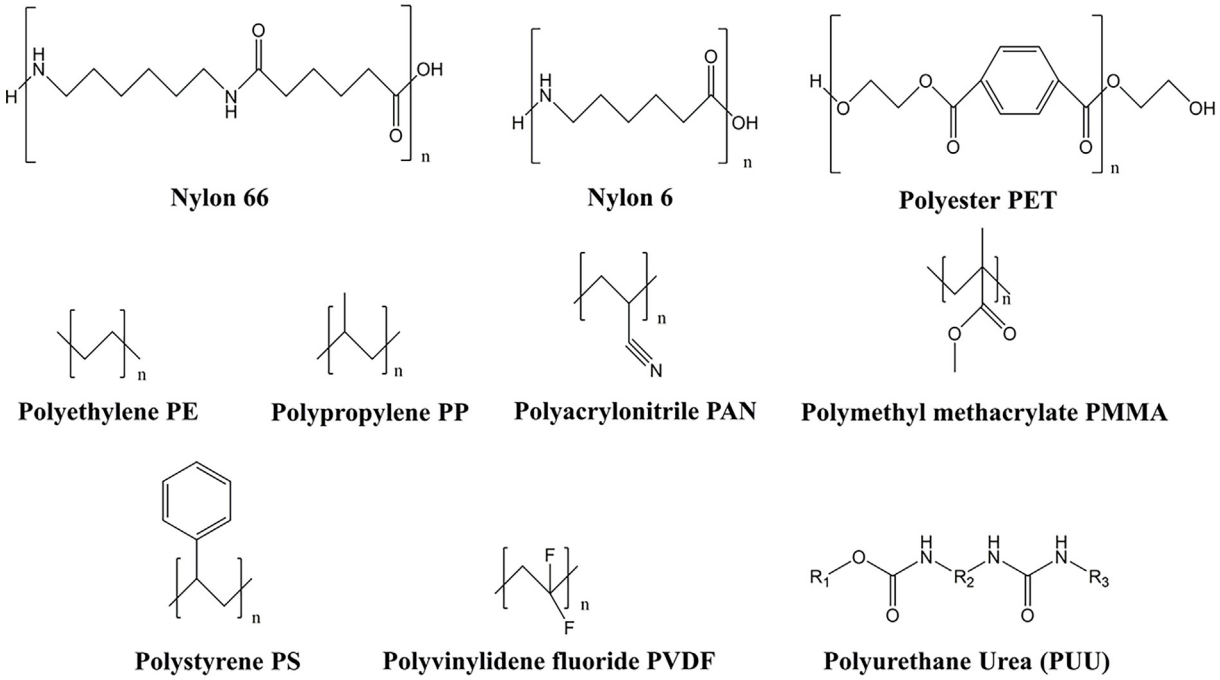


**Fig. 9.** Chemical structures of the polymers found in synthetic textiles.

icals and harsh conditions [173]. They are largely used in aerospace, construction, and automobile industries.

When carbon fibers are submitted to an activation step, they are called **Activated Carbon Fibers (ACFs)** (Fig. 8) [10]. The activation can be done using physical methods, such as hot gas, plasma or supercritical fluid, or chemical methods, with the incorporation of reagent ($ZnCl_2$, NaOH, etc.) in the carbon fibers. This leads to an increase of surface area by clearing pores and creating new ones [68]. The resulting specific surface area is up to 2.500 $m^2/g$ and the micropores are directly available at the surface of the fibers. These properties make ACFs particularly adapted for the adsorption and removal of toxic compounds (liquid or gas) [75,78,79,174,175]. Furthermore, ACFs fabrics are comfortable thanks to their low weight, flexibility and excellent air permeability. They are already manufactured as combat suits for NBC (Nuclear Biological Chemical) protection, with generally a 24 h protection against HD liquid and 6 h against HD vapors [10].

**Graphene** consists in a two-dimensional (2D) single layer of carbon atoms. The formation of graphene fibers is possible using the wet-spinning method and requires the precise alignment of graphene sheets along the fiber axis. Graphene fibers possess extraordinary mechanical properties, with a record tensile strength (130 GPa), excellent elastic modulus (1.1 TPa), and electronic transport efficiency, good stability, high thermal conductivity and notable flexibility [173].

**Graphene oxide** (GO), prepared by the oxidative exfoliation of graphite, combines the 2D structure of graphene and a large amount of oxygen-containing functional groups (hydroxyl, epoxide and carbonyl). These functional groups give to graphene oxide its hydrophilic nature, which is furthermore chemically stable and easy to fabricate [176]. Graphene as well as graphene oxide are well adapted for gas and liquid detection or separation [177-179]. They are of particular interest for CWAs garments protection, as they both possess high moisture permeability and are almost impermeable to small gases [180]. Combination with active species (*e.g.* $TiO_2$, $Zn(OH)_2$, ...) have also being used for the decomposition of CWAs [181-184].

*3.3.2.2. Synthetics organic fibers.* The development of synthetic fibers made from petrochemicals started in the early 20th century.

Nylon, from the polyamides family, was commercialized by DuPont industry in 1938 as the first synthetic polymer. The polyester polyethylene terephthalate (PET) was patented three years later by a British textile company and corresponds to the first ester-type fiber. Nowadays, 98 % of the synthetic fiber production include polyamides (nylon), polyolefin (i.e polyethylene and polypropylene), polyesters and polyacrylates. Their fast development is related to their properties associating strength, durability, chemical resistance, low moisture absorbency, and their durability versus crease [185]. The most common synthetic fibers (Fig. 9) used for the capture of CWA will be briefly described in the following paragraphs.

**Polyamide** fibers contain chains of aliphatic or aromatic subunits bonded by amide (RCO-NR'R") functions. Among them, the most common are aliphatic nylon 6 and nylon 6,6, which are described in Fig. 9. They possess a semi-crystalline structure with an excellent tensile strength, resistance to most chemicals and to abrasion, good elastic recovery and low initial modulus. Their applications are various like carpets fibers, parachute fabrics, ropes, fishing nets or safety airbags [185,186].

**Polyesters** correspond to polymers containing ester groups. The most known polyester being the thermoplastic polyethylene terephthalate (PET), which represents 60% of the worldwide synthetic fibers production. They are hydrophobic, allowing a quick drying of the fibers. They are recyclable and resistant (vs. stretching, abrasion, wrinkle, chemicals and mildews). They possess excellent tensile strength and have negligible shrinkage. These properties made polyesters excellent for technical textiles applications [185,186].

**Polyolefin** fibers are by definition composed of at least 85 % by mass of ethene, propene or other olefin $C_nH_{2n}$ units. The most used polyolefins fibers are the thermoplastic polypropylene (PP) (90% of the polyolefin fibers production) and polyethylene (PE). Theses fibers exhibit excellent chemical resistance (especially to acids, alkalis and organic solvents), high strength and toughness. These low-cost fibers are interesting for protective cloths due to their cut-resistance or in biomedical applications (implants or devices) [187].

**Polyacrylate** fibers contain at least 85 % of the acrylonitrile monomer, the most known being polyacrylonitrile (PAN) fibers. They were first developed by DuPont in 1941, under the name Orlon. To facilitate the fibers processing, acrylonitrile monomers can be combined with others monomers, such as methyl acrylate, methyl methacrylate (also known as plexiglass) or vinyl acetate. They have been commonly adapted for clothing due to their strength and warm properties. Furthermore, they are resistant to acids, oxidants, organic liquids and weak alkalis, and also to UV radiation and micro-organisms [187].

In addition to these families of synthetic fibers, some other polymers have been used as fibers in CWAs protective garments. Polystyrene (PS) is a thermoplastic polymer, which can be electrospun to produce fibers [188]. Polyvinylidene fluoride (PVDF) is biocompatible and possess high mechanical strength and thermal stability. It is mainly used in biomedical and energy harvesting systems [189]. Also, polyvinylidene fluoride was shown to be particularly adapted to MOFs deposition, which is an interesting point for the application aimed in this review [190]. Poly(urethane urea) (PUU) is formed by the combination of urethane –NH-COO- and urea –NH-CO-NH- functions, which give elastomeric properties by an alternation of hard and soft segments [191].

## 4. Porous textile composites (PTCs) synthesis

Composite materials used as active protective garments against CWAs combine textiles and active materials, in our case porous solids. The two constituents must present strong adherence to insure durable resistance and efficiency [192]. Common synthesis methods used to achieve these goals can be gathered into two groups: the direct integration of a porous material within the fibers, or the attachment of the adsorbent at the surface of the fiber [193-195]. Details and examples of these methods will be described in the next part, with a focus on MOFs and activated carbon fibers compounds, as they represent the prominent part of the compounds showing great performances for the capture and/or degradation of CWAs.

### *4.1. Direct integration by electrospinning*

Electrospinning is a well-adapted fabrication method to process solutions, mainly polymer-based, into continuous nano- or microfibers. The polymer solution is pushed through a needle and precipitated on the base collector to generate fibers following the application of a high voltage (Fig. 10.a) [193,196]. For about 10 years, the electrospinning technique was developed to mix various compounds, like metal sulfides or metal oxides, within the fiber matrix [197,198]. The particles (or their precursors) and the polymers solution are mixed to create the electrospun composite fibers. Depending on the nature of the particles and the polymer,

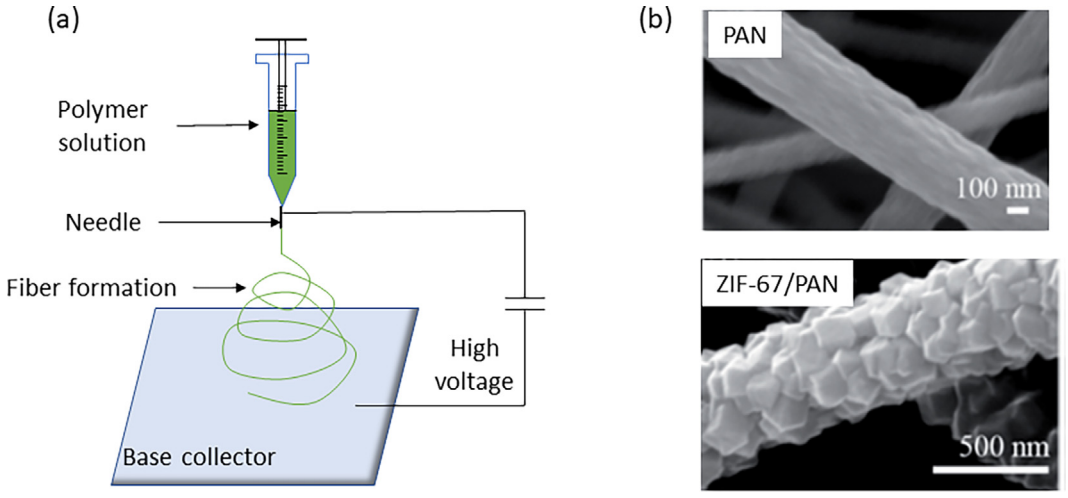


**Fig. 10.** (a) Scheme of electrospinning method and (b) SEM images of polyacrylonitrile (PAN) and ZIF-67/PAN electrospun fibers obtained by *in-situ* growth [219]. Reproduced with permission from the Royal Society of Chemistry.

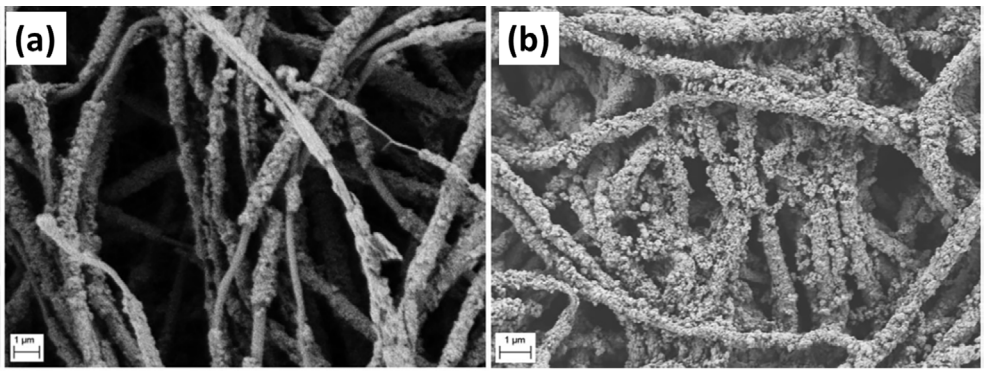


**Fig. 11.** SEM images of HKUST-1 deposited on (a) bare cotton fiber and (b) carboxymethylated fibers [239]. Reproduced with permission from Wiley Online Library.

optimization of the experimental conditions (viscosity of the mixture, particles concentration, chemical compatibility, . . .) is mandatory to obtain a homogeneous composite [193]. Therefore, the resulting fibers contain particles (from nm to µm) embedded within the polymer. This method was developed for many applications, such as energy storage systems (supercapacitors), mechanical enhancement or catalysis [197].

The first MOF-fiber composite obtained by direct electrospinning was produced from a mixture of zeolitic imidazolate framework called ZIF-8 and polyvinylpyrrolidone (PVP) [199]. Fibers of PVP with a diameter from 150 to 300 nm were obtained and homogeneous distribution of ZIF-8 was observed within the composite porous fibers (specific surface area: 530 $m^2/g$). Since then, numerous new combinations of MOF-polymer have been investigated via electrospinning, mainly using synthetic fibers [128,191,200-207]. Only a few works reported the direct electrospinning of natural fibers, more specifically to form chitosan-MIL-68(Al) and chitosan-MIL-101(Fe) composites, with high content of MOF (80 wt%) [208,209]. The obtained fibers have a spider web structure with excellent specific surface areas, up to 1460 and 3300 $m^2/g$ for MIL-68 and MIL-101(Fe), respectively.

One of the main limitations of the direct electrospinning of MOF-polymer composites is the inactivity of MOFs crystallites trapped within dense polymeric fibers. In this case, the external pores of the solids are blocked by organic matter, reducing the porosity and the efficiency of the composite [193]. To overcome these issues, Peterson *et al.* have investigated the effect of different solvents for the direct electrospinning of a suspension of polystyrene and UiO-66-$NH_2$ [210]. Pure DMF solvent led to a deposition of MOF crystals on the surface of the fibers while a DMF/THF solvent mixture resulted in the dispersion of crystallites within the fibers due to the formation of a yarn-like composite. The use of porous polymer fibers is a second strategy for limiting MOF inertia within the polymeric matrix, as exemplified with ZIF-8 [211-213]. Otherwise, simultaneous electrospinning of nylon-6 and electrospray of UiO-66 have been tested and resulted in a selective immobilization of the MOF at the surface of the fibers [214].

Alternatively, *in-situ* growth of MOF crystals onto the surface of fibers has been developed to keep MOF fully accessible, according two methods [193]. In the first one, called seed-assisted growth, MOF crystallites can be incorporated as a seed to the polymer solution prior to electrospinning deposition. The crystal growth is thus triggered by immersing the fibers in a solution containing MOFs precursors (metal salt and ligand) [193,215,216]. As an illustration, this approach was adapted to popular HKUST-1 and ZIF-8, which were grown under a solvothermal treatment of seeded polystyrene (PS) surfaces, resulting in defect-free and uniform coatings. A threefold enhancement of the specific surface area was measured after the secondary growth, from 300 to>900 $m^2/g$ for both MOFs [217]. The second method consists in adding a MOF precursor (metal ions or organic ligand) to the polymer solution. The crystallization and the growth of the porous solid will start after a second impregnation in a mixture containing the remaining reagents, needed for the MOF production [218-220]. For instance, a mixture of polyacrylonitrile (PAN) and $Co(AC)_2$ was electrospun and the generated fibers were then immersed into a 2-methylimidazole solution to form homogeneous ZIF-67 at the surface of the fiber (Fig. 10.b) [219].

### 4.2. Functionalization and surface decoration of the fibers

Due to the presence of numerous accessible functional groups (–OH, –COOH, $–NH_2$) at their surface, natural fibers are suitable for straightforward deposition. In the case of cotton, the available hydroxyl groups of cellulose are well adapted sites for the growth of MOFs, like HKUST-1 (Fig. 12) [221]. The same approach was also adjusted to inorganic zeolite crystals which can be directly deposited on cellulose fiber via classical methods such as hydrothermal treatment or spray-coating [222,223]. An original approach has been validated recently, using an ionic liquid welding technique to improve the anchoring of UiO-66-$NH_2$ on cotton [224]. Deposition of pre-formed MOFs by simple immersion of the textile in a suspension have also been reported for the deposit of MOF-808 on cotton [32]. Direct deposition of MOFs (HKUST-1, ZIF-8) is also possible on other natural fibers, like wool or silk, involving hydroxyl, carboxyl or amine functions [225-228].

To improve the anchoring of MOFs on fibers, functionalization of the fiber surface with a function analogous to one chemical group existing within the MOF structure has been usually exploited. Typically, these species are carboxylate (R-COO) mimicking ligand or hydroxyl groups (R-OH) analogous to those bridging cations in the inorganic clusters in the MOFs structures. For natural fibers, these chemical functions are easily produced by mercerization or carboxymethylation techniques (Fig. 12). Uniform and dense coatings of various MOFs have been successfully obtained on mercerized fibers using a layer-by-layer or a solvothermal techniques [229-235]. In the case of Zr-MOFs, Kim *et al.* used a solvothermal process to grow UiO-66-$NH_2$ from 60 to 200 nm large with excellent crystallinity on mercerized cotton [160]. Carboxymethylation has been successfully adapted to cotton and chitosan fibers for the anchoring of Cu, Zn or Zr-based MOFs [161,162,236-239]. The homogeneous deposition of MOFs on a carboxylate-bearing surface is well illustrated in the case of the composite cotton/HKUST-1, where SEM images clearly show partially covered fibers without carboxymethylation whereas pretreated fibers display an uniform growth of HKUST-1 over the whole surface (Fig. 11) [239].

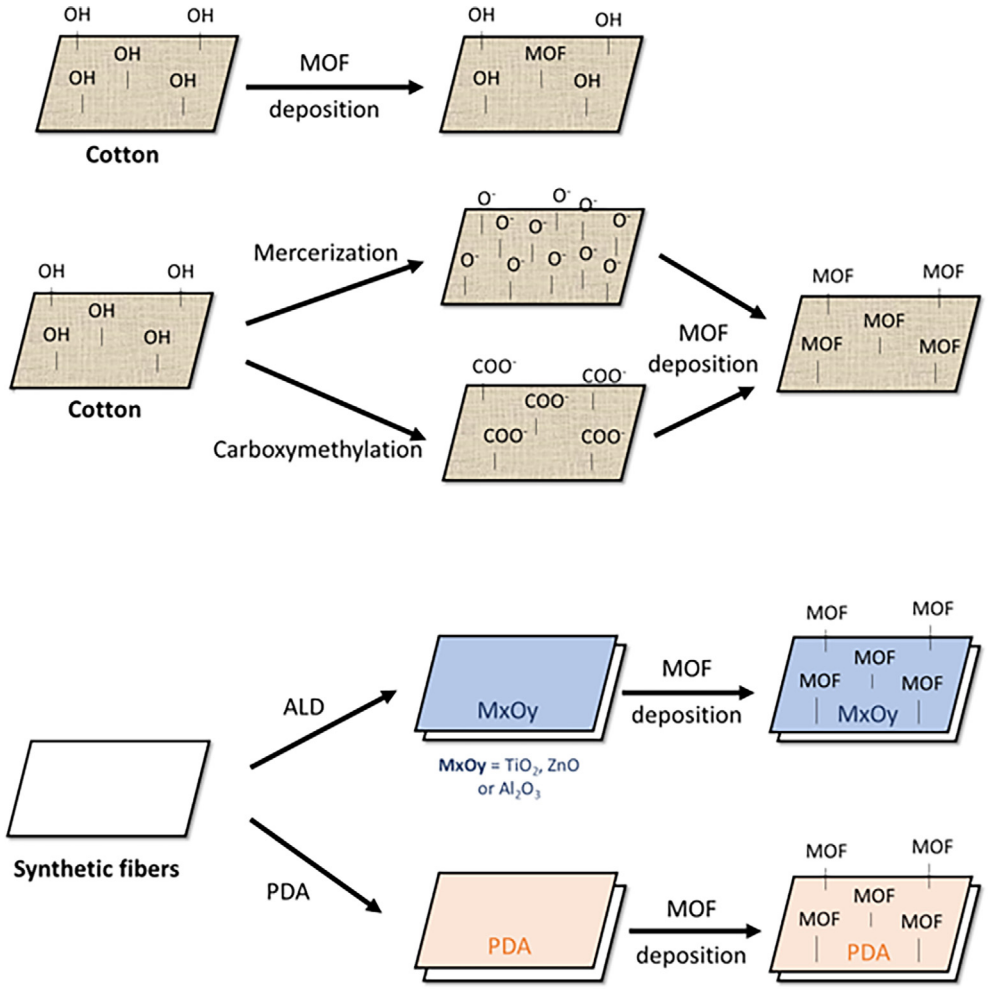


**Fig. 12.** Usual functionalization and surface decoration pathways of natural fibers (cotton) and synthetic fibers (ALD = Atomic Layer Deposition; PDA = Polydopamine).

For synthetic fibers, the absence of functionalization sites at the surface limits the anchoring of additional materials. This limitation can be bypassed with mixed natural-synthetic fibers. In the case of Nyco (mixed nylon-cotton fibers), Kalaj and Cohen developed a spray coating deposition of a post-synthetically modified UiO-66-$NH_2$ with excellent adhesion to the textile support, as evaluated by scratching and tape test [240]. On pure synthetic fibers, some examples of direct deposition were also mentioned [241-246]. Ma *et al.* described the solvothermal deposition for Zr-based solids (MOF-808 and UiO-66-$NH_2$) via a three-steps process (aggregation, formation of MOFs and growth), leading to the deposition of approximately 1 µm-thick layer of MOF on the polymer fibers (PE, PAN or PP) [246]. In this case, the efficiency of MOF deposition was associated to the use of trifluoroacetic acid as a synthesis modulator. Indeed, the higher acidity of trifluoroacetic acid slows down the crystallization in order to favor a continuous and homogeneous MOF crystallization on the fiber. Furthermore, the composite shows a particular resistance to vigorous washing, highlighting a strong binding between the fiber and the crystallites. Another solution for direct deposition of MOFs without fiber functionalization is the sorption-vapor synthesis [247]. The fiber is first submerged in a solution containing all the Zr-based MOF precursors and modulator. The adsorbed precursors on the fiber were then placed in a solvent/modulator mixture at 100 °C for several hours and the formation of a homogeneous growth of MOFs crystals on the fibers was observed.

Like natural fibers, synthetic supports can be also functionalized by various organic (polydopamine PDA, polyvinylamine, etc) [163,248-252] or inorganic chemical species ($Al_2O_3$, ZnO or $TiO_2$) [165,253,254] in order to facilitate solids deposition (Fig. 12). For example, polydopamine possesses various functional groups (i.e. amine, imine and catechol) and serves as nucleation centers for MOFs growth (*e.g.* HKUST-1, ZIF-8, MOF-5, MIL-100) on several fibers (PP, PE, PS and PVDF) [251,255,256]. The atomic layer deposition (ALD) route allows the functionalization of a large range of fibers (PP, PET, PA, cotton) by inorganic oxides like ZnO to facilitate the heterogeneous nucleation and growth of MOF particles. It is now a well-developed method and good results have been obtained using various polymers fibers and MOFs (HKUST-1, UiO-66, UiO-66-$NH_2$, UiO-67, Zn-MOF-74, Mg-MOF-74 and MOF-525). For all these composites, the target applications aimed were the detection and removal of toxic gaseous compounds ($H_2S$, $NH_3$, CWAs or simulants) [165,253,254,257-259]. However, the ALD method remains an expensive and time-consuming method, showing a possible lack of covalent attachment with the synthetic fibers [240].

### *4.3. Activated carbon fibers (ACFs) functionalization*

The porous properties of ACFs can be tuned by post synthetic modification, via the introduction of functional groups on the walls and/or the embedding of inorganic particles within the pores [73].

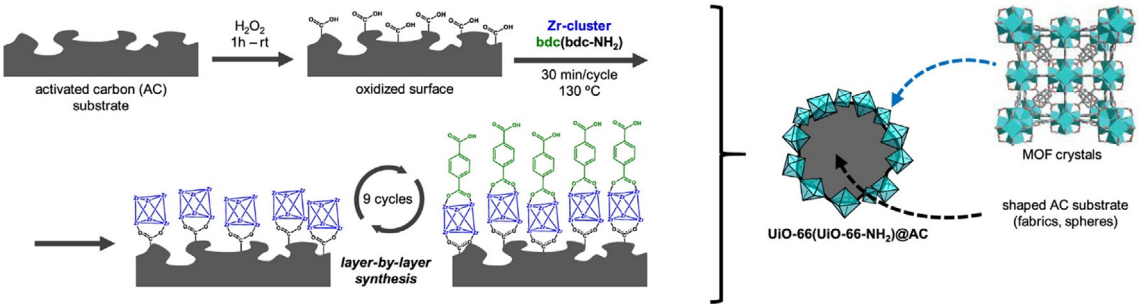


**Fig. 13.** Scheme of UiO-66 and UiO-66-$NH_2$ synthesis by a layer-by-layer deposition on functionalized activated carbons [283]. Reproduced with permission from the American Chemical Society.

**Table 2**
CWAs adsorption and detoxification using porous textile composites (PTC) containing ACFs.

| PTC | | | CWA and amount | Adsorption/Permeation | Degradation time | Degradation products | Ref |
|---|---|---|---|---|---|---|---|
| Composition | Amount or size | SSA ($m^2$/g) | | | | | |
| ACFs/Barium titanate nanospheres | 20 mg | 613 | CEES (20 µL) | 313 mg/g after 7 days | | Ace, EtOH, Eth-Cl, iPrOH, EVS and DEDS | [292] |
| ACFs | 20 mg | 956 | CEES (20 µL) | 324 mg/g after 7 days | | EVS, DEDS, Ace and Eth-Cl | [20] |
| ACFs | 200 mg | 939 to 1300 | CEES (70 ppm) | Maximum weight increase: 3.24 wt% | | | [25] |
| ACF/MgO or ACF/$Al_2O_3$ | 9 mg | | CEES (30 µL) | Adsorption rate constant: 4.8 $min^{-1}$ | $t_{1/2}$ = 16 min | | [281,282] |
| ACFs | | 483 | CEES (amount unknown) | ~ 20 mg/g-ACF | | | [290] |
| ACFs | | 483 | DIMP (amount unknown) | ~ 100 mg/g-ACF | | | [290] |
| ACF/$SiO_2$ NPs | 4 * 8 cm | | DMMP (100 ppm) | 0.824 g/g-ACF | | | [278] |
| ACF (A-15) | 0.08 g | 1500 | DMMP (2.55 mg/L) | 0.59 g/g-ACF at $t_B$ = 90 min | | | [83] |
| Ozonized ACF | 300–350 mg | | TMP (3 g) | 31.8 % after 336 h | | | [294] |
| ACF/UiO-66 | 40 mg | 840 | DIFP (1.25 µL) | | 80% in 1440 min | | [283] |
| ACF/UiO-66-$NH_2$ | 40 mg | 745 | DIFP (1.25 µL) | | 40 % in 1440 min | | [283] |

* Ace: acetaldehyde; Eth-Cl: chloroethane; EVS: ethyl vinyl sulfide; DEDS: diethyl disulfide; $t_{1/2}$: Half-life; $t_B$: breakthrough time.

Surface functionalization of ACFs is often realized through the addition of oxygen functional groups such as phenolic, carboxylic or lactonic groups or through nitridation to add amines, amides or pyridines groups. Several methods have been developed, such as chemical oxidation [260-263], nitridation [264,265], plasma treatment (oxygen [266,267] or nitrogen [268]), halogenation [269,270], gamma-ray irradiation [271] or electrochemical oxidation [272,273]. Whereas wall decoration is well adapted for enhancing gas sorption ($CO_2$, $SO_2$) [260,268], the decomposition of trapped species needs the presence of an embedded active material such as metal oxide nanoparticles within the framework [175,274]. Several difficulties have been identified such as pores obstruction of ACFs or the agglomeration of NPs which could reduce their activity [73]. Despite these obstacles, various NPs have been successfully implemented into the ACFs frameworks such as $TiO_2$, $Fe_2O_3$, $MnO_2$, CuO, Cu or Ag, making the composites particularly attractive for air [174,274-278] and water decontamination [73,175,279-282]. Recently, UiO-66 and UiO-66-$NH_2$ MOF have been deposited on functionalized ACFs using a layer-by-layer deposition (Fig. 13) [283]. The association of ACFs and MOFs is almost inexistent surprisingly [284], the combination of activated carbons and MOFs being more developed so far [285-288].

## 5. Activated carbon fibers (ACFs) composites for CWAs adsorption and decontamination

Due to their excellent properties of adsorption, non-functionalized ACFs have been mostly applied (and already commercialized) to the capture of CWAs rather than for detoxification. However, the functionalization of ACFs allows the combination of adsorption and detoxification properties. The next section (and Table 2) will therefore describe recent works on porous textile composites containing ACFs against mustard gas and nerve agents (or their simulants) and the results in term of adsorption and detoxification of CWAs, when available.

### 5.1. Mustard gas and its simulant CEES

ACFs efficiency for the protection against HD has been already proved in the literature and they are currently used in several military combinations [10,289]. Studies using bare ACFs suggest that the pore diameter needs to be controlled for optimizing the capture and the immobilization of toxic species [290]. Typically, the highest loading of CEES is obtained for mesoporous over microporous fabrics, with an optimum pore diameter of 2.9 nm [25]. This

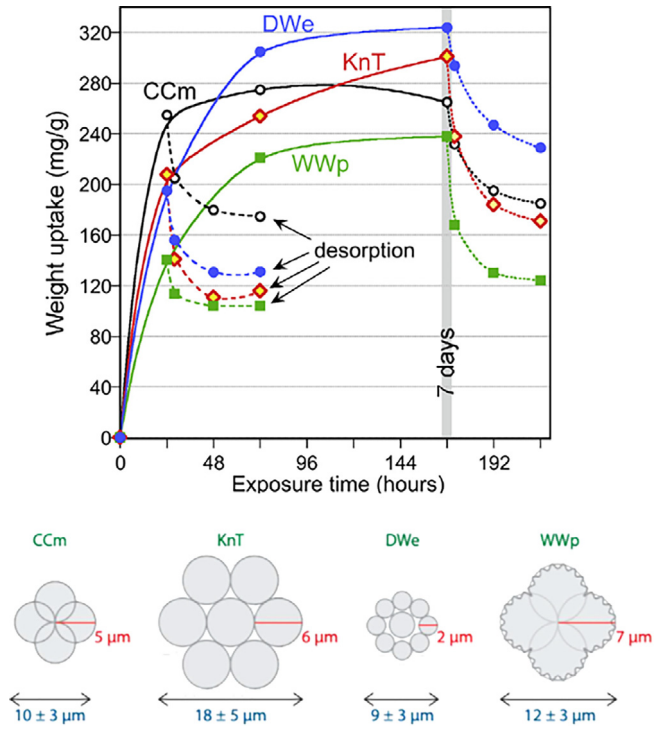


**Fig. 14.** Weight uptake and desorption evolution for 4 ACFs of various structures after exposure to CEES vapors up to 7 days (CCm: Stedcarb without the two outer protective nylon layers, KnT: Knitted ACF, DWe: Double Weave ACF, WWp: From the Oak Ridge National Laboratory. Structures are described in the scheme below the graph) [20]. Reproduced with permission from Elsevier Science & Technology Journal.

selectivity has been assigned to the slowest diffusion of CEES within ACF microporous apertures. A 1-day exposition shows weakly absorbed CEES in the largest pores but longer exposition times let gaseous compounds diffuse into micropores, where CEES is strongly adsorbed [20]. After 7 days, the uptake of CEES reached 324 mg/g, one of the best weight uptakes reported nowadays (Fig. 14).

Whereas the incorporation of reactive agents within ACFs could reduce the accessible specific surface area of the composite, this approach favors the degradation of the targeted species. While such studies are scarce on CWAs, a recent work dealing with the addition of barium titanate perovskite nanospheres on ACFs proved the efficiency of this strategy to detoxify CEES vapor or droplets [291,292]. Products of degradation were analyzed by GC–MS after 7 days of exposure to CEES vapors, showing high concentration of degradation products (acetaldehyde, ethyl vinyl sulfide, isopropanol and diethyl disulfide) which are not formed when using bare ACFs. In addition to the catalytic effect for the degradation of CEES, perovskite NPs enhances the retention of the adsorbed species, since only 14 wt% was released after 48 h of desorption, compared to 30 wt% after 24 h for non-modified ACFs. The other studies on ACFs including reactive species were made using various contents of crystalline MgO or amorphous $Al_2O_3$ NPs embedded in activated carbon fibers [281,282]. Detoxification of CEES was followed by GC giving half-life time between 16 and 78 min. The best result was obtained for a sample with 20 wt% of $Al_2O_3$ NPs due to a higher resulting specific surface area [282]. Unfortunately, no degradation product was mentioned in this last study.

### 5.2. Nerve agent simulants

Like mustard gas and its simulant, the studies involving ACFs versus nerve agent simulants remain focused on their capture (Table 2). To the best of our knowledge, no work about nerve agent detoxification by an ACF composite has been reported in the literature. Pore sizes and surface areas remain the main parameters driving the adsorption of nerve agent simulants [293]. For diisopropylmethyl phosphonate (DIMP), six different ACFs were tested, showing that the higher adsorption capacity was obtained with the solid having the larger micropores (11.6 Å) [290]. Also, a comparative study was carried on the removal efficiency of an ACF and metal-doped (Ag, Cu and Cr) activated carbon materials against DMMP vapor [83]. Better efficiency of the ACF was highlighted, as an adsorption of 0.585 g/g was measured, which is 7.4 times higher than the metal-impregnated activated carbons. Moreover, the authors have shown that the physically absorbed DMMP on the ACF can be totally removed by a short thermal treatment (121 °C, 30 min).

The functionalization of ACFs has been tested to improve the adsorption of nerve agent simulants (*e.g.* DMMP, trimethyl phosphate, . . .). Surface functionalization was studied by comparing trimethyl phosphate sorption efficiency with pristine and ozonized ACF [294]. The higher adsorption and retention measured with the ozonized ACF was associated to important hydrogen bonding between the oxygenated surface of ACF and trimethyl phosphate. Inorganic species such as $SiO_2$ NPs have also been incorporated to ACFs to test the adsorption capacity [278]. An important decrease of the adsorption capacity of DMMP was measured in the presence of $SiO_2$ NPs within the pores: 0.824 g/g of ACF vs 0.219 g/g of ACF-$SiO_2$ NPs. This was explained by the higher hydrophilic capacity on the modified ACF, which leads to an increased adsorption of $H_2O$, instead of DMMP. Recently, UiO-66 and UiO-66-$NH_2$ MOFs deposited on ACF were used to follow the degradation of diisopropylfluorophosphate (DIFP), with respectively 80 and 40 % of detoxification after 24 h [283]. The proposed mechanism was divided in three steps: (1) the strong adsorption of DIFP on the ACF materials, (2) the slow migration of physisorbed DIFP towards MOFs active sites due to desorption and (3) the hydrolysis by the Zr-MOF pore structure.

Table 2 summarizes the discussion above, confirming the predominance of studies on the adsorption of CWAs for ACFs. Functionalization of ACF is still scarce but has confirm its ability to detoxify some simulants. Moreover, the first combination of ACF and MOF is a promising idea to create a new type of protection, mixing the adsorption capacity of ACF and detoxification efficiency of MOF.

## 6. MOFs composites for CWAs

Contrary to ACFs, MOFs deposited on textiles for CWAs capture and/or detoxification is a quite new technology. What makes MOFs so interesting for CWAs detoxification is the combination of very high surface areas for adsorption with a significant catalytic activity brought by the metallic cluster (especially the Zr-based MOFs). Usually with MOFs, the detoxification path and by-products of mustard gas or its simulant, are identified by GC/MS analytical technique. For nerve agents, the presence of phosphorus allows to follow the degradation using $^{31}P$ NMR. UV–Visible spectroscopy can also be used in the case of colored products, such as DMNP and the p-nitrophenoxide. When comparing studies on CWA degrada-

tion, one has to pay attention to the analytical method and the *modus operandi*, since different approaches and additives (*e.g.* co-catalyst) are used in the literature. Next sections present the main results on the capture and/or detoxification of gas mustard or nerve agents (and their simulants) using MOFs deposited on various textile fibers, which are summed up in Tables 3 and 4. For an easier comparison, the analysis method and the addition of the N-ethylmorpholine (NEM) co-catalyst for the degradation of nerve agents have been specified in Table 4.

### 6.1. Mustard gas and simulants

While adsorption studies with ACFs discuss their performances on the basis of their gravimetric uptake, CWAs capture by MOFs are principally evaluated in terms of permeation or breakthrough time $t_B$ (i.e. when the permeation reaches 0.1 μg/(min.cm$^2$)). These two different approaches make difficult the comparison between these two families of materials. With HD, Kim *et al.* used an AVLAG (Aerosol Vapor Liquid Assessment Group) test cell to evaluate the permeation of their cotton/UiO-66-$NH_2$ composite [160]. They showed that the permeation rate of HD was decreased by a factor 10 in the presence of the amino functionalized MOF, passing from 184 μg/cm$^2$ with cotton to 16 μg/cm$^2$ with cotton/UiO-66-$NH_2$. Furthermore, after HD diffusion through the fiber, they were able to detect by GC/MS the formation of thiodiglycol (TDG), proving the hydrolysis of HD. With CEES, following the ASTM F739-12 norm, a breakthrough time ($t_B$) of 50 and 126 min were measured for UiO-66-$NH_2$ and MOF-808 deposited on PET respectively, while PET alone does not provide any protection [246]. Respecting the same standard (Fig. 15.a), a membrane composed of a block copolymer polystyrene-polyisoprene-polystyrene (SIS) was impregnated with various amounts of HKUST-1 (up to 50 wt%) [295]. The increased quantity of HKUST-1 delayed the breakthrough time up to 4000 min (Fig. 15.b). The same experiment was repeated on an aged sample (left 1 day in water), and CEES permeation through the composite was two times faster than prior exposure to water. This loss of efficiency was assigned to the partial MOF hydrolysis. In addition to the great performance of HKUST-1 for CEES capture, this MOF is a good optical detector for sulfur-based species, since the exposition to CEES leads to a color change from blue to yellow-green. This transformation is related to the reduction of copper Cu(II) → Cu(I) from HKUST-1 associated to the oxidation of CEES in sulfoxide or sulfone. Another study on CEES permeation over a HKUST-1 composite (PP/ZnO/HKUST-1) was made but only a steady-state permeation rate of 2.5 μg.cm$^{-2}$.min$^{-1}$ was mentioned [296].

Detoxification of HD (or its simulant) has been assessed using UV–Visible spectrometer, or MS/GC to analyze the degradation products and determine the degradation path (mainly hydrolysis or oxidation). Mustard gas degradation on chitosan fibers decorated with HKUST-1 or silver-doped MOF-5 (Chitosan/MOF-5/Ag) was followed by UV–Vis [236,238]. Excellent decontamination was achieved with both materials, reaching 87.3 % after 30 min for chitosan/HKUST-1 and 90.8 % after 120 min for chitosan/MOF-5/Ag. As discussed before with zeolites (section 2.2.1), the presence of Ag allows an enhancement of the HD uptake due to affinity of S or Cl atoms towards Ag/$Ag_2O$ [238]. In these two studies, the hydrolytic degradation path was deduced from the detection by GC/MS analysis of 2-HEES by-products from the detoxification of CEES. The same degradation path was reported with lithium *tert*-butoxide (LiOtBu)-doped Zr(IV) MOF materials deposited on silk fibroins, with a half-life of CEES of 8 min [297]. However, a surprising low half-life of approximately 75 min was measured for blank without any comments on this value. The analysis method and the solvents used ($H_2O$, EtOH, DMF) being quite standard, such low half-life for a blank could suggested an easy degradation of CEES in the conditions described and have certainly an impact in the degradation kinetic in the presence of MOFs.

When the degradation of CEES is undertaken following the oxidation path instead of hydrolysis (see section 1), a special care is necessary to avoid the formation of toxic 2-chloroethyl ethyl sulfone ($CEESO_2$). To produce solely non-toxic sulfoxide CEESO, a mild oxidant such as singlet oxygens $^1O_2$ need to be generated to favor selective oxidation (Fig. 16.a). The usual method to generate $^1O_2$ is

**Table 3**
HD and CEES adsorption and detoxification using PTC containing MOFs.

| PTC | | | Amount of CWA | Permeation or $t_B$ | Degradation efficiency | | | Degradation path and products | Ref |
|---|---|---|---|---|---|---|---|---|---|
| Composition | Amount or size | SSA (m$^2$/g) | | | Half-life $t_{1/2}$ (minutes) | η (%) | Time (minutes) | | |
| **Sulfur mustard HD** | | | | | | | | | |
| Cotton/UiO-66-$NH_2$ | 4.5 cm diameter | | 4 μL | 16 μg/cm$^2$ | | | | Hydrolysis to TDG | [160] |
| Chitosan/MOF-5(Zn)-Ag | 15 mg | | 4 μL | | 63 | 90.1 | 120 | | [238] |
| Chitosan/$Cu_3(BTC)_2$ | 15 mg | | 4 μL | | | 87.3 | 30 | | [236] |
| PP/PCN-222 | 14 mg | 120 | 0.7 μL | | 720 | 100 | 1440 | | [298] |
| PET/UiO-66-NH-Cl | 1 * 5 cm | | 3.4 μL | | ~ 3 | 80 | 5 | Selective oxidation to sulfoxide HDO | [300] |
| **CEES** | | | | | | | | | |
| PET/UiO-66-NH-Cl | 1 * 5 cm | | 3 μL | | | 99 | 5 | Selective oxidation to CEESO | [300] |
| PP/PCN-222 | 7 mg | 120 | 21.5 μL | | 6 [1] | 100 | 100 | | [298] |
| PP/Al-PMOF | 8.5 mg | 233 | 23 μL | | 4 [1] | ~ 100 | 20 | Selective oxidation to CEESO | [152] |
| Silk fibroins/UiO-66-LiOtBu | 20 mg | 130 | 2.5 μL | | 8 | ~ 100 | 40 | Hydrolysis to ESOH | [297] |
| Chitosan/MOF-5(Zn)-Ag | 20 mg | | 4 μL | | | | | Hydrolysis to 2-HEES | [238] |
| PP/$TiO_2$/MOF-525(Zr) | 14 mg | 104 | 21.5 μL | | | 100 [1] | 70 | | [259] |
| Polyester/MOF-808 | 1 in. diameter | 480 | 300 mg/m$^3$ | $t_B$: 126 min | | | | | [246] |
| Polyester/UiO-66-$NH_2$ | 1 in. diameter | 95 | 300 mg/m$^3$ | $t_B$: 50 min | | | | | [246] |
| SIS/HKUST-1 | 1.5 * 1.5 in. | | Flow rate: 300 mL/min | $t_B$: 67 h | | | | | [295] |
| PP/ZnO/HKUST-1 | 1 in. diameter | | 300 mg/m$^3$ | $t_B$ < 15 min | | | | | [296] |

* TDG: thiodiglycol; HDO: sulfoxide HD; CEESO: 2-chloroethyl ethyl sulfoxide; ESOH and HEES: 2-hydroxy ethyl ethyl sulfide; $t_B$: breakthrough time; SIS: polystyrene-block-polyisoprene-block-polystyrene.
[1] Under blue light irradiation.

**Table 4**
Nerve agents (and their simulants) adsorption and detoxification using porous textile composites containing MOFs.

| PTC | | | Amount of CWA | Permeation or $t_B$ | Analysis method | Degradation efficiency | | | Degradation products | Ref |
|---|---|---|---|---|---|---|---|---|---|---|
| Composition | Amount or size | SSA ($m^2/g$) | | | | Half-life $t_{1/2}$ (minutes) | η (%) | Time (minutes) | | |
| **Soman GD** | | | | | | | | | | |
| Cotton/UiO-66-$NH_2$ | 4.5 cm diameter | | 5 μL | 5 μg/$cm^2$ | | | | | PMPA and MPA | [160] |
| PA-6/$TiO_2$/UiO-66 | 14 mg | 143.9 | 2.6 μL | | $^{31}$P NMR (NEM buffer) | 3 | > 80 | 10 | PMPA | [257] |
| PA-6/$TiO_2$/UiO-66-$NH_2$ | 14 mg | 205.9 | 2.6 μL | | $^{31}$P NMR (NEM buffer) | 3.7 | > 80 | 10 | PMPA | [257] |
| PA-6/$TiO_2$/UiO-67 | 14 mg | 356.2 | 2.6 μL | | $^{31}$P NMR (NEM buffer) | 2.3 | > 80 | 10 | PMPA | [257] |
| Polyester PET/UiO-66-$NH_2$ | 0.5 * 5 mm | 95 | 2.5 μL | | $^{31}$P NMR (NEM buffer) | 8 | ~ 100 | 100 | Hydrolysis | [246] |
| Polyester PET/MOF-808(Zr) | 0.5 * 5 mm | 130 | 2.5 μL | | $^{31}$P NMR (NEM buffer) | 2 | ~ 100 | 20 | Hydrolysis | [246] |
| PS/UiO-66-$NH_2$ | 20 mg | 45 | 2.6 μL | | $^{31}$P NMR (No NEM) | 95 | 100 | 360 | PMPA | [210] |
| PVDF/UiO-66-$NH_2$ | 5 mg (1 $cm^2$) | 225 | 2.6 μL | | $^{31}$P NMR (No NEM) | 131 | | | PMPA | [303] |
| PA-6/UiO-66-$NH_2$ | 10–40 mg | 108 | Unknown amount | | GC/MS (No NEM) | | 65 | 1440 | | [247] |
| PVDF/$Ti(OH)_4$-UiO-66 | 1 * 2 cm | | 2.6 μL | | $^{31}$P NMR (No NEM) | 35 | 100 | 180 | PMPA and MPA | [309] |
| Cotton/MOF-808-PEI | 1 * 1 cm | | 2.4 μL | | $^{31}$P NMR (No NEM) | 12 | 96 | 60 | PMPA and MPA | [302] |
| Cotton/MOF-808/BPEIH | 1*1 cm | 220 | 3 μL | | GC/MS (No NEM) | ~ 10 | ~ 70 | 60 | Hydrolysis | [32] |
| PP/PCN-222 | 14 mg | 120 | 4.5 μL | | $^{31}$P NMR (No NEM) | 620 | 100 | 1700 | | [298] |
| PP/$TiO_2$/UiO-66-$NH_2$ | 1 $cm^2$ | | 3 μL | | $^{31}$P NMR (No NEM) | 177 | 100 | 600 | PMPA | [304] |
| **VX** | | | | | | | | | | |
| Cotton/MOF-808-PEI | 1 * 1 cm | | 2.4 μL | | $^{31}$P NMR (No NEM) | | 100 | 60 | EMPA and DESH | [302] |
| Cotton/MOF-808/BPEIH | 1*1 cm | 220 | 3 μL | | GC/MS (No NEM) | ~ 5 | > 90 | 10 | Hydrolysis | [32] |
| Cotton/MOF-808/DTNB | 1*1 cm | | 25 mM | | $^{31}$P NMR and LC/MS (MOPS buffer sol.) | 6 | > 90 | 30 | Hydrolysis | [310] |
| **Simulant DMNP** | | | | | | | | | | |
| Cotton/MOF-808(Zr)-PEI | 1 * 1 cm | | 4 μL | | $^{31}$P NMR (No NEM) | 24 | 100 | 240 | DMP | [302] |
| Cotton/MOF-808/BPEI | 1 * 1 cm | 220 | 4 μL | | $^{31}$P NMR (No NEM) | 1 | 99 | 15 | 4-NP | [32] |
| PP/PCN-222 | 14 mg | 120 | 4 μL | | UV–Vis (NEM buffer sol.) | 6 [1] | 100 | 90 | | [298] |
| PP/$TiO_2$/UiO-66-$NH_2$ | 14 mg | | 6.2 mg | | UV–Vis (NEM buffer sol.) | 4.9 | | | 4-NP | [304] |
| Polyester PET/ MOF-808 | 0.5 * 5 mm | 130 | 4 μL | | $^{31}$P NMR (NEM buffer) | > 0.5 | 100 | 1.5 | DMP | [246] |
| Polyester PET/ UiO-66-$NH_2$ | 0.5 * 5 mm | 95 | 4 μL | | $^{31}$P NMR (NEM buffer) | 5 | 100 | 15 | DMP | [246] |
| Cotton/UiO-66-$NH_2$ | | 125 | 4.5 μL | | UV–Vis (NEM buffer sol.) | ~ 50 | ~ 60 | 90 | 4-NP | [163] |
| PA-6/$TiO_2$/UiO-66 | 14 mg | 143.9 | 4 μL | | UV–Vis (NEM buffer sol.) | 135 | | | 4-NP | [257] |
| PA-6/$TiO_2$/UiO-66-$NH_2$ | 14 mg | 205.9 | 4 μL | | UV–Vis (NEM buffer sol.) | 7.3 | > 90 | 60 | 4-NP | [257] |
| PA-6/$TiO_2$/UiO-67 | 14 mg | 356.2 | 4 μL | | UV–Vis (NEM buffer sol.) | 7.4 | > 90 | 60 | 4-NP | [257] |
| PA-6/PDA/UiO-66-$NH_2$ | 17.6 mg | 270 | 4 μL | | UV–Vis (NEM buffer sol.) | 0.5 [2] | > 95 | 3 [2] | 4-NP | [251] |
| PA-6/UiO-66-$NH_2$ | 14 mg | 280 | 4 μL | | UV–Vis (NEM buffer sol.) | 7.4 | | | | [247] |
| PVDF/UiO-66-$NH_2$ | 12 mg | 225 | 4 μL | | UV–Vis (NEM buffer sol.) | 12 | ~ 70 | 30 | 4-NP | [303] |
| PMMA/$Ti(OH)_4$ /$TiO_2$/UiO-66-$NH_2$ | 12 mg | 264 | 4 μL | | UV–Vis (NEM buffer sol.) | 26 | ~ 90 | 120 | 4-NP | [307] |
| PMMA/$Ti(OH)_4$/UiO-66 | 3 mg | 185 | 4 μL | | UV–Vis (NEM buffer sol.) | 29 | 94 | 120 | 4-NP | [308] |
| PP/ZnO/UiO-66-$NH_2$ | 17.6 mg | 211 | 6.2 mg | | UV–Vis (NEM buffer sol.) | 2.8 | > 95 | 90 | 4-NP | [258] |
| PP/$TiO_2$/MOF-525(Zr) | 14 mg | 104 | 4 μL | | UV–Vis (NEM buffer sol.) | ~ 80 | ~ 65 | 120 | 4-NP | [259] |
| PP/ZnO/UiO-66-$NH_2$ | 14 mg | 145 | 6.2 mg | | UV–Vis (NEM buffer sol.) | 10 | 90 | 60 | 4-NP | [253] |
| Graphene oxide/UiO-66-$NH_2$ | 20 mg | 305 | 4 μL | | UV–Vis (NEM buffer sol.) | 1.6 [3] | > 99 | 30 [3] | DMP and 4-NP | [244] |
| Cotton/UiO-66-$NH_2$ | | 58 | Unknown amount | | UV–Vis (NEM buffer sol.) | 4 | | | 4-NP | [224] |
| PAN/PDA/UiO-66-$NH_2$ | 12 mg | 254 | 4 μL | 79.9 mg/g | UV–Vis (NEM buffer sol.) | 1.8 min [4] | 100 | 30 [4] | 4-NP | [306] |
| PIM/PAN/UiO-66-$NH_2$ | 15–18 mg | 574 | 4 μL | | UV–Vis (NEM buffer sol.) | ~ 45 | 70 | 140 | 4-NP | [128] |
| PA-66/UiO-66-$NH_2$ | 3 +/- 0.2 mg | 107 | 25 mM | | UV–Vis (NEM buffer sol.) | Hydrolysis rate: ~ 35 mM/sec x$10^6$ | | | 4-NP | [252] |
| Nyco/UiO-66-NCS-PTU | | ~ 0 | 10 μL | | UV–Vis (NEM buffer sol.) | Hydrolysis rate: 320 mM/sec x$10^{-6}$ | | | | [240] |
| PUU/UiO-66 | 12 * 8 mm | 8.7 | 20 μL | | UV–Vis (NEM buffer sol.) | Hydrolysis rate 4.8 mM.$sec^{-1}$.$mg^{-1}$ × $10^{-6}$ | | | 4-NP | [191] |

(*continued on next page*)

**Table 4** (*continued*)

| PTC | | | Amount of CWA | Permeation or $t_B$ | Analysis method | Degradation efficiency | | | Degradation products | Ref |
|---|---|---|---|---|---|---|---|---|---|---|
| Composition | Amount or size | SSA ($m^2/g$) | | | | Half-life $t_{1/2}$ (minutes) | η (%) | Time (minutes) | | |
| PUU/UiO-66-$NH_2$ | 12 * 8 mm | | 20 µL | | UV–Vis (NEM buffer sol.) | Hydrolysis rate 19.5 $mM.sec^{-1}.mg^{-1} \times 10^{-6}$ | | | 4-NP | [191] |
| PVDF/Ti(OH)$_4$–UiO-66/TEA | 12 mg | | 4 µL | | UV–Vis (NEM buffer sol.) | | ~ 40 | 120 | 4-NP | [309] |
| **Other nerve agent simulants** | | | | | | | | | | |
| Cotton/MOF-808/BPEI | 1 * 1 cm | 220 | DEMP (4.2 µL) | | $^{31}$P NMR (No NEM) | < 1 | 100 | 10 | Hydrolysis EMPA | [32] |
| PVDF/Ti(OH)$_4$–UiO-66/TEA | 1 $cm^2$ | | DFP (1 µL) | | $^{31}$P NMR (No NEM) | 744 | | | IDP and DP | [309] |
| ACF/UiO-66 | 40 mg | 840 | DIFP (1.25 µL) | | GC (No NEM) | ~ 240 | 80 | 1440 | Hydrolysis | [283] |
| ACF/UiO-66-$NH_2$ | 40 mg | 745 | DIFP (1.25 µL) | | GC (No NEM) | | 40 | 1440 | Hydrolysis | [283] |
| Silk fibroins/UiO-66-LiOtBu | 20 mg | 130 | DIFP (2.5 µL) | | GC and $^{31}$P NMR (No NEM) | 20 | | | Hydrolysis | [297] |
| Silk fibroins/UiO-66-LiOtBu | 20 mg | 130 | DMMP (2.5 µL) | | GC and $^{31}$P NMR (No NEM) | 50 | | | Hydrolysis | [297] |
| Cotton/HKUST-1-g-$C_3N_4$ | 20 mg | | DMCP (40 µL) | 6.7 g/g of Cu after 192 h | | | | | DMP | [221] |

* PDA: Polydopamine; Nyco: Nylon and cotton blend; NCS: isothiocyanate; PTU: Polythiourea; PUU: poly (urethane urea); PEI: Polyethylenimine; BPEIH: Branched polyethylenimine hydrogel; DEMP: O,S-diethyl methylphosphonothioate; DMCP: Dimethyl Chlorophosphonate; PMPA: Pinacolyl Methylphosphonic Acid; MPA: Methylphosphonic Acid; EMPA: Ethyl Methyl Phosphonic Acid; DESH: 2-(Diisopropylamino)Ethanethiol; DMP: Dimethyl Phosphate; 4-NP: p-Nitrophenoxide; IDP: Isopropyl Dihydrogen Phosphate; DP: Diisopropylphosphate; DTNB: ditopic 5,5-dithiobis(2-nitrobenzoic acid); MOPS: morpholinopropylsulfonic acid.

[1] Under blue light irradiation.
[2] Under simulated solar light irradiation.
[3] Under solar light irradiation.
[4] Under near-infrared light irradiation.

the use of using photosensitizers such as porphyrins [24,298]. These groups can be integrated to MOFs as the organic linker [23,151] or by post-synthetic modification [299]. In the case of MOF-PTC, an Al-porphyrin-based MOF on polypropylene was prepared and the photocatalytic properties of the ligand was used to generate $^1O_2$. A short half-life of 4 min was obtained for CEES degradation under blue LED irradiation and CEESO was the only product detected (Fig. 16 b and c) [152]. The same porphyrin linker was used to synthetize Zr-based PCN-222 attached on polypropylene fibers, tested for sulfur-based agents (HD, CEES) detoxification [298]. For theses toxics, blue light irradiation induces higher degradation rates, passing from 35 % degradation in dark to 100 % after 24 h for HD, and <10 % to 100 % degradation under irradiation for CEES after 100 min. Recently, a new method for the selective oxidation of HD and CEES was proposed by using haloamine groups, which are known to be efficient oxidants for sulfur-containing compounds [300]. With the formation of UiO-66-NH-Cl on polyethylene terephthalate fibers, half-life under 3 min were noted for both CEES and HD, and the unique products detected were the sulfoxide ones.

According to the data sum up in Table 3, the higher degradation efficiency against both HD and CEES has been obtained by oxidative detoxification using a UiO-66-NH-Cl composite, with impressive half-life under 5 min. Concerning the permeation, the combination of block copolymer polystyrene-polyisoprene-poly styrene SIS and HKUST-1 gave the best protection with a breakthrough time of 67 h.

### 6.2. Nerve agents and simulants

Farha *et coll.* proposed that the hydrolytic pathway is the most suited route to detoxify efficiently organophosphorus compounds. Efficiency of materials relies to different steps (Fig. 17) [12]. First, the toxic organophosphorus species is coordinated to an open metal site and its hydrolysis is possible thanks to a nearby water molecules adsorbed on the terminal hydroxyl group. After this step, the addition of a basic agents is needed to release the coordinated phosphorous species. In this case, the basic function acts as a co-catalyst removing acidic by-products connected to the metallic center and regenerating the MOF catalyst. The positive effect of basic species or basic chemical groups was already mentioned for other family of materials [3].

In the case of Zr(IV) based MOFs, the very strong Lewis acidity associated to the inorganic cation makes this family of stable MOFs very attractive for nerve agents detoxification. This efficiency is reinforced by their functionalization with amine groups (Brönsted base), connected to the ligand or adsorbed at the MOF surface.

However, to further optimize the detoxification of organophosphorus compounds, the addition of an additional base as a co-catalyst has been largely developed [32,297,301]. The most famous one is the N-ethylmorpholine (NEM), based on the protocol proposed by Fahra *et coll.* in 2014 for DMNP degradation [142]. In this case, NEM buffer solution is added to a suspension containing the MOF phase and DMNP, and the reaction is monitored by UV–Vis spectroscopy (evolution of p-nitrophenoxide absorbance band at 407 nm). Nevertheless, while the addition of NEM is feasible in solution for tests, it is impossible to integrate this volatile and toxic molecule into protective garments. To bypass this difficulty, several studies are currently in progress, such as mixing basic polymers like polyethylenimine (PEI), poly(amidoamine) dendrimer (PAMAM) or lithium alkoxide directly with the MOF-textile composite [297,301,302]. The comparison of experiments done with or without a co-catalyst is very difficult, as a same MOF could have a high variation of efficiency depending on the presence of a co-catalyst. Therefore, for an easier comparison, this section has been divided into three subparts, i.e. the first describes the results

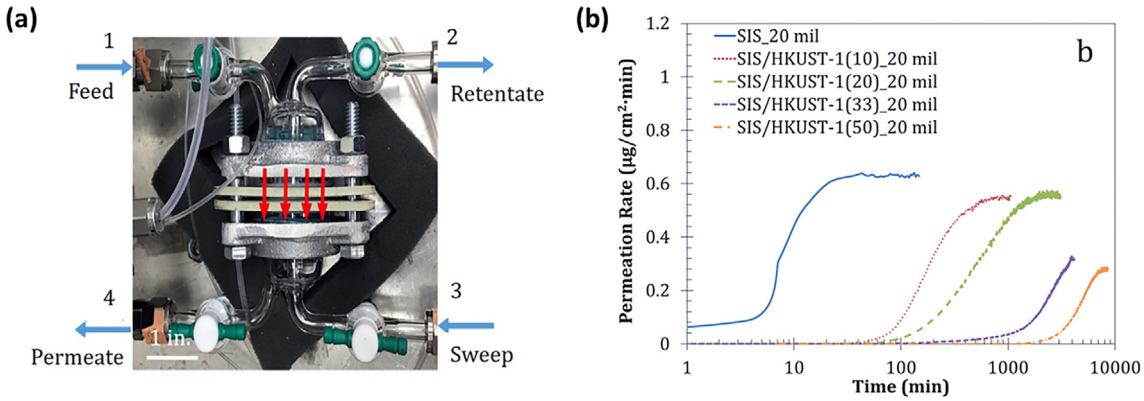


**Fig. 15.** (a) Photograph of a permeation test cell and (b) CEES permeation on block copolymer polystyrene-polyisoprene-polystyrene SIS/HKUST-1 membranes [295]. Reproduced with permission from the American Chemical Society.

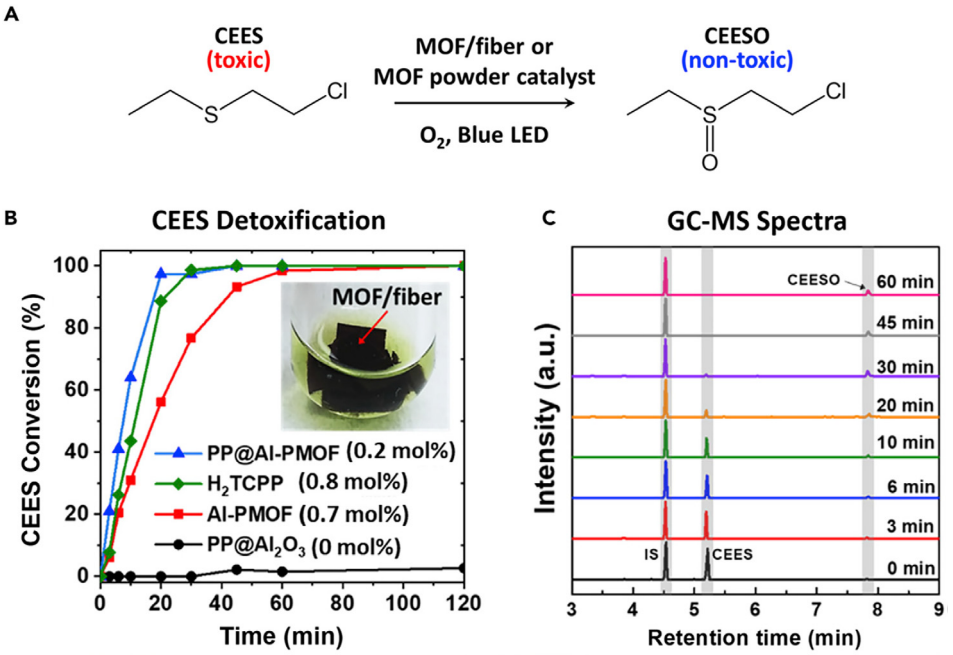


**Fig. 16.** (a) Scheme of selective photo-oxidative degradation of CEES, (b) CEES conversion to CEESO over time under blue LED irradiation, (c) GC–MS spectrums of CEES degradation over time [152]. Reproduced with permission from Elsevier Science & Technology Journal. (For interpretation of the references to color in this figure legend, the reader is referred to the web version of this article.)

obtained without the use of a co-catalyst, the second with the use of NEM, and the last subpart details the use of other co-catalysts.

*6.2.1. Detoxification without co-catalyst*

Without co-catalyst, the use of MOFs and textiles against nerve agents have been focused on the GD detoxification [160,210,247,298,303,304]. Using polyvinylidene fluoride PVDF/UiO-66-$NH_2$ composite fabrics with a loading of 33 wt% of MOF, a half-life of 131 min was measured [303]. GD degradation produces pinacolyl methylphosphonic acid (PMPA) via P-F bond cleavage while no methylphosphonic acid was detected (Fig. 3). A similar composite based on the combination of polystyrene (PS) and UiO-66-$NH_2$ (PS/UiO-66-$NH_2$) was used and GD half-life decreased to 95 min [210]. According to several studies, the contribution of fibers in CWA detoxification is minor [246,252,253,258]. Therefore, a possible reason for this faster reaction could be the largest amount of composite used in the system (5 mg vs 20 mg), while the loading of MOF and the amount of Soman remained similar. Furthermore, these two studies highlighted that the most relevant parameter for GD removal is the homogeneous dispersion of MOF to assure good accessibility. Other parameters analyzed in these works, such as MOFs loading, its localization (in or at the surface of the fibers) or the diameter of the fibers have less impact on the removal efficiency. In comparison, GD detoxification has been tested by a similar process with PCN-222, a zirconium-porphyrin based MOF, deposited on PP and a related half-life of 710 min was monitored [298]. This difference could be due to the utilization of a larger and more hydrophobic linker (5,10,15,20-tetrakis(4-carboxyphenyl) porphyrin) compared to UiO-66-$NH_2$. Another long degradation time was measured using a polyamide PA/UiO-66-$NH_2$ sample, with 65 % GD degradation after 24 h, despite reasonable MOF content (~10 wt%) and specific surface area (108 $m^2$/g) [247]. Recently, a PP/$TiO_2$/UiO-66-$NH_2$ was used to study GD diffusion and degradation, but also the breathability capacity of the

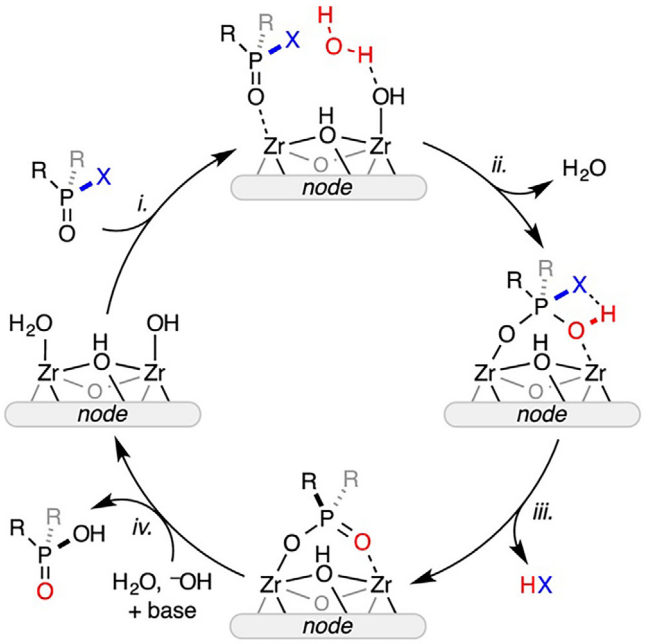


**Fig. 17.** Proposed mechanism of organophosphorus compounds hydrolysis [12]. (i) Coordination of the organophosphorus species to the open metal site; (ii) nucleophile reaction of the hydroxyl group on the phosphorous compound; (iii) departure of a HX leaving group; (iv) departure of the hydrolyzed organophosphorus species. Reproduced with permission from the American Chemical Society.

composite [304]. It showed a good detoxification capacity with a half-life of 177 min while keeping a high moisture vapor transport rate (MVTR, 15600 $g.m^{-2}.day^{-1}$) and impeding GD diffusion through the material. The vapor adsorption and degradation of GD has also been studied on a cotton fabric functionalized with UiO-66-$NH_2$ using a specific AVLAG cell [160]. The addition of UiO-66-$NH_2$ on cotton decreases by a factor 20 the permeation of the fabric towards GD (120 $\mu g.cm^{-2}$ vs 5 $\mu g.cm^{-2}$), and GC–MS analysis confirmed the catalytic activity of the MOF with the formation of pinacolyl methylphosphonic acid and methylphosphonic acid.

*6.2.2. Detoxification in the presence of NEM:*

To understand the effect of NEM, Zr-based MOFs (UiO-66, UiO-66-$NH_2$ and NU-1000) were tested for DMNP detoxification in pure water or in NEM solution (0.45 M) [244,257,304,305]. While the determined degradation was below 50 % after 24 h in pure water, UiO-66-$NH_2$ and NU-1000 presented half-life under 10 min in presence of NEM [305]. The same tendency was observed on graphene fibers with UiO-66-$NH_2$, where the increase of NEM concentration from 0 to 0.45 M enhances the conversion rate from 49.1 to 99.5 % (Fig. 18) [244]. Another work aiming to detoxify GD has shown that its half-life shifted from 4 min with NEM to>300 min without it using PA/$TiO_2$/Zr-MOF (UiO-66, UiO-66-$NH_2$ or UiO-67) composites [257]. According to these studies, NEM allows an easier hydrolysis by deprotonating water and neutralizing acidic by-products, which could poison the MOF catalytic sites [244,257,305].

Owing to the use of NEM, the first half-life under 10 min for GD on composite textiles was reported by Zhao *et al.* in 2016 [257]. A polyamide-6 was first coated by $TiO_2$ through the atomic layer deposition (ALD) method. A Zr-MOF (UiO-66, UiO-66-$NH_2$ or UiO-67) was deposited subsequently using a classical solvothermal method, with resulting mass loadings between 8.8 and 15.4 wt%.

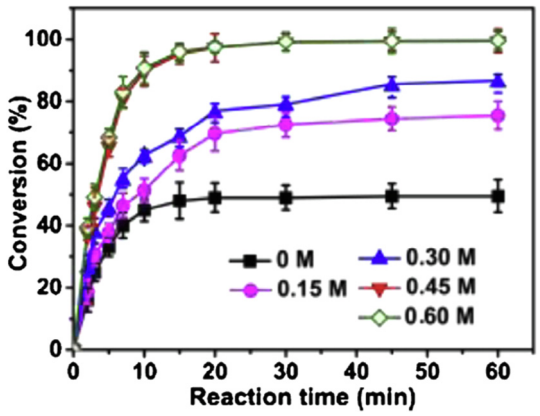


**Fig. 18.** Effect of the concentration of the N-ethylmorpholine (NEM) buffer solution on the conversion rate of DMNP [244]. Reproduced with permission from Elsevier.

These three composites gave respectively half-lives of 3.0 min, 3.7 min and 2.3 min and more than 80 % conversion within 10 min. The fastest reaction with UiO-67 was explained by the larger pores size of this solid (up to 17 Å) allowing faster diffusion of the reactants through the porosity. To date, the most efficient composite against GD was prepared by Ma *et al.* in 2019: PET/MOF-808 composites with 6.5 wt% of MOF, which gave a half-life of 2 min (Fig. 19) [246]. Compared to UiO-66-$NH_2$, this higher catalytic activity has been attributed to a large pore size (4.8 and 18 Å diameter) associated to the lower connectivity on the Zr site (6-connected vs 12-connected for UiO-66).

Concerning the DMNP detoxification (Fig. 20.a), a majority of porous textile composites containing MOFs are focused on the use of the UiO-66 family and particularly UiO-66-$NH_2$, which has shown high efficiency in numerous studies, with half-lives generally under 30 min (Table 4) [149,163,191,224,244,246,247,251-253,257,258,283,303,304,306-308]. This high activity has been linked to the amine moiety of UiO-66-$NH_2$, since the basicity of this function enhances the catalytic activity by transferring protons during the catalytic reaction [306]. This effect was clearly proved by Shen *et al.* who have shown that the conversion rate of DMNP is divided by a factor 20 using UiO-66 instead of UiO-66-$NH_2$ [149].

High degradation efficiencies towards DMNP (i.e. half-lives under 10 min) with UiO-66-$NH_2$ composites were obtained either using the photothermal effect [244,251,306], some specific synthesis deposition [224,246,247] or by adding an intermediate ALD layer between the fiber and the MOF [253,257,258,304]. The photothermal method converts photon into heat thanks to photothermal agents such as polydopamine (PDA) or graphene. It promotes efficient collisions of molecules and mass transfer, especially within the porosity of MOFs. For instance, PDA deposited as an intermediate layer between the fiber (PA or PAN) and UiO-66-$NH_2$ was used as a photothermal agent [251]. Under room light, DMNP half-life is 4 min, while simulated solar light (SSL, 0.6 $W.cm^{-2}$) decreases the half-life to 0.5 min due to heat transfer from PDA to UiO-66-$NH_2$ (Fig. 20). Graphene oxide fibers were also used as a photothermal agent with UiO-66-$NH_2$, showing half-lives of 3.4 and 1.6 min without irradiation and under SSL, respectively [244]. Concerning the high efficiency of composites containing an oxide-based layer formed by atomic layer deposition (ALD), the nucleation and rapid growth of accessible MOFs was the proposed explanation [253,257,258]. Indeed, in these last articles, the MOF contents typically found in the literature (15 wt% to 30 wt%) cannot explain the high DMNP degradation. Apart from these photothermal and ALD methods, a few innovative chemical depositions of UiO-66-$NH_2$ have shown exceptional DMNP degradation efficiency. Bunge *et al.* achieved an impressive half-life of 4 min with an ionic liquid welding deposition technique on cotton

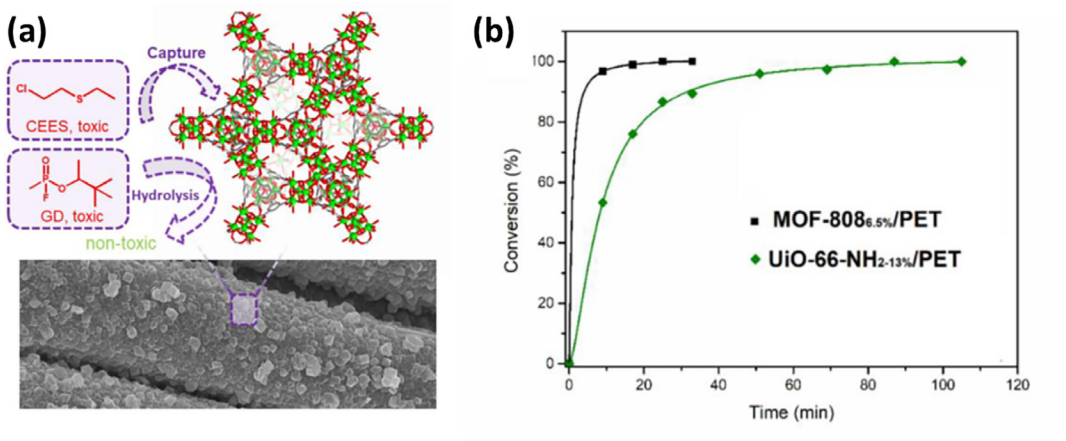


**Fig. 19.** (a) Scheme of CWA degradation by MOF-Fiber with SEM image of the corresponding MOF-PET Fiber and (b) catalytic degradation of GD using MOF-coated fibers [246]. Reproduced with permission from the American Chemical Society.

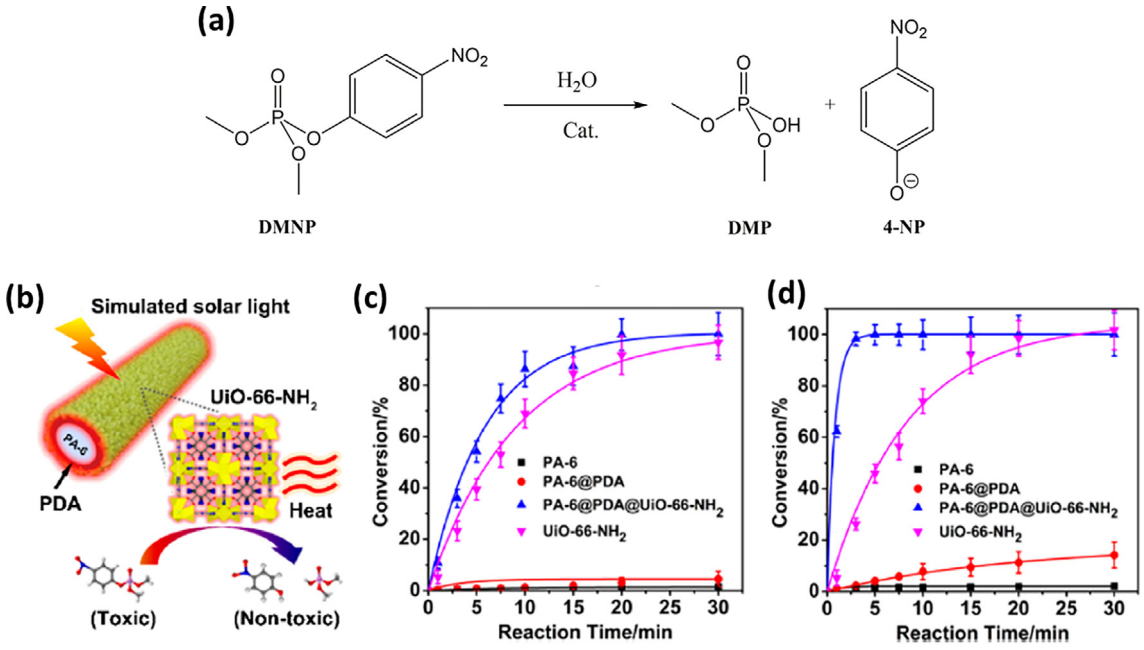


**Fig. 20.** (a) Degradation pathway of DMNP (b) Schematic illustration of the PTC and photo-degradation reaction of DMNP, (c) conversion rate under room light and (d) simulated solar light [251]. Reproduced with permission from the American Chemical Society.

[224]. In another study, trifluoroacetic acid was used as a modulator for a uniform coverage of Zr-MOF (MOF-808 and UiO-66-$NH_2$) on the fiber, giving a half-life under 0.5 min for MOF-808 and of 5 min for UiO-66-$NH_2$ [246]. Finally, a sorption-vapor synthesis of PA/UiO-66-$NH_2$ led to a fast degradation of DMNP as well, with a 7.4 min half-life [247].

Apart from the UiO-n family, some other Zr-MOFs have been studied for an integration in protective garments, like MOF-808, PCN-222 and MOF-525 [246,259,298]. This latter does not present much interest, as the best half-life against DMNP obtained is 80 min [259]. Thanks to a porphyrin linker, PCN-222 deposited on polypropylene fabrics have shown photocatalytic activity against DMNP for the first time, with a decreased half-life from 22 to 6 min under blue light irradiation [298]. This result is close to the best DMNP half-life obtained with a porous textile composites containing non-photoactive MOF, making photo-hydrolysis an interesting path for future research. So far, the fastest degradation rate towards DMNP was recorded with MOF-808 deposited on polyethylene terephthalate (PET), with an impressing half-life under 0.5 min and full degradation after 1.5 min [246].

Interestingly, some studies compared the degradation efficiency of a same composite on DMNP and on Soman GD [246,247,257,303,309]. Some of them have shown a higher activity against GD than DMNP, like PA/$TiO_2$/UiO-66-$NH_2$, where a decrease from 7.3 min (DMNP) to 2.3 min (GD) was noted [257] or with PVDF/$Ti(OH)_4$/UiO-66 sample with a shift from 151 min for DMNP to 35 min for GD [309]. However, an opposite trend was noted with others. PVDF/UiO-66-$NH_2$ presented an increased half-life from 12 min for DMNP to 131 min for GD [303]. The same behavior was observed on PET/MOF-808 and PET/UiO-66-$NH_2$, with half-lives remaining under 10 min [246]. A PA-6/UiO-66-$NH_2$ showed an increase from 7.4 min for DMNP to more than15 h for GD [247]. To these days, no clear explanation was proposed to explain this difference of behavior between DMNP and GD

on these close composites. The difference of analytical technique (UV–Vis or $^{31}$P NMR, done with or without NEM) is insufficient to propose a satisfying explication.

As it seems impossible to predict which type of CWA might be used, a few MOF-based PTC have been tested for their dual function, i.e. the capacity to detoxify both nerve agents and sulfur mustard agents [11,259,297,298]. The first study was done in 2015 on a UiO-66/Li*O*tBu deposited on silk, with hydrolysis half-lives for CEES, DMMP and DIFP of 8, 50 and 20 min, respectively [297]. A PP/$TiO_2$/MOF-525 showed also higher activity against CEES than the nerve agent simulant, with a full degradation of CEES in 70 min while DMNP half-life was 80 min [259]. Finally, a PP/PCN-222 was tested against a larger variety of CWAs (GD, HD) and simulants (DMNP, CEES) [298]. While the degradation of simulants showed good results (half-lives under 30 min), the degradation of CWA remains slow (half-lives of 620 and 720 min for GD and HD, respectively).

*6.2.3. Detoxification with a co-catalyst (different from NEM):*

Analyses involving aqueous NEM solution highlighted the importance of the presence of a base to enhance the catalytic activity of MOFs for nerve agent detoxification. In the same idea, a similar compound to NEM was tested recently, the morpholinopropylsulfonic acid (MOPS) for the sensing and detoxification of VX [310]. The reaction of VX on a cotton/MOF-808/DTNB (5,5-dithiobis(2-nitrobenzoic acid)) showed an efficient hydrolysis of VX with $t_{1/2}$ of 6 min but also a color change from white to orange with VX amounts down to 2.5 µg. However, in the case of protective garments, the direct integration of basic species with the MOF-textile is mandatory for an efficient use. To replace NEM, investigations have been focused on amines with a lower vapor pressure than NEM such as polyethyleimine (PEI, linear or branched), poly(amidoamine) (PAMAM) dendrimers, triethanolamine (TEA) or imidazole compounds [301,309,311,312]. Among those, PEI and TEA have already been integrated to MOF-textile composites and tested for nerve agent detoxification. Thanks to its viscosity compatible with the electrospinning process and a pKa close to that of NEM, TEA was integrated to PVDF/Ti$(OH)_4$/UiO-66 electrospun fibers [309]. However, TEA gave mitigated performances, as it allows to decrease the half-life of DMNP (from 151 min to 89 min), but it increases the one of GD (from 35 min to 47 min) and di-isopropyl fluorophosphate (DFP) shows no degradation up to 12.4 h. Comparing DFP and GD, the authors hypothesized that TEA can potentially lower the activation barrier of the DFP reaction, while GD possess already a low barrier energy. Concerning polyethyleimine addition, a composite MOF-808/PEI deposited on cotton showed exceptional detoxification of DMNP ($t_{1/2}$ = 24 min, vs 24 h without PEI), GD and VX (completely hydrolyzed in 1 h) [302]. With a half-life of 12 min for GD, this composite possesses one of the best detoxification efficiencies ever reported. A similar composite was prepared by immerging cotton in a MOF-808 and branched polyethyleimine hydrogel (BPEIH) solution [32]. The latter presents the significant advantage of combining a high amine density with an abundant supply of water. This cotton/MOF-808/BPEIH showed impressive detoxification efficiency against nerve agents ($t_{1/2}$ under 10 min for GD and VX) and its simulants ($t_{1/2}$ under 1 min DMNP and DEMP). These exceptional results were linked to the presence of the three components required for hydrolysis of nerve agent, namely acid Lewis sites (from MOF-808), a base (PEI) for the catalyst regeneration and water (from hydrogel) to facilitate hydrolysis (Fig. 17). Apart from amine species, highly basic lithium alkoxide Li$O^t$Bu have been integrated in UiO-66 MOF by photosynthetic modification [313] and deposited on silk fibroins fabrics [297]. The composite showed high efficiency with half-life of 20 min for DIFP and 50 min for DMMP, due to a synergic combination of alkoxide basicity (LiOtBu) and acidic Zr metal center.

Enhancement of nerve agent detoxification have also been reported thanks to photoactivity without NEM. With porphyrin-based PCN-222, GD degradation was slightly higher under light exposition (45 % vs 60 % approximately after 12 h), and the half-life remains long (610 min) compared to those discussed above [298]. Graphitic carbon nitride oxidized has also exhibited consequent photoreactive activity when associated to cotton/HKUST-1 fiber [221]. This composite was utilized for dimetyl chlorophosphate (DMCP) detection, capture and detoxification. The color change of the composite from blue-green to yellow-orange after contact with dimetyl chlorophosphate, was linked to the formation of new Cu-Cl bonds and allowed to monitor the simulant decomposition, as well as the exhaustion level of the protective media (Fig. 21). An important adsorption was measured, with a weight uptake of almost 7 g of dimetyl chlorophosphate per gram of Cu after 192 h of exposure time. Furthermore, the presence of photoactive graphitic carbon nitride oxidized promotes the methanolysis by forming methanol and $H_3PO_4$ by-products.

The recyclability and reusability of the composites have been rarely investigated in the literature. Besides the detoxification efficiency, other aspects of protective garments are important to consider for their wearing in real life conditions, like the good adhesion of the active species to the textiles or the structural stability and reusability of the composite. According to the literature, various methods were explored. In the case of adhesion control, a composite was stirred in ethanol for 24 h and no mass loss was detected [258]. Tape tests and scratching with a spatula were also used on a UiO-66-NCS (isothiocyanate)-PTU (polythiourea) deposited on Nyco, with no significant loss [240]. However, the same tests conducted without polythiourea or without -NCS function showed an abundant loss of MOF. Durability was also tested by washing the composite with water and soap for 3 h at room temperature to mimic laundry conditions. No structural modification or loss of activity against DMNP were measured, highlighting the stability of the overall composite. About long-term stability of the composites, a PA-6/UiO-66-$NH_2$ was kept 9 months in lab air [247]. No significant difference in terms of GD detoxification was noted, highlighting its good stability towards moisture and air. Finally, a larger study was conducted on a cotton/MOF-808/BPEIH to evaluate its tolerance versus time (3 months), humidity, atmospheric $CO_2$, organic contaminant (octane) and sweat [32]. The catalytic activity remains almost unchanged after these various treatments, denoting the high stability of this composite (Fig. 22).

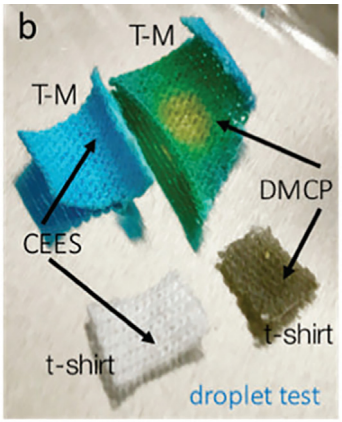


**Fig. 21.** Direct exposure of cotton/HKUST-1 (T-M) to CEES and dimetyl chlorophosphate (DMCP) droplets (4 µL) [221]. Reproduced with permission from the Royal Society of Chemistry.

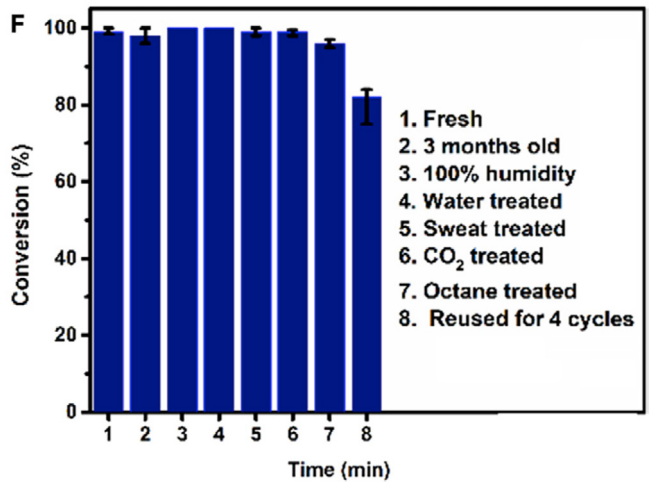


**Fig. 22.** DMNP conversion of cotton/MOF-808/BPEIH after various stability tests (reaction time: 15 min) [32]. Reproduced with permission from Elsevier Science & Technology Journal.

To test the reusability of a composite, cycles of DMNP detoxification (4–5 times) were separated by a washing step (usually in buffer solution or ethanol) between each cycle. A loss of activity was noted on PA-6/$TiO_2$/UiO-66-$NH_2$, where the half-life of DMNP shift from 7.3 min to 96.3 min after 3 cycles [257]. This drastic loss of catalytic efficiency was associated to potential secondary contamination during regeneration from unidentified species. A declining activity was also observed on a PAN/DPA/UiO-66-$NH_2$ composite, varying from 80% degradation of DMNP to 55% after 5 cycles [306]. In contrast, a stable activity after 4 to 5 cycles has been measured on a graphene/UiO-66-$NH_2$ and a PA-66/UiO-66-$NH_2$ composites [244,252].

Table 4 highlights the use of Zr-based MOF in porous textile composites, especially those incorporating UiO-66-$NH_2$ and MOF-808 which gave the best results in term of nerve agent decontamination. Researches of these last years showed the need for a co-catalyst integrable in the MOF-textile composite, such as polyethyleimine or lithium alkoxide, to strongly detoxify nerve agents. Nowadays, the next challenges for MOF-based PTC are long term efficiency and large-scale production.

## 7. Other porous textile composites for CWAs degradation

Despite the existence of various porous catalytic materials other than MOFs or ACFs with interesting results in terms of adsorption or detoxification of CWAs (zeolites, aerogels, etc. - see section 2.2.), their incorporation in textiles has not been largely developed. Only a few of them have been added in PTC (Table 5).

Hydrogen-bonded Organic Framework HOF-102 with 1,3,6,8-tetra(6-carboxynaphthalen-2-yl) pyrene ($H_4$TNAPy) linker supported on cotton, was deposited by simple dropcast approach prior to solvent evaporation [150]. Using the pyrene chromophore trapped within the porous structure, the composite HOF-102/cotton was used as a photocatalyst for CEES degradation. Full and selective conversion of CEES to CEESO was done in 30 min, and the composite maintained its stability after 3 cycles. For nerve agent simulants degradation, a PIM-1 (Polymer of Intrinsic Microporosity) with amidoxime groups was electrospun and tested against DMNP, in a basic borate-based buffer solution [130]. After 48 h, an 84 % degradation was measured with the formation of methyl 4-nitrophenyl phosphate (M4NP) mostly. Concerning zeolite compounds, to the best of our knowledge, only two articles in the literature mention the use of this family of microporous materials grafted on textiles for CWA decontamination. Satya *et al.* described the fabrication of cellulose/PET nanofibers coated with zeolites LTA and Mordenite by electrospray [223]. Unfortunately, almost no details were given on the detoxification of paraoxon.

The other study combining zeolites and fibers concerns the efficiency of an organic/inorganic barrier composed of an ionic liquid polymer (poly[1-(2,3-dihydroxypropyl)-3- vinylimidazolium bis(trifluoro-methanesulfon-imide)]), blended with NaY zeolite. This composite was tested for blocking the passage of CEES, while allowing the transport of water vapor [314]. A 22 h protection from CEES penetration was measured, with a high-water vapor transport of 1800 $g.m^{-2}.day^{-1}$, which is close to a breathable fabric (>2000 $g.m^{-2}.day^{-1}$). Finally, Peng *et al.* proposed to replace traditional protective garments with activated carbon by a lighter graphene oxide-based membrane, as a protective barrier against CEES and DMMP with high moisture transmission rate [180]. The selected membrane was a combination of Poly(ether ether ketone)-Ethylenediamine-Graphene oxide-Polyurethane, also called PEEK-EDA-GO-PU. The ethylenediamine serves as a cross-linking agent, while polyurethane is an anti-scratching layer and PEEK is a microporous hydrophobic membrane. This composite

**Table 5**
CWA simulants adsorption and detoxification using porous textile composites other than ACFs and MOFs.

| PTC | | | Simulants and amount | Permeation or $t_B$ | Degradation efficiency | | | Degradation products | Ref |
|---|---|---|---|---|---|---|---|---|---|
| Composition | Amount or size | SSA ($m^2/g$) | | | Half-life $t_{1/2}$ (minutes) | η (%) | Time (minutes) | | |
| Cotton/HOF-102 | 11.8 mg | | CEES (23 µL) | | ~ 5 [1] | 100 % | 30 | Selective reaction for CEESO | [150] |
| PIM-1-AX | | 605 | DMNP | | | 84 % | 2880 | Hydrolysis to M4NP and DMP | [130] |
| Diol-poly(RTIL)/NaY | 2.85 $cm^2$ | | CEES (3 µL) | $t_B$: 22 h | | | | | [314] |
| GO membrane | 1 in. diameter | | CEES (300 mg/$m^3$) | $t_B$: 16.2 min | | | | | [180] |
| | 8 mg | | DMMP | Blocked for 15 days | | | | | |
| Cellulose/PET nanofibers + zeolite mordenite or LTA | | | Paraoxon | | | | | | [223] |

* HOF: Hydrogen-bonded Organic Framework; PIM: Polymer of intrinsic microporosity; AX: Amidoxime; RTIL: Room Temperature Ionic Liquid; GO: Graphene oxide.
[1] Under 450 nm irradiation.

leads to an efficient blockage of DMMP during 15 days, and a relative long breakthrough time $t_B$ of 16.2 min was measured for CEES.

## 8. Conclusion

Chemical Warfare Agents (CWAs) adsorption and decontamination can be achieved using various sorbents and/or catalytic materials, such as mesoporous metal oxides, zeolites, aerogels, POPs, MOFs or ACFs. However, in the case of protective garments, the addition of such compounds to textile fibers creates an additional difficulty, as a good accessibility and anchoring of active porous materials to the fibers is necessary. Moreover, the comfort of the protective garments is an important parameter, with specific properties expected such as proper flexibility, efficient moisture vapor transport or low weight. Due to these difficulties, only few compounds were used for the fabrication of porous textile composites, and the large majority of the current studies are focused on fibers involving ACFs or MOFs, making microporous textiles composites the most studied protective garments so far.

Concerning activated carbons, and more specifically the ACFs, their use is mainly limited to the study of CWAs (or their simulants) adsorption. Due to their high specific surface area and adapted pores size (microporous), they have already proved excellent adsorption efficiencies towards CWAs and their simulants. Nowadays, these composites are incorporated in protective garments used by several armies from different countries. However, due to problems of CWAs saturation or desorption, performance enhancements of this type of protective garments are needed. The addition of catalytic species or porous materials to enhance the capture and/or the decontamination would lead to PTC active garments with very good efficiency. Few recent examples from the literature indeed prove that this path is very interesting for further investigations.

Porous textile composites containing MOFs are currently the most studied compounds for CWA detoxification. The integration of MOFs on the surface or within the fibers have been developed using mainly two techniques. The first one implies an electrospinning method, with a mixture of MOF particles or precursors with the fiber precursors. This approach leads to an excellent anchoring of MOFs but their accessibility is generally reduced, limiting the overall efficiency of the composite. A more preferred technique consists in the surface deposition of MOFs on the fiber surface, with straightforward synthesis routes (i.e. spray coating, solution impregnation). In this method, the MOFs anchoring can be optimized by the pre-functionalization of the supports.

Among all known MOFs existing, Zr-based compounds are particularly efficient and showed rapid degradation of various CWAs and their simulants. Indeed, the Lewis acidity of tetravalent Zr (IV) centers promotes the hydrolysis of organophosphorus compounds. However, this porous solid requires the help of a basic co-catalyst to reach high detoxification rates of nerve agents. This co-catalyst can be directly integrated in the composite (polyethyleimine, LiOtBu, etc ...) or added when testing the decontamination efficiency in solution (NEM especially). This addition largely improved the degradation of nerve agents, with half-lives down to < 5 min for MOF-based porous textile composites. Among all the MOF-composites referenced in this review, those involving the combination of ACF and Zr-MOF or the use of basic hydrogel appears very promising. In the case of sulfur mustard and its simulants, whereas hydrolysis degradation is an effective method for their decomposition, selective oxidation is now the preferred route. In this case, the use of photosensitizers-based MOFs has been developed, showing quick degradation time (<10 min) using several composites. Finally, dual functions PTCs have emerged, able to both detoxify organophosphorus nerve agents and sulfur mustard. These recent results of porous textile composites with a dual functionality might have an encouraging future for protective garments against CWAs.

## CRediT authorship contribution statement

**Nelly Couzon:** Writing-Original draft preparation, visualization. **Jérémy Dhainaut:** Writing - Review & Editing. **Christine Campagne:** Writing - Review & Editing. **Sébastien Royer:** Writing - Review & Editing. **Thierry Loiseau:** Writing - Review & Editing. **Christophe Volkringer:** Project administration, Supervision, Funding acquisition, Writing- Reviewing and Editing.

## Declaration of Competing Interest

The authors declare the following financial interests/personal relationships which may be considered as potential competing interests: Couzon reports financial support was provided by French National Research Agency-Agence Nationale de la Recherche.

## Acknowledgments

This work was supported by the National Agency of Research (ANR) through the TEXMOF project (ANR-19-ASTR-0015). The authors would like to thank the AID/ DGA (Defense Innovation Agency/French Ministry of Defense) for their support.

## References

[1] K. Ganesan, S.K. Raza, R. Vijayaraghavan, Chemical warfare agents, J. Pharm. Bioallied Sci. 2 (2010) 166–178, https://doi.org/10.4103/0975-7406.68498.
[2] A.H. Nurfaizey, N. Tucker, J. Stanger, M.P. Staiger, Functional nanofibers in clothing for protection against chemical and biological hazards, Funct. Nanofibers Their Appl., Elsevier (2012) 236–261, https://doi.org/10.1533/9780857095640.2.236.
[3] Y.J. Jang, K. Kim, O.G. Tsay, D.A. Atwood, D.G. Churchill, Update 1 of: destruction and detection of chemical warfare agents, Chem. Rev. 115 (2015) PR1–PR76, https://doi.org/10.1021/acs.chemrev.5b00402.
[4] B. Picard, I. Chataigner, J. Maddaluno, J. Legros, Introduction to chemical warfare agents, relevant simulants and modern neutralisation methods, Org. Biomol. Chem. 17 (2019) 6528–6537, https://doi.org/10.1039/C9OB00802K.
[5] P. Lodewyckx, Adsorption of chemical warfare agents, in: Act. Carbon Surf. Environ. Remediat., n.d.
[6] Q. Truong, E. Wilusz, Advances in chemical and biological protective clothing, in: Smart Text. Prot., Elsevier, 2013: pp. 364–377. 10.1533/9780857097620.2.364.
[7] L. Oudejans, J. O'Kelly, A.S. Evans, B. Wyrzykowska-Ceradini, A. Touati, D. Tabor, E.G. Snyder, Decontamination of personal protective equipment and related materials contaminated with toxic industrial chemicals and chemical warfare agent surrogates, J. Environ. Chem. Eng. 4 (2016) 2745–2753, https://doi.org/10.1016/j.jece.2016.05.022.
[8] M. Guidotti, C. Evangelisti, A. Rossodivita, M.C. Ranghieri, Nano-structured Solids and Heterogeneous Catalysts for the Selective Decontamination of Chemical Warfare Agents, in: J. Banoub (Ed.), Detect. Chem. Biol. Radiol. Nucl. Agents Prev. Terror., Springer Netherlands, Dordrecht, 2014: pp. 275–284. 10.1007/978-94-017-9238-7_17.
[9] T.G. Grissom, A.M. Plonka, C.H. Sharp, A.M. Ebrahim, Y. Tian, D.L. Collins-Wildman, A.L. Kaledin, H.J. Siegal, D. Troya, C.L. Hill, A.I. Frenkel, D.G. Musaev, W.O. Gordon, C.J. Karwacki, M.B. Mitchell, J.R. Morris, Metal−organic framework- and polyoxometalate-based sorbents for the uptake and destruction of chemical warfare agents, ACS Appl. Mater. Interfaces. 12 (2021) 14641–14661.
[10] V.B. Thakare, N.K. Tripathi, V.V. Singh, M. Sathe, B. Singh, Activated Carbon Fabric: An Adsorbent Material for Chemical Protective Clothing, Def. Sci. J. 68 (2017) 83. 10.14429/dsj.68.11734.
[11] Y. Liu, A.J. Howarth, N.A. Vermeulen, S.-Y. Moon, J.T. Hupp, O.K. Farha, Catalytic degradation of chemical warfare agents and their simulants by metal-organic frameworks, Coord. Chem. Rev. 346 (2017) 101–111, https://doi.org/10.1016/j.ccr.2016.11.008.
[12] K.O. Kirlikovali, Z. Chen, T. Islamoglu, J.T. Hupp, O.K. Farha, Zirconium-based metal-organic frameworks for the catalytic hydrolysis of organophosphorus nerve agents, ACS Appl. Mater. Interfaces. 12 (2020) 14702–14720, https://doi.org/10.1021/acsami.9b20154.
[13] A. Phadatare, B. Kandasubramanian, Metal organic framework functionalized fabrics for detoxification of chemical warfare agents, Ind. Eng. Chem. Res. 59 (2020) 569–586, https://doi.org/10.1021/acs.iecr.9b06695.

[14] S. Balasubramanian, A.J. Kulandaisamy, K.J. Babu, A. Das, J.B. Balaguru Rayappan, Metal Organic Framework Functionalized Textiles as Protective Clothing for the Detection and Detoxification of Chemical Warfare Agents—A Review, Ind. Eng. Chem. Res. (2021) acs.iecr.0c06096. 10.1021/acs.iecr.0c06096.
[15] G. Hoog, A. Steinmetz, eds., 9. Convention on the Prohibition of the Development, Production, Stockpiling and Use of Chemical Weapons and on their Destruction, in: Int. Conv. Prot. Humanity Environ., De Gruyter, 1993: pp. 332–364. 10.1515/9783110874815-026.
[16] What is a Chemical Weapon?, OPCW. (n.d.). https://www.opcw.org/our-work/what-chemical-weapon (accessed May 27, 2021).
[17] M. Wattana, T. Bey, Mustard gas or sulfur mustard: an old chemical agent as a new terrorist threat, Prehospital Disaster Med. 24 (2009) 19–29, https://doi.org/10.1017/S1049023X0000649X.
[18] H. Thiermann, F. Worek, K. Kehe, Limitations and challenges in treatment of acute chemical warfare agent poisoning, Chem. Biol. Interact. 206 (2013) 435–443, https://doi.org/10.1016/j.cbi.2013.09.015.
[19] D.A. Giannakoudakis, T.J. Bandosz, Detoxification of chemical warfare agents, Springer International Publishing, Cham, 2018, 10.1007/978-3-319-70760-0.
[20] D.A. Giannakoudakis, M. Barczak, M. Florent, T.J. Bandosz, Analysis of interactions of mustard gas surrogate vapors with porous carbon textiles, Chem. Eng. J. 362 (2019) 758–766, https://doi.org/10.1016/j.cej.2019.01.064.
[21] N.B. Munro, S.S. Talmage, G.D. Griffin, L.C. Waters, A.P. Watson, J.F. King, V. Hauschild, The sources, fate, and toxicity of chemical warfare agent degradation products, Environ. Health Perspect. 107 (1999) 933–974, https://doi.org/10.1289/ehp.99107933.
[22] R. Osovsky, D. Kaplan, I. Nir, H. Rotter, S. Elisha, I. Columbus, Decontamination of adsorbed chemical warfare agents on activated carbon using hydrogen peroxide solutions, Environ. Sci. Technol. 48 (2014) 10912–10918, https://doi.org/10.1021/es502981y.
[23] Y. Liu, C.T. Buru, A.J. Howarth, J.J. Mahle, J.H. Buchanan, J.B. DeCoste, J.T. Hupp, O.K. Farha, Efficient and selective oxidation of sulfur mustard using singlet oxygen generated by a pyrene-based metal–organic framework, J. Mater. Chem. A. 4 (2016) 13809–13813, https://doi.org/10.1039/C6TA05903A.
[24] N.S. Bobbitt, M.L. Mendonca, A.J. Howarth, T. Islamoglu, J.T. Hupp, O.K. Farha, R.Q. Snurr, Metal–organic frameworks for the removal of toxic industrial chemicals and chemical warfare agents, Chem. Soc. Rev. 46 (2017) 3357–3385, https://doi.org/10.1039/C7CS00108H.
[25] R. Kaiser, A. Kulczyk, D. Rich, R.J. Willey, J. Minicucci, B. MacIver, Effect of pore size distribution of commercial activated carbon fabrics on the adsorption of CWA simulants from the liquid phase, Ind. Eng. Chem. Res. 46 (2007) 6126–6132, https://doi.org/10.1021/ie061429n.
[26] J. Lavoie, S. Srinivasan, R. Nagarajan, Using cheminformatics to find simulants for chemical warfare agents, J. Hazard. Mater. 194 (2011) 85–91, https://doi.org/10.1016/j.jhazmat.2011.07.077.
[27] S.L. Bartelt-Hunt, D.R.U. Knappe, M.A. Barlaz, A review of chemical warfare agent simulants for the study of environmental behavior, Crit. Rev. Environ. Sci. Technol. 38 (2008) 112–136, https://doi.org/10.1080/10643380701643650.
[28] Meridian Medical Technologies | ATNAA, (n.d.). https://www.meridianmeds.com/products/atnaa (accessed December 9, 2020).
[29] Chemical Agent Health-Based Standards and Guidelines Summary Table 1: Criteria for Airborne Exposures as of July 2011, (2011).
[30] M. Agrawal, D.F. Sava Gallis, J.A. Greathouse, D.S. Sholl, How useful are common simulants of chemical warfare agents at predicting adsorption behavior?, J Phys. Chem. C. 122 (2018) 26061–26069, https://doi.org/10.1021/acs.jpcc.8b08856.
[31] I. Candel, M.D. Marcos, R. Martínez-Máñez, F. Sancenón, A.M. Costero, M. Parra, S. Gil, C. Guillem, F. Pérez-Plá, P. Amorós, Hydrolysis of DCNP (a Tabun mimic) catalysed by mesoporous silica nanoparticles, Microporous Mesoporous Mater. 217 (2015) 30–38, https://doi.org/10.1016/j.micromeso.2015.05.041.
[32] K. Ma, M.C. Wasson, X. Wang, X. Zhang, K.B. Idrees, Z. Chen, Y. Wu, S.-J. Lee, R. Cao, Y. Chen, L. Yang, F.A. Son, T. Islamoglu, G.W. Peterson, J.J. Mahle, O.K. Farha, Near-instantaneous catalytic hydrolysis of organophosphorus nerve agents with zirconium-based MOF/hydrogel composites, Chem Catal. 1 (2021) 721–733, https://doi.org/10.1016/j.checat.2021.06.008.
[33] M.A.R. Bhuiyan, L. Wang, A. Shaid, R.A. Shanks, J. Ding, Advances and applications of chemical protective clothing system, J. Ind. Text. 49 (2019) 97–138, https://doi.org/10.1177/1528083718779426.
[34] R.B. Ormond, R.L. Barker, Chemical, biological, radiological and nuclear (CBRN) protective clothing, Prot. Cloth., Elsevier (2014) 112–145, https://doi.org/10.1533/9781782420408.1.112.
[35] A. Gugliuzza, E. Drioli, A review on membrane engineering for innovation in wearable fabrics and protective textiles, J. Membr. Sci. 446 (2013) 350–375, https://doi.org/10.1016/j.memsci.2013.07.014.
[36] P. Lodewyckx, Activated Carbon Surfaces in Environmental Remediation, Chapiter 10, T.J. Bandosz, 2006.
[37] H.L. Schreuder-Gibson, Q. Truong, J.E. Walker, J.R. Owens, J.D. Wander, W.E. Jones, Chemical and biological protection and detection in fabrics for protective clothing, MRS Bull. 28 (2003) 574–578, https://doi.org/10.1557/mrs2003.168.
[38] GORE® CHEMPAK® Chemical Protection | GORE-TEX Professional, (n.d.). https://www.goretexprofessional.com/technologies/gore-chempak (accessed June 11, 2021).
[39] R. Ramaseshan, S. Sundarrajan, Y. Liu, R.S. Barhate, N.L. Lala, S. Ramakrishna, Functionalized polymer nanofibre membranes for protection from chemical warfare stimulants, Nanotechnology 17 (2006) 2947–2953, https://doi.org/10.1088/0957-4484/17/12/021.
[40] V.H. Grassian, S.C. Larsen, Applications of Nanocrystalline Zeolites to CWA Decontamination, in: R. Nagarajan, W. Zukas, T.A. Hatton, S. Lee (Eds.), Nanosci. Nanotechnol. Chem. Biol. Def., American Chemical Society, Washington DC, 2009: pp. 249–260. 10.1021/bk-2009-1016.ch019.
[41] J.P. Kumar, R. P.V.R.K., P. G.K., B. Singh, Montmorillonites supported with metal oxide nanoparticles for decontamination of sulfur mustard, Appl. Clay Sci. 116–117 (2015) 263–272, https://doi.org/10.1016/j.clay.2015.04.007.
[42] D.L. Bish, Parallels and Distinctions Between Clay Minerals and Zeolites, in: Dev. Clay Sci., Elsevier, 2013: pp. 783–800. 10.1016/B978-0-08-098258-8.00026-2.
[43] D. Costenaro, C. Bisio, F. Carniato, S.L. Safronyuk, T.V. Kramar, M.V. Taran, M.F. Starodub, A.M. Katsev, M. Guidotti, Physico-chemical properties, biological and environmental impact of Nb-saponites catalysts for the oxidative degradation of chemical warfare agents, ChemistrySelect 2 (2017) 1812–1819, https://doi.org/10.1002/slct.201700042.
[44] E. Koohsaryan, M. Anbia, Nanosized and hierarchical zeolites: A short review, Chin. J. Catal. 37 (2016) 447–467, https://doi.org/10.1016/S1872-2067(15)61038-5.
[45] M. Moshoeshoe, M.S. Nadiye-Tabbiruka, V. Obuseng, A review of the chemistry, structure, properties and applications of zeolites, Am. J. Mater. Sci. (2017) 26.
[46] M.V. Opanasenko, W.J. Roth, J. Čejka, Two-dimensional zeolites in catalysis: current status and perspectives, Catal. Sci. Technol. 6 (2016) 2467–2484, https://doi.org/10.1039/C5CY02079D.
[47] F. Carniato, C. Bisio, C. Evangelisti, R. Psaro, V. Dal Santo, D. Costenaro, L. Marchese, M. Guidotti, Iron-montmorillonite clays as active sorbents for the decontamination of hazardous chemical warfare agents, Dalton Trans. 47 (2018) 2939–2948, https://doi.org/10.1039/C7DT03859C.
[48] A. Roul, C.-A.-K. Le, M.-P. Gustin, E. Clavaud, B. Verrier, F. Pirot, F. Falson, Comparison of four different fuller's earth formulations in skin decontamination, J. Appl. Toxicol. 37 (2017) 1527–1536, https://doi.org/10.1002/jat.3506.
[49] C.M. Boone, Present state of CBRN decontamination methodologies, TNO (2007).
[50] A. Michalkova, L. Gorb, M. Ilchenko, O.A. Zhikol, O.V. Shishkin, J. Leszczynski, Adsorption of Sarin and Soman on Dickite: An ab Initio ONIOM Study, J. Phys. Chem. B. 108 (2004) 1918–1930, https://doi.org/10.1021/jp030391e.
[51] L. Bromberg, C.M. Straut, A. Centrone, E. Wilusz, T.A. Hatton, Montmorillonite functionalized with pralidoxime as a material for chemical protection against organophosphorous compounds, ACS Appl. Mater. Interfaces. 3 (2011) 1479–1484, https://doi.org/10.1021/am200041e.
[52] R. Osovsky, S. Cherf, S. Karagach, L. Aviram, Y. Mishael, Decontamination of sarin in water by designed oxime-clay composites, Appl. Clay Sci. 192 (2020), https://doi.org/10.1016/j.clay.2020.105620 105620.
[53] D. Plachá, K. Rosenbergová, J. Slabotínský, K.M. Kutláková, S. Študentová, G.S. Martynková, Modified clay minerals efficiency against chemical and biological warfare agents for civil human protection, J. Hazard. Mater. 271 (2014) 65–72, https://doi.org/10.1016/j.jhazmat.2014.01.059.
[54] F. Carniato, C. Bisio, R. Psaro, L. Marchese, M. Guidotti, Niobium(V) saponite clay for the catalytic oxidative abatement of chemical warfare agents, Angew. Chem. Int. Ed. 53 (2014) 10095–10098, https://doi.org/10.1002/anie.201405134.
[55] Y.R. Son, M.-K. Kim, S.G. Ryu, H.S. Kim, Rapid capture and hydrolysis of a sulfur mustard gas in silver-ion-exchanged zeolite Y, ACS Appl. Mater. Interfaces. 10 (2018) 40651–40660, https://doi.org/10.1021/acsami.8b15362.
[56] X. Li, P.K. Dutta, Interaction of dimethylmethylphosphonate with zeolite Y: impedance-based sensor for detecting nerve agent simulants, J. Phys. Chem. C. 114 (2010) 7986–7994, https://doi.org/10.1021/jp100088w.
[57] A.J. Bellamy, Reaction of gaseous sulfur mustard with zeolite 1 3 X t, J. Chem. Soc. Perkin Trans. (1994) 4.
[58] G.W. Wagner, P.W. Bartram, Reactions of VX, HD, and their simulants with NaY and AgY Zeolites. Desulfurization of VX on AgY, Langmuir 15 (1999) 8113–8118, https://doi.org/10.1021/la990716b.
[59] V.V. Singh, B. Jurado-Sánchez, S. Sattayasamitsathit, J. Orozco, J. Li, M. Galarnyk, Y. Fedorak, J. Wang, Multifunctional silver-exchanged zeolite micromotors for catalytic detoxification of chemical and biological threats, Adv. Funct. Mater. 25 (2015) 2147–2155, https://doi.org/10.1002/adfm.201500033.
[60] M. Sadeghi, S. Yekta, D. Mirzaei, A novel CuO NPs/AgZSM-5 zeolite composite adsorbent: Synthesis, identification and its application for the removal of sulfur mustard agent simulant, J. Alloys Compd. 748 (2018) 995–1005, https://doi.org/10.1016/j.jallcom.2018.03.239.
[61] K. Meenu, N. Kumar, K.R. Tiwari, T. Yadav, R. Tomar, A.K. Gupta, Synthesis and characterization of zeolite Linde Type W and its metal oxide composite Ag-O-LTW used for the decontamination of chemical warfare agent simulant, Phosphorus Sulfur Silicon Relat. Elem. (2020) 1–8, https://doi.org/10.1080/10426507.2020.1762193.
[62] X. Ji, W. Yao, J. Peng, N. Ren, J. Zhou, Y. Huang, Evaluation of Cu-ZSM-5 zeolites as QCM sensor coatings for DMMP detection, Sens. Actuators B Chem. 166–167 (2012) 50–55, https://doi.org/10.1016/j.snb.2011.12.014.
[63] S.-W. Yang, D.C. Doetschman, J.T. Schulte, J.B. Sambur, C.W. Kanyi, J.D. Fox, C. O. Kowenje, B.R. Jones, N.D. Sherma, Sodium X-type faujasite zeolite decomposition of dimethyl methylphosphonate (DMMP) to

methylphosphonate: Nucleophilic zeolite reactions I, Microporous Mesoporous Mater. 92 (2006) 56–60, https://doi.org/10.1016/j.micromeso.2005.12.018.
[64] M. Sadeghi, H. Ghaedi, S. Yekta, E. Babanezhad, Decontamination of toxic chemical warfare sulfur mustard and nerve agent simulants by NiO NPs/Ag-clinoptilolite zeolite composite adsorbent, J. Environ. Chem. Eng. 4 (2016) 2990–3000, https://doi.org/10.1016/j.jece.2016.06.008.
[65] Q. Meng, D.C. Doetschman, A.K. Rizos, M.-H. Lee, J.T. Schulte, A. Spyros, C.W. Kanyi, Adsorption of organophosphates into microporous and mesoporous NaX zeolites and subsequent chemistry, Environ. Sci. Technol. 45 (2011) 3000–3005, https://doi.org/10.1021/es1030678.
[66] W. Chen, X. Liu, R.L. He, T. Lin, Q.F. Zeng, X.G. Wang, Activated carbon powders from wool fibers, Powder Technol. 234 (2013) 76–83, https://doi.org/10.1016/j.powtec.2012.09.026.
[67] K.-L. Chiu, D.H.L. Ng, Synthesis and characterization of cotton-made activated carbon fiber and its adsorption of methylene blue in water treatment, Biomass Bioenergy. 46 (2012) 102–110, https://doi.org/10.1016/j.biombioe.2012.09.023.
[68] Z. Yue, J. Economy, Carbonization and activation for production of activated carbon fibers, in: Act. Carbon Fiber Text., Elsevier, 2017: pp. 61–139. 10.1016/B978-0-08-100660-3.00004-3.
[69] Y. Boutillara, J.L. Tombeur, G. De Weireld, P. Lodewyckx, In-situ copper impregnation by chemical activation with CuCl2 and its application to SO2 and H2S capture by activated carbons, Chem. Eng. J. 372 (2019) 631–637, https://doi.org/10.1016/j.cej.2019.04.183.
[70] H. Yuan, L.-Y. Meng, S.-J. Park, KOH-activated graphite nanofibers as $CO_2$ adsorbents, Carbon Lett. 19 (2016) 99–103, https://doi.org/10.5714/CL.2016.19.099.
[71] Yu, Son, Yoo, Cha, Lee, Kim, Chitosan-Derived Porous Activated Carbon for the Removal of the Chemical Warfare Agent Simulant Dimethyl Methylphosphonate, Nanomaterials. 9 (2019) 1703. 10.3390/nano9121703.
[72] B. Cojocaru, Ş. Neaţu, V.I. Pârvulescu, V. Şomoghi, N. Petrea, G. Epure, M. Alvaro, H. Garcia, Synergism of activated carbon and undoped and nitrogen-doped $TiO_2$ in the photocatalytic degradation of the chemical warfare agents soman, VX, and Yperite, ChemSusChem. 2 (2009) 427–436, https://doi.org/10.1002/cssc.200800246.
[73] A. Gopinath, K. Kadirvelu, Strategies to design modified activated carbon fibers for the decontamination of water and air, Environ. Chem. Lett. 16 (2018) 1137–1168, https://doi.org/10.1007/s10311-018-0740-9.
[74] M.F. Hassan, M.A. Sabri, H. Fazal, A. Hafeez, N. Shezad, M. Hussain, Recent trends in activated carbon fibers production from various precursors and applications—A comparative review, J. Anal. Appl. Pyrolysis. 145 (2020), https://doi.org/10.1016/j.jaap.2019.104715 104715.
[75] N.H. Phan, S. Rio, C. Faur, L. Le Coq, P. Le Cloirec, T.H. Nguyen, Production of fibrous activated carbons from natural cellulose (jute, coconut) fibers for water treatment applications, Carbon. 44 (2006) 2569–2577, https://doi.org/10.1016/j.carbon.2006.05.048.
[76] D. Wang, Z. Wang, X. Zheng, M. Tian, Activated carbon fiber derived from the seed hair fibers of Metaplexis japonica: Novel efficient adsorbent for methylene blue, Ind. Crops Prod. 148 (2020), https://doi.org/10.1016/j.indcrop.2020.112319 112319.
[77] L. Zhang, L. Tu, Y. Liang, Q. Chen, Z. Li, C. Li, Z. Wang, W. Li, Coconut-based activated carbon fibers for efficient adsorption of various organic dyes, RSC Adv. 8 (2018) 42280–42291, https://doi.org/10.1039/C8RA08990F.
[78] D. Das, V. Gaur, N. Verma, Removal of volatile organic compound by activated carbon fiber, Carbon. 42 (2004) 2949–2962, https://doi.org/10.1016/j.carbon.2004.07.008.
[79] K.J. Lee, N. Shiratori, G.H. Lee, J. Miyawaki, I. Mochida, S.-H. Yoon, J. Jang, Activated carbon nanofiber produced from electrospun polyacrylonitrile nanofiber as a highly efficient formaldehyde adsorbent, Carbon. 48 (2010) 4248–4255, https://doi.org/10.1016/j.carbon.2010.07.034.
[80] O. Ursini, G. Angelini, F. Cataldo, Adsorption of dinitrogen tetroxide on activated carbon fabric derived from novolacs, Fuller. Nanotub. Carbon Nanostructures. 25 (2017) 589–601, https://doi.org/10.1080/1536383X.2017.1353975.
[81] P. Wang, J. Lang, S. Xu, X. Wang, Nitrogen-containing activated carbon fibers derived from silk fibers for CO2 capture, Mater. Lett. 152 (2015) 145–147, https://doi.org/10.1016/j.matlet.2015.03.027.
[82] Z. Yue, J. Economy, Nanoparticle and nanoporous carbon adsorbents for removal of trace organic contaminants from water, J. Nanoparticle Res. 7 (2005) 477–487, https://doi.org/10.1007/s11051-005-4719-7.
[83] S.-K. Ryu, S.-R. Choi, Activated carbon fibers for the removal of chemical warfare simulants, J. Ceram. Soc. Jpn. 112 (2004) 1539–1542.
[84] S.C. Kang, J.S. Im, S.-H. Lee, T.-S. Bae, Y.-S. Lee, High-sensitivity gas sensor using electrically conductive and porosity-developed carbon nanofiber, Colloids Surf. Physicochem. Eng. Asp. 384 (2011) 297–303, https://doi.org/10.1016/j.colsurfa.2011.04.001.
[85] J. Kim, S.H. Lee, S.-J. Park, Y.-S. Lee, Preparation and gas-sensing properties of pitch-based carbon fiber prepared using a melt-electrospinning method, Res. Chem. Intermed. 40 (2014) 2571–2581, https://doi.org/10.1007/s11164-014-1670-1.
[86] S. Hu, S. Zhang, N. Pan, Y.-L. Hsieh, High energy density supercapacitors from lignin derived submicron activated carbon fibers in aqueous electrolytes, J. Power Sources. 270 (2014) 106–112, https://doi.org/10.1016/j.jpowsour.2014.07.063.
[87] H.-M. Lee, L.-K. Kwac, K.-H. An, S.-J. Park, B.-J. Kim, Electrochemical behavior of pitch-based activated carbon fibers for electrochemical capacitors, Energy Convers. Manag. 125 (2016) 347–352, https://doi.org/10.1016/j.enconman.2016.06.006.
[88] B. Xu, F. Wu, R. Chen, G. Cao, S. Chen, Y. Yang, Mesoporous activated carbon fiber as electrode material for high-performance electrochemical double layer capacitors with ionic liquid electrolyte, J. Power Sources. 195 (2010) 2118–2124, https://doi.org/10.1016/j.jpowsour.2009.09.077.
[89] S.S. Kistler, Coherent Expanded Aerogels and Jellies, Nature. 127 (1931) 741.
[90] A.C. Pierre, G.M. Pajonk, Chemistry of Aerogels and Their Applications, Chem. Rev. 102 (2002) 4243–4266, https://doi.org/10.1021/cr0101306.
[91] E. Barrios, D. Fox, Y.Y. Li Sip, R. Catarata, J.E. Calderon, N. Azim, S. Afrin, Z. Zhang, L. Zhai, Nanomaterials in advanced, high-performance aerogel composites: a review, Polymers 11 (2019) 726, https://doi.org/10.3390/polym11040726.
[92] G. Gan, X. Li, S. Fan, L. Wang, M. Qin, Z. Yin, G. Chen, Carbon aerogels for environmental clean-up: carbon aerogels for environmental clean-up, Eur. J. Inorg. Chem. 2019 (2019) 3126–3141, https://doi.org/10.1002/ejic.201801512.
[93] J.E. Amonette, J. Matyáš, Functionalized silica aerogels for gas-phase purification, sensing, and catalysis: A review, Microporous Mesoporous Mater. 250 (2017) 100–119, https://doi.org/10.1016/j.micromeso.2017.04.055.
[94] U. Berardi, Aerogel-enhanced insulation for building applications, in: Nanotechnol. Eco-Effic. Constr., Elsevier, 2019: pp. 395–416. 10.1016/B978-0-08-102641-0.00017-7.
[95] L. Hu, R. He, H. Lei, D. Fang, Carbon aerogel for insulation applications: A review, Int. J. Thermophys. 40 (2019) 39, https://doi.org/10.1007/s10765-019-2505-5.
[96] J. Stergar, U. Maver, Review of aerogel-based materials in biomedical applications, J. Sol-Gel Sci. Technol. 77 (2016) 738–752, https://doi.org/10.1007/s10971-016-3968-5.
[97] V. Štengl, S. Bakardjieva, M. Maøíková, J. Šubrt, F. Opluštil, M. Olšanská, Aerogel nanoscale aluminium oxides as a destructive sorbent for mustard gas, (2003) 6.
[98] V. Štengl, S. Bakardjieva, M. Maříková, J. Šubrt, F. Opluštil, M. Olšanská, Aerogel nanoscale magnesium oxides as a destructive sorbent for toxic chemical agents, Open Chem. 2 (2004), https://doi.org/10.2478/BF02476182.
[99] Q. Han, L. Yang, Q. Liang, M. Ding, Three-dimensional hierarchical porous graphene aerogel for efficient adsorption and preconcentration of chemical warfare agents, Carbon. 122 (2017) 556–563, https://doi.org/10.1016/j.carbon.2017.05.031.
[100] M. McEntee, W.O. Gordon, A. Balboa, D. Delia, C. Pitman, A. Pennington, D.R. Rolison, J. Pietron, P.A. DeSario, Mesoporous Cu Nanoparticle/$TiO_2$ Aerogels for Room-Temperature Hydrolytic Decomposition of Chemical Warfare Simulant Dimethyl Methylphosphonate, ACS Appl. Nano Mater. (2020) acsanm.0c00228. 10.1021/acsanm.0c00228.
[101] Y. Ren, Z. Ma, P.G. Bruce, Ordered mesoporous metal oxides: synthesis and applications, Chem. Soc. Rev. 41 (2012) 4909, https://doi.org/10.1039/c2cs35086f.
[102] J. Praveen Kumar, G.K. Prasad, P.V.R.K. Ramacharyulu, P. Garg, K. Ganesan, Mesoporous CuO–ZnO binary metal oxide nanocomposite for decontamination of sulfur mustard, Mater. Chem. Phys. 142 (2013) 484–490, https://doi.org/10.1016/j.matchemphys.2013.07.034.
[103] J. Praveen Kumar, G.K. Prasad, J.A. Allen, P.V.R.K. Ramacharyulu, K. Kadirvelu, B. Singh, Synthesis of mesoporous metal aluminate nanoparticles and studies on the decontamination of sulfur mustard, J. Alloys Compd. 662 (2016) 44–53, https://doi.org/10.1016/j.jallcom.2015.11.181.
[104] J. Praveen Kumar, G.K. Prasad, P.V.R.K. Ramacharyulu, B. Singh, T. Gopi, R. Krishna, Mesoporous binary metal oxide nanocomposites: Synthesis, characterization and decontamination of sulfur mustard, Mater. Chem. Phys. 173 (2016) 168–178, https://doi.org/10.1016/j.matchemphys.2016.01.063.
[105] T.H. Mahato, G.K. Prasad, B. Singh, K. Batra, K. Ganesan, Mesoporous manganese oxide nanobelts for decontamination of sarin, sulphur mustard and chloro ethyl ethyl sulphide, Microporous Mesoporous Mater. 132 (2010) 15–21, https://doi.org/10.1016/j.micromeso.2009.05.035.
[106] M.E. Martin, R.M. Narske, K.J. Klabunde, Mesoporous metal oxides formed by aggregation of nanocrystals. Behavior of aluminum oxide and mixtures with magnesium oxide in destructive adsorption of the chemical warfare surrogate 2-chloroethylethyl sulfide, Microporous Mesoporous Mater. 83 (2005) 47–50, https://doi.org/10.1016/j.micromeso.2005.04.003.
[107] G.K. Prasad, P.V.R.K. Ramacharyulu, K. Batra, B. Singh, A.R. Srivastava, K. Ganesan, R. Vijayaraghavan, Decontamination of Yperite using mesoporous mixed metal oxide nanocrystals, J. Hazard. Mater. 183 (2010) 847–852, https://doi.org/10.1016/j.jhazmat.2010.07.104.
[108] C.R. Ringenbach, S.R. Livingston, D. Kumar, C.C. Landry, Vanadium-Doped Acid-Prepared Mesoporous Silica: Synthesis, Characterization, and Catalytic Studies on the Oxidation of a Mustard Gas Analogue, Chem. Mater. 17 (2005) 5580–5586, https://doi.org/10.1021/cm051372f.
[109] M. Sadeghi, S. Yekta, H. Ghaedi, Synthesis and application of Pb-MCM-41/ZnNiO 2 as a novel mesoporous nanocomposite adsorbent for the decontamination of chloroethyl phenyl sulfide (CEPS), Appl. Surf. Sci. 400 (2017) 471–480, https://doi.org/10.1016/j.apsusc.2016.12.224.

[110] A. Saxena, A.K. Srivastava, B. Singh, A. Goyal, Removal of sulphur mustard, sarin and simulants on impregnated silica nanoparticles, J. Hazard. Mater. 211–212 (2012) 226–232, https://doi.org/10.1016/j.jhazmat.2011.07.117.
[111] A.-T. Vu, S. Jiang, K. Ho, J.B. Lee, C.-H. Lee, Mesoporous magnesium oxide and its composites: Preparation, characterization, and removal of 2-chloroethyl ethyl sulfide, Chem. Eng. J. 269 (2015) 82–93, https://doi.org/10.1016/j.cej.2015.01.089.
[112] V. Štengl, J. Bludská, F. Opluštil, T. Němec, Mesoporous titanium–manganese dioxide for sulphur mustard and soman decontamination, Mater. Res. Bull. 46 (2011) 2050–2056, https://doi.org/10.1016/j.materresbull.2011.07.003.
[113] V. Štengl, D. Králová, F. Opluštil, T. Němec, Mesoporous manganese oxide for warfare agents degradation, Microporous Mesoporous Mater. 156 (2012) 224–232, https://doi.org/10.1016/j.micromeso.2012.02.031.
[114] V. Štengl, T.M. Grygar, J. Bludská, F. Opluštil, T. Němec, Mesoporous iron–manganese oxides for sulphur mustard and soman degradation, Mater. Res. Bull. 47 (2012) 4291–4299, https://doi.org/10.1016/j.materresbull.2012.09.015.
[115] M. Alvaro, B. Cojocaru, A.A. Ismail, N. Petrea, B. Ferrer, F.A. Harraz, V.I. Parvulescu, H. Garcia, Visible-light photocatalytic activity of gold nanoparticles supported on template-synthesized mesoporous titania for the decontamination of the chemical warfare agent Soman, Appl. Catal. B Environ. 99 (2010) 191–197, https://doi.org/10.1016/j.apcatb.2010.06.019.
[116] T.G. Woo, B.J. Cha, Y.D. Kim, H.O. Seo, Positive Effects of Impregnation of Fe-oxide in Mesoporous Al-Oxides on the Decontamination of Dimethyl Methylphosphonate, Catalysts. 9 (2019) 898, https://doi.org/10.3390/catal9110898.
[117] S.M.J. Rogge, A. Bavykina, J. Hajek, H. Garcia, A.I. Olivos-Suarez, A. Sepúlveda-Escribano, A. Vimont, G. Clet, P. Bazin, F. Kapteijn, M. Daturi, E.V. Ramos-Fernandez, F.X. Llabrés i Xamena, V. Van Speybroeck, J. Gascon,, Metal–organic and covalent organic frameworks as single-site catalysts, Chem. Soc. Rev. 46 (2017) 3134–3184, https://doi.org/10.1039/C7CS00033B.
[118] S.-Y. Ding, W. Wang, Covalent organic frameworks (COFs): from design to applications, Chem Soc Rev. 42 (2013) 548–568, https://doi.org/10.1039/C2CS35072F.
[119] Y. Zhang, S.N. Riduan, Functional porous organic polymers for heterogeneous catalysis, Chem Soc Rev. 41 (2012) 2083–2094, https://doi.org/10.1039/C1CS15227K.
[120] K. Geng, T. He, R. Liu, S. Dalapati, K.T. Tan, Z. Li, S. Tao, Y. Gong, Q. Jiang, D. Jiang, Covalent Organic Frameworks: Design, Synthesis, and Functions, Chem. Rev. (2020) acs.chemrev.9b00550. 10.1021/acs.chemrev.9b00550.
[121] H. Vardhan, A. Nafady, A.M. Al-Enizi, S. Ma, Pore surface engineering of covalent organic frameworks: structural diversity and applications, Nanoscale. 11 (2019) 21679–21708, https://doi.org/10.1039/C9NR07525A.
[122] C.L. McGann, G.C. Daniels, S.L. Giles, R.B. Balow, J.L. Miranda-Zayas, J.G. Lundin, J.H. Wynne, Air Activated Self-Decontaminating Polydicyclopentadiene PolyHIPE Foams for Rapid Decontamination of Chemical Warfare Agents, Macromol Rapid Commun. 39 (2018) 1800194, https://doi.org/10.1002/marc.201800194.
[123] R.K. Totten, Y.-S. Kim, M.H. Weston, O.K. Farha, J.T. Hupp, S.T. Nguyen, Enhanced Catalytic Activity through the Tuning of Micropore Environment and Supercritical CO $_2$ Processing: Al(Porphyrin)-Based Porous Organic Polymers for the Degradation of a Nerve Agent Simulant, J. Am. Chem. Soc. 135 (2013) 11720–11723, https://doi.org/10.1021/ja405495u.
[124] P. Kaur, J.T. Hupp, S.T. Nguyen, Porous Organic Polymers in Catalysis: Opportunities and Challenges, ACS Catal. 1 (2011) 819–835, https://doi.org/10.1021/cs200131g.
[125] R.K. Totten, M.H. Weston, J.K. Park, O.K. Farha, J.T. Hupp, S.T. Nguyen, Catalytic Solvolytic and Hydrolytic Degradation of Toxic Methyl Paraoxon with La(catecholate)-Functionalized Porous Organic Polymers, ACS Catal. 3 (2013) 1454–1459, https://doi.org/10.1021/cs4001738.
[126] Y. Zhi, Z. Yao, W. Jiang, H. Xia, Z. Shi, Y. Mu, X. Liu, Conjugated Microporous Polymers as Heterogeneous Photocatalysts for Efficient Degradation of a Mustard-Gas Simulant, ACS Appl. Mater. Interfaces. 11 (2019) 37578–37585, https://doi.org/10.1021/acsami.9b10958.
[127] Z.-H. He, S.-D. Gong, S.-L. Cai, Y.-L. Yan, G. Chen, X.-L. Li, S.-R. Zheng, J. Fan, W.-G. Zhang, A Benzimidazole-Containing Covalent Organic Framework-Based QCM Sensor for Exceptional Detection of CEES, Cryst. Growth Des. 19 (2019) 3543–3550, https://doi.org/10.1021/acs.cgd.9b00409.
[128] S. Wang, N.L. Pomerantz, Z. Dai, W. Xie, E.E. Anderson, T. Miller, S.A. Khan, G. N. Parsons, Polymer of intrinsic microporosity (PIM) based fibrous mat: combining particle filtration and rapid catalytic hydrolysis of chemical warfare agent simulants into a highly sorptive, breathable, and mechanically robust fiber matrix, Mater. Today Adv. 8 (2020), https://doi.org/10.1016/j.mtadv.2020.100085 100085.
[129] D. Jung, P. Das, A. Atilgan, P. Li, J.T. Hupp, T. Islamoglu, J.A. Kalow, O.K. Farha, Reactive Porous Polymers for Detoxification of a Chemical Warfare Agent Simulant, Chem. Mater. 32 (2020) 9299–9306, https://doi.org/10.1021/acs.chemmater.0c03160.
[130] D. Jung, K.O. Kirlikovali, Z. Chen, K.B. Idrees, A. Atilgan, R. Cao, T. Islamoglu, O. K. Farha, An Amidoxime-Functionalized Porous Reactive Fiber against Toxic Chemicals, ACS Mater. Lett. 3 (2021) 320–326, https://doi.org/10.1021/acsmaterialslett.0c00598.
[131] S. Royuela, R. Gil-San Millán, M.J. Mancheño, M.M. Ramos, J.L. Segura, J.A.R. Navarro, F. Zamora, Catalytically Active Imine-based Covalent Organic Frameworks for Detoxification of Nerve Agent Simulants in Aqueous Media, Materials. 12 (2019) 1974. 10.3390/ma12121974.
[132] O.K. Farha, I. Eryazici, N.C. Jeong, B.G. Hauser, C.E. Wilmer, A.A. Sarjeant, R.Q. Snurr, S.T. Nguyen, A.O. Yazaydin, J.T. Hupp, Metal−Organic Framework Materials with Ultrahigh Surface Areas: Is the Sky the Limit ?, J Am. Chem. Soc. 134 (2012) 15016–15021, https://doi.org/10.1021/ja3055639.
[133] C. Janiak, J.K. Vieth, MOFs, MILs and more: concepts, properties and applications for porous coordination networks (PCNs)w, New J. Chem. 34 (2010) 2366–2388.
[134] P. Silva, S.M.F. Vilela, J.P.C. Tomé, F.A. Almeida Paz, Multifunctional metal–organic frameworks: from academia to industrial applications, Chem. Soc. Rev. 44 (2015) 6774–6803, https://doi.org/10.1039/C5CS00307E.
[135] F. Millange, C. Serre, G. Férey, Synthesis, structure determination and properties of MIL-53as and MIL-53ht: the first Criii hybrid inorganic–organic microporous solids: Criii(OH)·{O2C–C6H4–CO2}·{HO2C–C6H4–CO2H}xElectronic supplementary information (ESI) available: crystal data, atomic coordinates and metrical parameters for MIL-53as and MIL-53ht. See http://www.rsc.org/suppdata/cc/b2/b201381a/, Chem. Commun. (2002) 822–823. 10.1039/b201381a.
[136] S.S. Chui, A Chemically Functionalizable Nanoporous Material [Cu3(TMA)2(H2O)3]n, Science. 283 (1999) 1148–1150, https://doi.org/10.1126/science.283.5405.1148.
[137] H. Li, M. Eddaoudi, M. O'Keeffe, O.M. Yaghi, Design and synthesis of an exceptionally stable and highly porous metal-organic framework, Nature. 402 (1999) 276–279, https://doi.org/10.1038/46248.
[138] J.H. Cavka, S. Jakobsen, U. Olsbye, N. Guillou, C. Lamberti, S. Bordiga, K.P. Lillerud, A New Zirconium Inorganic Building Brick Forming Metal Organic Frameworks with Exceptional Stability, J. Am. Chem. Soc. 130 (2008) 13850–13851, https://doi.org/10.1021/ja8057953.
[139] R. Zou, R. Zhong, S. Han, H. Xu, A.K. Burrell, N. Henson, J.L. Cape, D.D. Hickmott, T.V. Timofeeva, T.E. Larson, Y. Zhao, A Porous Metal−Organic Replica of α-PbO $_2$ for Capture of Nerve Agent Surrogate, J. Am. Chem. Soc. 132 (2010) 17996–17999, https://doi.org/10.1021/ja101440z.
[140] A. Roy, A.K. Srivastava, B. Singh, D. Shah, T.H. Mahato, A. Srivastava, Kinetics of degradation of sulfur mustard and sarin simulants on HKUST-1 metal organic framework, Dalton Trans. 41 (2012) 12346, https://doi.org/10.1039/c2dt31888a.
[141] F.-J. Ma, S.-X. Liu, C.-Y. Sun, D.-D. Liang, G.-J. Ren, F. Wei, Y.-G. Chen, Z.-M. Su, A Sodalite-Type Porous Metal−Organic Framework with Polyoxometalate Templates: Adsorption and Decomposition of Dimethyl Methylphosphonate, J. Am. Chem. Soc. 133 (2011) 4178–4181, https://doi.org/10.1021/ja109659k.
[142] M.J. Katz, J.E. Mondloch, R.K. Totten, J.K. Park, S.T. Nguyen, O.K. Farha, J.T. Hupp, Simple and Compelling Biomimetic Metal-Organic Framework Catalyst for the Degradation of Nerve Agent Simulants, Angew. Chem. 126 (2014) 507–511, https://doi.org/10.1002/ange.201307520.
[143] M.R. Mian, T. Islamoglu, U. Afrin, S. Goswami, R. Cao, K.O. Kirlikovali, M.G. Hall, G.W. Peterson, O.K. Farha, Catalytic Degradation of an Organophosphorus Agent at Zn−OH Sites in a Metal−Organic Framework, Chem Mater. 32 (2020) 6998–7004.
[144] S. Wang, L. Bromberg, H. Schreuder-Gibson, T.A. Hatton, Organophophorous Ester Degradation by Chromium(III)Terephthalate Metal−Organic Framework (MIL-101) Chelated to N, N-Dimethylaminopyridine and Related Aminopyridines, ACS Appl. Mater. Interfaces. 5 (2013) 1269–1278.
[145] K. Vellingiri, L. Philip, K.-H. Kim, Metal–organic frameworks as media for the catalytic degradation of chemical warfare agents, Coord. Chem. Rev. 353 (2017) 159–179, https://doi.org/10.1016/j.ccr.2017.10.010.
[146] A.J. Howarth, Y. Liu, P. Li, Z. Li, T.C. Wang, J.T. Hupp, O.K. Farha, Chemical, thermal and mechanical stabilities of metal–organic frameworks, Nat. Rev. Mater. 1 (2016) 15018, https://doi.org/10.1038/natrevmats.2015.18.
[147] G.W. Peterson, S.-Y. Moon, G.W. Wagner, M.G. Hall, J.B. DeCoste, J.T. Hupp, O. K. Farha, Tailoring the Pore Size and Functionality of UiO-Type Metal−Organic Frameworks for Optimal Nerve Agent Destruction, Inorg. Chem. 54 (2015) 9684–9686.
[148] J.Y. Seo, Y. Song, J.-H. Lee, H. Kim, S. Cho, K.-Y. Baek, Robust Nanocellulose/Metal–Organic Framework Aerogel Composites: Superior Performance for Static and Continuous Disposal of Chemical Warfare Agent Simulants, ACS Appl. Mater. Interfaces. 13 (2021) 33516–33523, https://doi.org/10.1021/acsami.1c08138.
[149] C. Shen, Z. Mao, H. Xu, L. Zhang, Y. Zhong, B. Wang, X. Feng, C. Tao, X. Sui, Catalytic MOF-loaded cellulose sponge for rapid degradation of chemical warfare agents simulant, Carbohydr. Polym. 213 (2019) 184–191, https://doi.org/10.1016/j.carbpol.2019.02.044.
[150] K. Ma, P. Li, J.H. Xin, Y. Chen, Z. Chen, S. Goswami, X. Liu, S. Kato, H. Chen, X. Zhang, J. Bai, M.C. Wasson, R.R. Maldonado, R.Q. Snurr, O.K. Farha, Ultrastable Mesoporous Hydrogen-Bonded Organic Framework-Based Fiber Composites toward Mustard Gas Detoxification, Cell Rep. Phys. Sci. 1 (2020), https://doi.org/10.1016/j.xcrp.2020.100024 100024.
[151] Y. Liu, A.J. Howarth, J.T. Hupp, O.K. Farha, Selective Photooxidation of a Mustard-Gas Simulant Catalyzed by a Porphyrinic Metal-Organic Framework, Angew. Chem. 127 (2015) 9129–9133, https://doi.org/10.1002/ange.201503741.
[152] D.T. Lee, J.D. Jamir, G.W. Peterson, G.N. Parsons, Protective fabrics: metal-organic framework textiles for rapid photocatalytic sulfur mustard simulant detoxification, Matter. 2 (2020) 404–415, https://doi.org/10.1016/j.matt.2019.11.005.
[153] W.-Q. Zhang, K. Cheng, H. Zhang, Q.-Y. Li, Z. Ma, Z. Wang, J. Sheng, Y. Li, X. Zhao, X.-J. Wang, Highly efficient and selective photooxidation of sulfur

mustard simulant by a triazolobenzothiadiazole-moiety-functionalized metal–organic framework in air, Inorg. Chem. 57 (2018) 4230–4233.
[154] Y. Yue, G. Han, Q. Wu, Transitional Properties of Cotton Fibers from Cellulose I to Cellulose II Structure, BioResources. 8 (2013) 6460–6471. 10.15376/biores.8.4.6460-6471.
[155] J. Hu, B. Kumar, J. Lu, Handbook of Fibrous Materials, Volume 1 Production and Characterization Volume 2 Applications in Energy, Environmental Science and Healthcare, Wiley-VCH, 2020.
[156] S.K. Ramamoorthy, M. Skrifvars, A. Persson, A review of natural fibers used in biocomposites: plant, animal and regenerated cellulose fibers, Polym. Rev. 55 (2015) 107–162, https://doi.org/10.1080/15583724.2014.971124.
[157] M. Gomes, H. Azevedo, P. Malafaya, S. Silva, J. Oliveira, G. Silva, R.S. João Mano, R. Reis, Natural Polymers in Tissue Engineering Applications, in: Handb. Biopolym. Biodegrad. Plast., Elsevier, 2013: pp. 385–425. 10.1016/B978-1-4557-2834-3.00016-1.
[158] Y. Qin, A brief description of textile fibers, in: Med. Text. Mater., Elsevier, 2016: pp. 23–42. 10.1016/B978-0-08-100618-4.00003-0.
[159] A.K. Yetisen, H. Qu, A. Manbachi, H. Butt, M.R. Dokmeci, J.P. Hinestroza, M. Skorobogatiy, A. Khademhosseini, S.H. Yun, Nanotechnology in textiles, ACS Nano. 10 (2016) 3042–3068, https://doi.org/10.1021/acsnano.5b08176.
[160] M.-K. Kim, S.H. Kim, M. Park, S.G. Ryu, H. Jung, Degradation of chemical warfare agents over cotton fabric functionalized with UiO-66-$NH_2$, RSC Adv. 8 (2018) 41633–41638, https://doi.org/10.1039/C8RA06805D.
[161] H.N. Rubin, B.H. Neufeld, M.M. Reynolds, Surface-anchored metal-organic framework–cotton material for tunable antibacterial copper delivery, ACS Appl. Mater. Interfaces. 10 (2018) 15189–15199, https://doi.org/10.1021/acsami.7b19455.
[162] M. da Silva Pinto, C.A. Sierra-Avila, J.P. Hinestroza, In situ synthesis of a Cu-BTC metal–organic framework (MOF 199) onto cellulosic fibrous substrates: cotton, Cellulose. 19 (2012) 1771–1779, https://doi.org/10.1007/s10570-012-9752-y.
[163] M.A. Bunge, A.B. Davis, K.N. West, C.W. West, T.G. Glover, Synthesis and characterization of UiO-66-NH $_2$ metal-organic framework cotton composite textiles, Ind. Eng. Chem. Res. 57 (2018) 9151–9161, https://doi.org/10.1021/acs.iecr.8b01010.
[164] I. Mirkovic, L. Lei, D. Ljubic, S. Zhu, Crystal growth of metal-organic framework-5 around cellulose-based fibers having a necklace morphology, ACS Omega. 4 (2019) 169–175, https://doi.org/10.1021/acsomega.8b02332.
[165] J. Zhao, M.D. Losego, P.C. Lemaire, P.S. Williams, B. Gong, S.E. Atanasov, T.M. Blevins, C.J. Oldham, H.J. Walls, S.D. Shepherd, M.A. Browe, G.W. Peterson, G. N. Parsons, Highly adsorptive, MOF-functionalized nonwoven fiber mats for hazardous gas capture enabled by atomic layer deposition, Adv. Mater. Interfaces. 1 (2014) 1400040, https://doi.org/10.1002/admi.201400040.
[166] M.A. Khan, M. Mujahid, A review on recent advances in chitosan based composite for hemostatic dressings, Int. J. Biol. Macromol. 124 (2019) 138–147, https://doi.org/10.1016/j.ijbiomac.2018.11.045.
[167] S. Islam, M.A.R. Bhuiyan, M.N. Islam, Chitin and chitosan: structure, properties and applications in biomedical engineering, J. Polym. Environ. 25 (2017) 854–866, https://doi.org/10.1007/s10924-016-0865-5.
[168] C.H. Dalton, C.A. Hall, H.L. Lydon, J.K. Chipman, J.S. Graham, J. Jenner, R.P. Chilcott, Development of haemostatic decontaminants for the treatment of wounds contaminated with chemical warfare agents. 2: Evaluation of *in vitro* topical decontamination efficacy using undamaged skin: Wound decontamination: Topical efficacy, J. Appl. Toxicol. 35 (2015) 543–550, https://doi.org/10.1002/jat.3060.
[169] A.R. Murphy, D.L. Kaplan, Biomedical applications of chemically-modified silk fibroin, J. Mater. Chem. 19 (2009) 6443, https://doi.org/10.1039/b905802h.
[170] P.M. Gore, M. Naebe, X. Wang, B. Kandasubramanian, Progress in silk materials for integrated water treatments: Fabrication, modification and applications, Chem. Eng. J. 374 (2019) 437–470, https://doi.org/10.1016/j.cej.2019.05.163.
[171] J. Chen, H. Venkatesan, J. Hu, Chemically modified silk proteins, Adv. Eng. Mater. 20 (2018) 1700961, https://doi.org/10.1002/adem.201700961.
[172] X. Huang, Fabrication and properties of carbon fibers, Materials. 2 (2009) 2369–2403, https://doi.org/10.3390/ma2042369.
[173] Z. Xu, C. Gao, Graphene fiber: a new trend in carbon fibers, Mater. Today. 18 (2015) 480–492, https://doi.org/10.1016/j.mattod.2015.06.009.
[174] S. Giraudet, P. Le Cloirec, Activated carbon filters for filtration–adsorption, in: Act. Carbon Fiber Text., Elsevier, 2017: pp. 211–243. 10.1016/B978-0-08-100660-3.00009-2.
[175] D. Zhao, Y. Yu, J.P. Chen, Fabrication and testing of zirconium-based nanoparticle-doped activated carbon fiber for enhanced arsenic removal in water, RSC Adv. 6 (2016) 27020–27030, https://doi.org/10.1039/C5RA25030G.
[176] V.V. Singh, A.K. Nigam, S.S. Yadav, B.K. Tripathi, A. Srivastava, M. Boopathi, B. Singh, Graphene oxide as carboelectrocatalyst for in situ electrochemical oxidation and sensing of chemical warfare agent simulant, Sens. Actuators B Chem. 188 (2013) 1218–1224, https://doi.org/10.1016/j.snb.2013.08.013.
[177] K. Huang, G. Liu, Y. Lou, Z. Dong, J. Shen, W. Jin, A graphene oxide membrane with highly selective molecular separation of aqueous organic solution, Angew. Chem. Int. Ed. 53 (2014) 6929–6932, https://doi.org/10.1002/anie.201401061.
[178] R. Spitz Steinberg, M. Cruz, N.G.A. Mahfouz, Y. Qiu, R.H. Hurt, Breathable vapor toxicant barriers based on multilayer graphene oxide, ACS Nano. 11 (2017) 5670–5679, https://doi.org/10.1021/acsnano.7b01106.
[179] B.M. Yoo, J.E. Shin, H.D. Lee, H.B. Park, Graphene and graphene oxide membranes for gas separation applications, Curr. Opin. Chem. Eng. 16 (2017) 39–47, https://doi.org/10.1016/j.coche.2017.04.004.
[180] C. Peng, Z. Iqbal, K.K. Sirkar, G.W. Peterson, Graphene oxide-based membrane as a protective barrier against toxic vapors and gases, ACS Appl. Mater. Interfaces. 12 (2020) 11094–11103, https://doi.org/10.1021/acsami.0c00615.
[181] D.A. Giannakoudakis, J.A. Arcibar-Orozco, T.J. Bandosz, Effect of GO phase in Zn(OH)2/GO composite on the extent of photocatalytic reactive adsorption of mustard gas surrogate, Appl. Catal. B Environ. 183 (2016) 37–46, https://doi.org/10.1016/j.apcatb.2015.10.014.
[182] J. Henych, A. Mattsson, J. Tolasz, V. Štengl, L. Österlund, Solar light decomposition of warfare agent simulant DMMP on TiO $_2$ /graphene oxide nanocomposites, Catal. Sci. Technol. 9 (2019) 1816–1824, https://doi.org/10.1039/C9CY00059C.
[183] V.V. Singh, A. Martin, K. Kaufmann, S.D.S. de Oliveira, J. Wang, Zirconia/graphene oxide hybrid micromotors for selective capture of nerve agents, Chem. Mater. 27 (2015) 8162–8169, https://doi.org/10.1021/acs.chemmater.5b03960.
[184] M. Šťastný, J. Tolasz, V. Štengl, J. Henych, D. Žižka, Graphene oxide/MnO 2 nanocomposite as destructive adsorbent of nerve-agent simulants in aqueous media, Appl. Surf. Sci. 412 (2017) 19–28, https://doi.org/10.1016/j.apsusc.2017.03.228.
[185] B.L. Deopura, N.V. Padaki, Synthetic Textile Fibres, in, Text. Fash., Elsevier (2015) 97–114, https://doi.org/10.1016/B978-1-84569-931-4.00005-2.
[186] A.R. Bunsell, Textile Institute (Manchester, England), eds, Second edition, Woodhead Publishing an imprint of Elsevier, Duxford, United Kingdom, Handbook of properties of textile and technical fibres, 2018.
[187] R.R. Mather, Synthetic Textile Fibres, in: Text. Fash., Elsevier, 2015: pp. 115–138. 10.1016/B978-1-84569-931-4.00006-4.
[188] S. Jiang, G. Duan, E. Zussman, A. Greiner, S. Agarwal, Highly flexible and tough concentric triaxial polystyrene fibers, ACS Appl. Mater. Interfaces. 6 (2014) 5918–5923, https://doi.org/10.1021/am500837s.
[189] P.K. Szewczyk, A. Gradys, S.K. Kim, L. Persano, M. Marzec, A. Kryshtal, T. Busolo, A. Toncelli, D. Pisignano, A. Bernasik, S. Kar-Narayan, P. Sajkiewicz, U. Stachewicz, Enhanced piezoelectricity of electrospun polyvinylidene fluoride fibers for energy harvesting, ACS Appl. Mater. Interfaces. 12 (2020) 13575–13583, https://doi.org/10.1021/acsami.0c02578.
[190] R. Semino, J.C. Moreton, N.A. Ramsahye, S.M. Cohen, G. Maurin, Understanding the origins of metal–organic framework/polymer compatibility, Chem. Sci. 9 (2018) 315–324, https://doi.org/10.1039/C7SC04152G.
[191] J.M. Palomba, D.M. Wirth, J.Y. Kim, M. Kalaj, E.M. Clarke, G.W. Peterson, J.K. Pokorski, S.M. Cohen, Strong, ductile MOF–Poly(urethane urea) composites, Chem Mater. 33 (2021) 3164–3171.
[192] H. Amid, B. Mazé, M.C. Flickinger, B. Pourdeyhimi, Hybrid adsorbent nonwoven structures: a review of current technologies, J. Mater. Sci. 51 (2016) 4173–4200, https://doi.org/10.1007/s10853-016-9741-x.
[193] Y. Dou, W. Zhang, A. Kaiser, Electrospinning of metal-organic frameworks for energy and environmental applications, Adv. Sci. 7 (2020) 1902590, https://doi.org/10.1002/advs.201902590.
[194] K. Ma, K.B. Idrees, F.A. Son, R. Maldonado, M.C. Wasson, X. Zhang, X. Wang, E. Shehayeb, A. Merhi, B.R. Kaafarani, T. Islamoglu, J.H. Xin, O.K. Farha, Fiber composites of metal-organic frameworks, Chem. Mater. 32 (2020) 7120–7140, https://doi.org/10.1021/acs.chemmater.0c02379.
[195] G.W. Peterson, D.T. Lee, H.F. Barton, T.H. Epps, G.N. Parsons, Fibre-based composites from the integration of metal–organic frameworks and polymers, Nat. Rev. Mater. 6 (2021) 605–621, https://doi.org/10.1038/s41578-021-00291-2.
[196] A. Greiner, J.H. Wendorff, Electrospinning: A fascinating method for the preparation of ultrathin fibers, Angew. Chem. Int. Ed. 46 (2007) 5670–5703, https://doi.org/10.1002/anie.200604646.
[197] C.-L. Zhang, S.-H. Yu, Nanoparticles meet electrospinning: recent advances and future prospects, Chem. Soc. Rev. 43 (2014) 4423, https://doi.org/10.1039/c3cs60426h.
[198] W. Zhu, Y. Cheng, C. Wang, N. Pinna, X. Lu, Transition metal sulfides meet electrospinning: versatile synthesis, distinct properties and prospective applications, Nanoscale. 13 (2021) 9112–9146, https://doi.org/10.1039/D1NR01070K.
[199] R. Ostermann, J. Cravillon, C. Weidmann, M. Wiebcke, B.M. Smarsly, Metal–organic framework nanofibers viaelectrospinning, Chem Commun. 47 (2011) 442–444, https://doi.org/10.1039/C0CC02271C.
[200] M. Rose, B. Böhringer, M. Jolly, R. Fischer, S. Kaskel, MOF processing by electrospinning for functional textiles, Adv. Eng. Mater. 13 (2011) 356–360, https://doi.org/10.1002/adem.201000246.
[201] L.E. Lange, F.O. Ochanda, S.K. Obendorf, J.P. Hinestroza, CuBTC metal-organic frameworks enmeshed in polyacrylonitrile fibrous membrane remove methyl parathion from solutions, Fibers Polym. 15 (2014) 200–207, https://doi.org/10.1007/s12221-014-0200-5.
[202] K. Wahiduzzaman, J. Allmond, S. Stone, K. Harp, Mujibur, Synthesis and Electrospraying of Nanoscale MOF (Metal Organic Framework) for High-Performance CO2 Adsorption Membrane, Nanoscale Res. Lett. 12 (2017) 6, https://doi.org/10.1186/s11671-016-1798-6.
[203] Y. Zhang, S. Yuan, X. Feng, H. Li, J. Zhou, B. Wang, Preparation of nanofibrous metal-organic framework filters for efficient air pollution control, J. Am. Chem. Soc. 138 (2016) 5785–5788, https://doi.org/10.1021/jacs.6b02553.

[204] Z. Hao, J. Wu, C. Wang, J. Liu, Electrospun polyimide/metal-organic framework nanofibrous membrane with superior thermal stability for efficient PM $_{2.5}$ capture, ACS Appl. Mater. Interfaces. 11 (2019) 11904–11909, https://doi.org/10.1021/acsami.8b22415.
[205] J. Ren, N.M. Musyoka, P. Annamalai, H.W. Langmi, B.C. North, M. Mathe, Electrospun MOF nanofibers as hydrogen storage media, Int. J. Hydrog. Energy. 40 (2015) 9382–9387, https://doi.org/10.1016/j.ijhydene.2015.05.088.
[206] X. Wang, W. Xu, J. Gu, X. Yan, Y. Chen, M. Guo, G. Zhou, S. Tong, M. Ge, Y. Liu, C. Chen, MOF-based fibrous membranes adsorb PM efficiently and capture toxic gases selectively, Nanoscale. 11 (2019) 17782–17790, https://doi.org/10.1039/C9NR05795A.
[207] G.W. Peterson, H. Wang, K. Au, T.H. Epps, METAL–ORGANIC FRAMEWORK POLYMER composite enhancement via acyl chloride modification, Polym. Int. 70 (2021) 783–789, https://doi.org/10.1002/pi.6151.
[208] M. Asiabi, A. Mehdinia, A. Jabbari, Electrospun biocompatible Chitosan/MIL-101 (Fe) composite nanofibers for solid-phase extraction of Δ9-tetrahydrocannabinol in whole blood samples using Box-Behnken experimental design, J. Chromatogr. A. 1479 (2017) 71–80, https://doi.org/10.1016/j.chroma.2016.12.024.
[209] M. Asiabi, A. Mehdinia, A. Jabbari, Spider-web-like chitosan/MIL-68(Al) composite nanofibers for high-efficient solid phase extraction of Pb(II) and Cd(II), Microchim. Acta. 184 (2017) 4495–4501, https://doi.org/10.1007/s00604-017-2473-z.
[210] G.W. Peterson, A.X. Lu, T.H. Epps, Tuning the morphology and activity of electrospun polystyrene/UiO-66-NH $_2$ metal-organic framework composites to enhance chemical warfare agent removal, ACS Appl. Mater. Interfaces. 9 (2017) 32248–32254, https://doi.org/10.1021/acsami.7b09209.
[211] Z. Li, J. Zhang, L. Yu, J. Zhang, Electrospun porous nanofibers for electrochemical energy storage, J. Mater. Sci. 52 (2017) 6173–6195, https://doi.org/10.1007/s10853-017-0794-2.
[212] X. Dai, X. Li, X. Wang, Morphology controlled porous poly(lactic acid)/zeolitic imidazolate framework-8 fibrous membranes with superior PM2.5 capture capacity, Chem. Eng. J. 338 (2018) 82–91, https://doi.org/10.1016/j.cej.2018.01.025.
[213] M.R. Armstrong, B. Shan, S.V. Maringanti, W. Zheng, B. Mu, Hierarchical pore structures and high ZIF-8 loading on matrimid electrospun fibers by additive removal from a blended polymer precursor, Ind. Eng. Chem. Res. 55 (2016) 9944–9951, https://doi.org/10.1021/acs.iecr.6b02479.
[214] J.Y. Seo, K.Y. Cho, J.-H. Lee, M.W. Lee, K.-Y. Baek, Continuous flow composite membrane catalysts for efficient decomposition of chemical warfare agent simulants, ACS Appl. Mater. Interfaces. 12 (2020) 32778–32787, https://doi.org/10.1021/acsami.0c08276.
[215] Y. Xu, Y. Wen, W. Zhu, Y. Wu, C. Lin, G. Li, Electrospun nanofibrous mats as skeletons to produce MOF membranes for the detection of explosives, Mater. Lett. 87 (2012) 20–23, https://doi.org/10.1016/j.matlet.2012.07.076.
[216] Y. Zhang, Y. Zhang, X. Wang, J. Yu, B. Ding, Ultrahigh metal-organic framework loading and flexible nanofibrous membranes for efficient CO $_2$ capture with long-term, ultrastable recyclability, ACS Appl. Mater. Interfaces. 10 (2018) 34802–34810, https://doi.org/10.1021/acsami.8b14197.
[217] Y. Wu, F. Li, H. Liu, W. Zhu, M. Teng, Y. Jiang, W. Li, D. Xu, D. He, P. Hannam, G. Li, Electrospun fibrous mats as skeletons to produce free-standing MOF membranes, J. Mater. Chem. 22 (2012) 16971, https://doi.org/10.1039/c2jm32570e.
[218] Liu, Cai, Chan, Yu, Development and Applications of MOFs Derivative One-Dimensional Nanofibers via Electrospinning: A Mini-Review, Nanomaterials. 9 (2019) 1306. 10.3390/nano9091306.
[219] Y. Bian, R. Wang, S. Wang, C. Yao, W. Ren, C. Chen, L. Zhang, Metal–organic framework-based nanofiber filters for effective indoor air quality control, J. Mater. Chem. A. 6 (2018) 15807–15814, https://doi.org/10.1039/C8TA04539A.
[220] H. Talmoudi, N. Khenoussi, D. Adolphe, A.H. Said, L. Schacher, An in situ crystal growth of metal organic frameworks-5 on electrospun PVA nanofibers, Autex Res. J. 18 (2018) 308–313, https://doi.org/10.1515/aut-2017-0024.
[221] D.A. Giannakoudakis, Y. Hu, M. Florent, T.J. Bandosz, Smart textiles of MOF/g-C $_{3\,N}$ 4 nanospheres for the rapid detection/detoxification of chemical warfare agents, Nanoscale Horiz. 2 (2017) 356–364, https://doi.org/10.1039/C7NH00081B.
[222] L. Yu, X. Shang, H. Chen, L. Xiao, Y. Zhu, J. Fan, A tightly-bonded and flexible mesoporous zeolite-cotton hybrid hemostat, Nat. Commun. 10 (2019) 1932, https://doi.org/10.1038/s41467-019-09849-9.
[223] A. Satya, S. Subramanian, R. Seeram, Functionalized cellulose PET polymer fibers with zeolites for detoxification against nerve agents, J. Inorg. Mater. 27 (2012), https://doi.org/10.3724/SP.J.1077.2011.11558.
[224] M.A. Bunge, E. Pasciak, J. Choi, L. Haverhals, W.M. Reichert, T.G. Glover, Ionic liquid welding of the UIO-66-NH $_2$ MOF to cotton textiles, Ind. Eng. Chem. Res. 59 (2020) 19285–19298, https://doi.org/10.1021/acs.iecr.0c03763.
[225] R.M. Abdelhameed, H.E. Emam, Design of ZIF(Co & Zn)@wool composite for efficient removal of pharmaceutical intermediate from wastewater, J. Colloid Interface Sci. 552 (2019) 494–505, https://doi.org/10.1016/j.jcis.2019.05.077.
[226] R.M. Abdelhameed, H.E. Emam, J. Rocha, A.M.S. Silva, Cu-BTC metal-organic framework natural fabric composites for fuel purification, Fuel Process. Technol. 159 (2017) 306–312, https://doi.org/10.1016/j.fuproc.2017.02.001.
[227] H.E. Emam, R.M. Abdelhameed, In-situ modification of natural fabrics by Cu-BTC MOF for effective release of insect repellent (N, N-diethyl-3-methylbenzamide), J. Porous Mater. 24 (2017) 1175–1185, https://doi.org/10.1007/s10934-016-0357-y.
[228] J. Li, X. Yuan, Y. Wu, X. Ma, F. Li, B. Zhang, Y. Wang, Z. Lei, Z. Zhang, From powder to cloth: Facile fabrication of dense MOF-76(Tb) coating onto natural silk fiber for feasible detection of copper ions, Chem. Eng. J. 350 (2018) 637–644, https://doi.org/10.1016/j.cej.2018.05.144.
[229] L. Lu, C. Hu, Y. Zhu, H. Zhang, R. Li, Y. Xing, Multi-functional finishing of cotton fabrics by water-based layer-by-layer assembly of metal–organic framework, Cellulose. 25 (2018) 4223–4238, https://doi.org/10.1007/s10570-018-1838-8.
[230] R.M. Abdelhameed, H.R. el-deib, F.M.S.E. El-Dars, H.B. Ahmed, H.E. Emam, Applicable strategy for removing liquid fuel nitrogenated contaminants using MIL-53-NH $_2$ @natural fabric composites, Ind. Eng. Chem. Res. 57 (2018) 15054–15065, https://doi.org/10.1021/acs.iecr.8b03936.
[231] D.K. Yoo, S.H. Jhung, Effect of functional groups of metal-organic frameworks, coated on cotton, on removal of particulate matters via selective interactions, ACS Appl. Mater. Interfaces. 11 (2019) 47649–47657, https://doi.org/10.1021/acsami.9b19646.
[232] S. Khanjani, A. Morsali, Layer by layer growth of nano porous lead(ii) coordination polymer on natural silk fibers and its application in removal and recovery of iodide, CrystEngComm. 14 (2012) 8137, https://doi.org/10.1039/c2ce25696g.
[233] A.R. Abbasi, J. ad-Din Aali, A. Azadbakht, A. Morsali, V. Safarifard, Synthesis and characterization of TMU-16-NH2 metal-organic framework nanostructure upon silk fiber: Study of structure effect on morphine and methyl orange adsorption affinity, Fibers Polym. 16 (2015) 1193–1200, https://doi.org/10.1007/s12221-015-1193-4.
[234] A.R. Abbasi, M. Yousefshahi, A. Azadbakht, Synthesis and characterization of azine-functionalized zinc cation metal–organic frameworks nanostructures upon silk fibers under ultrasound irradiation, study of pores effect on morphine adsorption affinity, Colloids Surf. Physicochem. Eng. Asp. 498 (2016) 58–65, https://doi.org/10.1016/j.colsurfa.2016.02.038.
[235] S. Khanjani, A. Morsali, Ultrasound-promoted coating of MOF-5 on silk fiber and study of adsorptive removal and recovery of hazardous anionic dye "congo red", Ultrason. Sonochem. 21 (2014) 1424–1429, https://doi.org/10.1016/j.ultsonch.2013.12.012.
[236] L. Zhang, J. Sun, Y. Zhou, Y. Zhong, Y. Ying, Y. Li, Y. Liu, Z. Zuhra, C. Huang, Layer-by-layer assembly of Cu $_3$ (BTC) $_2$ on chitosan non-woven fabrics: a promising haemostatic decontaminant composite material against sulfur mustard, J. Mater. Chem. B. 5 (2017) 6138–6146, https://doi.org/10.1039/C7TB01489A.
[237] M. Schelling, M. Kim, E. Otal, J. Hinestroza, Decoration of Cotton Fibers with a Water-Stable Metal-Organic Framework (UiO-66) for the Decomposition and Enhanced Adsorption of Micropollutants in Water, Bioengineering. 5 (2018) 14, https://doi.org/10.3390/bioengineering5010014.
[238] L. Liu, E. Ping, J. Sun, L. Zhang, Y. Zhou, Y. Zhong, Y. Zhou, Y. Wang, Multifunctional Ag@MOF-5@chitosan non-woven cloth composites for sulfur mustard decontamination and hemostasis, Dalton Trans. 48 (2019) 6951–6959, https://doi.org/10.1039/C9DT00503J.
[239] E. Laurila, J. Thunberg, S.P. Argent, N.R. Champness, S. Zacharias, G. Westman, L. Öhrström, Enhanced Synthesis of metal-organic frameworks on the surface of electrospun cellulose nanofibers: enhanced synthesis of metal-organic frameworks, Adv. Eng. Mater. 17 (2015) 1282–1286, https://doi.org/10.1002/adem.201400565.
[240] M. Kalaj, S.M. Cohen, Spray-coating of catalytically active MOF–polythiourea through postsynthetic polymerization, Angew. Chem. Int. Ed. 59 (2020) 13984–13989, https://doi.org/10.1002/anie.202004205.
[241] C. Liu, Y. Wu, C. Morlay, Y. Gu, B. Gebremariam, X. Yuan, F. Li, General deposition of metal-organic frameworks on highly adaptive organic-inorganic hybrid electrospun fibrous substrates, ACS Appl. Mater. Interfaces. 8 (2016) 2552–2561, https://doi.org/10.1021/acsami.5b10078.
[242] L. Zhang, H. Chen, X. Bai, S. Wang, L. Li, L. Shao, W. He, Y. Li, T. Wang, X. Zhang, J. Chen, Y. Fu, Fabrication of 2D metal–organic framework nanosheet@fiber composites by spray technique, Chem. Commun. 55 (2019) 8293–8296, https://doi.org/10.1039/C9CC02614B.
[243] K. Zhang, Q. Huo, Y.-Y. Zhou, H.-H. Wang, G.-P. Li, Y.-W. Wang, Y.-Y. Wang, Textiles/metal–organic frameworks composites as flexible air filters for efficient particulate matter removal, ACS Appl. Mater. Interfaces. 11 (2019) 17368–17374, https://doi.org/10.1021/acsami.9b01734.
[244] L. Song, T. Zhao, D. Yang, X. Wang, X. Hao, Y. Liu, S. Zhang, Z.-Z. Yu, Photothermal graphene/UiO-66-NH2 fabrics for ultrafast catalytic degradation of chemical warfare agent simulants, J. Hazard. Mater. 393 (2020), https://doi.org/10.1016/j.jhazmat.2020.122332 122332.
[245] A. Centrone, Y. Yang, S. Speakman, L. Bromberg, G.C. Rutledge, T.A. Hatton, Growth of metal−organic frameworks on polymer surfaces, J. Am. Chem. Soc. 132 (2010) 15687–15691, https://doi.org/10.1021/ja106381x.
[246] K. Ma, T. Islamoglu, Z. Chen, P. Li, M.C. Wasson, Y. Chen, Y. Wang, G.W. Peterson, J.H. Xin, O.K. Farha, Scalable and template-free aqueous synthesis of zirconium-based metal-organic framework coating on textile fiber, J. Am. Chem. Soc. 141 (2019) 15626–15633, https://doi.org/10.1021/jacs.9b07301.
[247] S.E. Morgan, A.M. O'Connell, A. Jansson, G.W. Peterson, J.J. Mahle, T.B. Eldred, W. Gao, G.N. Parsons, Stretchable and multi-metal–organic framework fabrics via high-yield rapid sorption-vapor synthesis and their application in chemical warfare agent hydrolysis, ACS Appl. Mater. Interfaces. 13 (2021) 31279–31284, https://doi.org/10.1021/acsami.1c07366.

[248] M. Meilikhov, K. Yusenko, E. Schollmeyer, C. Mayer, H.-J. Buschmann, R.A. Fischer, Stepwise deposition of metal organic frameworks on flexible synthetic polymer surfaces, Dalton Trans. 40 (2011) 4838, https://doi.org/10.1039/c0dt01820a.
[249] L. Qiu, L. Wang, M. Zhang, M. Zhang, M. Wang, C. Yang, R. Li, G. Wu, A facile strategy for fabrication of HKUST-1 on a flexible polyethylene nonwoven fabric with a high MOF loading, Microporous Mesoporous Mater. 292 (2020), https://doi.org/10.1016/j.micromeso.2019.109723 109723.
[250] M.A. Bunge, K.N. Ruckart, S. Leavesley, G.W. Peterson, N. Nguyen, K.N. West, T.G. Glover, Modification of Fibers with Nanostructures Using Reactive Dye Chemistry, Ind. Eng. Chem. Res. 54 (2015) 3821–3827, https://doi.org/10.1021/acs.iecr.5b00089.
[251] A. Yao, X. Jiao, D. Chen, C. Li, Bio-Inspired Polydopamine-Mediated Zr-MOF Fabrics for Solar Photothermal-Driven Instantaneous Detoxification of Chemical Warfare Agent Simulants, ACS Appl. Mater. Interfaces. 12 (2020) 18437–18445, https://doi.org/10.1021/acsami.9b22242.
[252] M. Kalaj, M.S. Denny, K.C. Bentz, J.M. Palomba, S.M. Cohen, Nylon–MOF Composites through Postsynthetic Polymerization, Angew. Chem. Int. Ed. 58 (2019) 2336–2340, https://doi.org/10.1002/anie.201812655.
[253] D.T. Lee, J. Zhao, C.J. Oldham, G.W. Peterson, G.N. Parsons, UiO-66-NH $_2$ Metal-Organic Framework (MOF) Nucleation on $TiO_2$, ZnO, and $Al_2O_3$ Atomic Layer Deposition-Treated Polymer Fibers: Role of Metal Oxide on MOF Growth and Catalytic Hydrolysis of Chemical Warfare Agent Simulants, ACS Appl. Mater. Interfaces. 9 (2017) 44847–44855, https://doi.org/10.1021/acsami.7b15397.
[254] J. Zhao, B. Gong, W.T. Nunn, P.C. Lemaire, E.C. Stevens, F.I. Sidi, P.S. Williams, C.J. Oldham, H.J. Walls, S.D. Shepherd, M.A. Browe, G.W. Peterson, M.D. Losego, G.N. Parsons, Conformal and highly adsorptive metal–organic framework thin films via layer-by-layer growth on ALD-coated fiber mats, J. Mater. Chem. A. 3 (2015) 1458–1464, https://doi.org/10.1039/C4TA05501B.
[255] Y. Liu, M. Zhu, M. Chen, L. Ma, B. Yang, L. Li, W. Tu, A polydopamine-modified reduced graphene oxide (RGO)/MOFs nanocomposite with fast rejection capacity for organic dye, Chem. Eng. J. 359 (2019) 47–57, https://doi.org/10.1016/j.cej.2018.11.105.
[256] M. Zhou, J. Li, M. Zhang, H. Wang, Y. Lan, Y. Wu, F. Li, G. Li, A polydopamine layer as the nucleation center of MOF deposition on ‘‘inert” polymer surfaces to fabricate hierarchically structured porous films, Chem. Commun. 51 (2015) 2706–2709, https://doi.org/10.1039/C4CC08796H.
[257] J. Zhao, D.T. Lee, R.W. Yaga, M.G. Hall, H.F. Barton, I.R. Woodward, C.J. Oldham, H.J. Walls, G.W. Peterson, G.N. Parsons, Ultra-Fast Degradation of Chemical Warfare Agents Using MOF-Nanofiber Kebabs, Angew. Chem. Int. Ed. 55 (2016) 13224–13228, https://doi.org/10.1002/anie.201606656.
[258] D.T. Lee, J. Zhao, G.W. Peterson, G.N. Parsons, Catalytic ‘‘MOF-Cloth” Formed via Directed Supramolecular Assembly of UiO-66-NH $_2$ Crystals on Atomic Layer Deposition-Coated Textiles for Rapid Degradation of Chemical Warfare Agent Simulants, Chem. Mater. 29 (2017) 4894–4903, https://doi.org/10.1021/acs.chemmater.7b00949.
[259] H.F. Barton, A.K. Davis, G.N. Parsons, The Effect of Surface Hydroxylation on MOF Formation on ALD Metal Oxides: MOF-525 on TiO $_2$ /Polypropylene for Catalytic Hydrolysis of Chemical Warfare Agent Simulants, ACS Appl. Mater. Interfaces. (2020) acsami.9b20910. 10.1021/acsami.9b20910.
[260] B.C. Bai, E.A. Kim, C.W. Lee, Y.-S. Lee, J.S. Im, Effects of surface chemical properties of activated carbon fibers modified by liquid oxidation for CO2 adsorption, Appl. Surf. Sci. 353 (2015) 158–164, https://doi.org/10.1016/j.apsusc.2015.06.046.
[261] A. Perrard, L. Retailleau, R. Berjoan, J.-P. Joly, Liquid phase oxidation kinetics of an ex-cellulose activated carbon cloth by NaOCl, Carbon. 50 (2012) 2226–2234, https://doi.org/10.1016/j.carbon.2012.01.039.
[262] Z. Wang, H. Jin, K. Wang, Y. Xie, J. Ning, Y. Tu, Y. Chen, H. Liu, H. Zeng, A two-step method for the integrated removal of HCl, SO2 and NO at low temperature using viscose-based activated carbon fibers modified by nitric acid, Fuel. 239 (2019) 272–281, https://doi.org/10.1016/j.fuel.2018.11.002.
[263] R.N. Fallah, S. Azizian, Removal of thiophenic compounds from liquid fuel by different modified activated carbon cloths, Fuel Process. Technol. 93 (2012) 45–52, https://doi.org/10.1016/j.fuproc.2011.09.012.
[264] L. Xu, J. Guo, F. Jin, H. Zeng, Removal of SO2 from O2-containing flue gas by activated carbon fiber (ACF) impregnated with NH3, Chemosphere. 62 (2006) 823–826, https://doi.org/10.1016/j.chemosphere.2005.04.070.
[265] C.L. Mangun, J.A. DeBarr, J. Economy, Adsorption of sulfur dioxide on ammonia-treated activated carbon fibers, Carbon. 39 (2001) 1689–1696, https://doi.org/10.1016/S0008-6223(00)00300-6.
[266] S.-J. Park, B.-J. Kim, Influence of oxygen plasma treatment on hydrogen chloride removal of activated carbon fibers, J. Colloid Interface Sci. 275 (2004) 590–595, https://doi.org/10.1016/j.jcis.2004.03.011.
[267] K. Okajima, K. Ohta, M. Sudoh, Capacitance behavior of activated carbon fibers with oxygen-plasma treatment, Electrochimica Acta. 50 (2005) 2227–2231, https://doi.org/10.1016/j.electacta.2004.10.005.
[268] B.C. Bai, H.-U. Lee, C.W. Lee, Y.-S. Lee, J.S. Im, N 2 plasma treatment on activated carbon fibers for toxic gas removal: Mechanism study by electrochemical investigation, Chem. Eng. J. 306 (2016) 260–268, https://doi.org/10.1016/j.cej.2016.07.046.
[269] M.-J. Jung, J.W. Kim, J.S. Im, S.-J. Park, Y.-S. Lee, Nitrogen and hydrogen adsorption of activated carbon fibers modified by fluorination, J. Ind. Eng. Chem. 15 (2009) 410–414, https://doi.org/10.1016/j.jiec.2008.11.001.
[270] Y. Yao, V. Velpari, J. Economy, In search of brominated activated carbon fibers for elemental mercury removal from power plant effluents, J. Mater. Chem. A. 1 (2013) 12103, https://doi.org/10.1039/c3ta11465a.
[271] S. Gao, L. Zhu, L. Liu, A. Gao, F. Liao, M. Shao, Improved Energy Storage Performance Based on Gamma-Ray Irradiated Activated Carbon Cloth, Electrochimica Acta. 191 (2016) 908–915, https://doi.org/10.1016/j.electacta.2016.01.151.
[272] S.-J. Park, B.-J. Park, S.-K. Ryu, Electrochemical treatment on activated carbon fibers for increasing the amount and rate of Cr(VI) adsorption, Carbon. 37 (1999) 1223–1226, https://doi.org/10.1016/S0008-6223(98)00318-2.
[273] Z. Tabti, R. Ruiz-Rosas, C. Quijada, D. Cazorla-Amorós, E. Morallón, Tailoring the Surface Chemistry of Activated Carbon Cloth by Electrochemical Methods, ACS Appl. Mater. Interfaces. 6 (2014) 11682–11691, https://doi.org/10.1021/am502475v.
[274] Z. Dai, X. Yu, C. Huang, M. Li, J. Su, Y. Guo, H. Xu, Q. Ke, Nanocrystalline MnO $_2$ on an activated carbon fiber for catalytic formaldehyde removal, RSC Adv. 6 (2016) 97022–97029, https://doi.org/10.1039/C6RA15463H.
[275] M. Li, B. Lu, Q.-F. Ke, Y.-J. Guo, Y.-P. Guo, Synergetic effect between adsorption and photodegradation on nanostructured TiO2/activated carbon fiber felt porous composites for toluene removal, J. Hazard. Mater. 333 (2017) 88–98, https://doi.org/10.1016/j.jhazmat.2017.03.019.
[276] B.C. Bai, Y.-S. Lee, J.S. Im, Activated carbon fibers for toxic gas removal based on electrical investigation: Mechanistic study of p-type/n-type junction structures, Sci. Rep. 9 (2019) 14458, https://doi.org/10.1038/s41598-019-50707-x.
[277] S. Kang, J. Hwang, Fabrication of hollow activated carbon nanofibers (HACNFs) containing manganese oxide catalyst for toluene removal via two-step process of electrospinning and thermal treatment, Chem. Eng. J. 379 (2020), https://doi.org/10.1016/j.cej.2019.122315 122315.
[278] H. Emamipour, D.L. Johnsen, M.J. Rood, M. Jain, G. Skandan, Novel activated carbon fiber cloth filter with functionalized silica nanoparticles for adsorption of toxic industrial chemicals, Adsorption. 21 (2015) 265–272, https://doi.org/10.1007/s10450-015-9668-6.
[279] L. Huang, S. Zhou, F. Jin, J. Huang, N. Bao, Characterization and mechanism analysis of activated carbon fiber felt-stabilized nanoscale zero-valent iron for the removal of Cr(VI) from aqueous solution, Colloids Surf. Physicochem. Eng. Asp. 447 (2014) 59–66, https://doi.org/10.1016/j.colsurfa.2014.01.037.
[280] E.J. Park, H.J. Kim, S.W. Han, J.H. Jeong, I.H. Kim, H.O. Seo, Y.D. Kim, Assembly of PDMS/SiO 2 -PTFE and activated carbon fibre as a liquid water–resistant gas sorbent structure, Chem. Eng. J. 325 (2017) 433–441, https://doi.org/10.1016/j.cej.2017.05.088.
[281] S. Dadvar, H. Tavanai, M. Morshed, M. Ghiaci, The Removal of 2-Chloroethyl Ethyl Sulfide Using Activated Carbon Nanofibers Embedded with MgO and Al $_{2\,O}$ 3 Nanoparticles, J. Chem. Eng. Data. 57 (2012) 1456–1462, https://doi.org/10.1021/je201328s.
[282] S. Dadvar, H. Tavanai, M. Morshed, M. Ghiaci, A study on the kinetics of 2-chloroethyl ethyl sulfide adsorption onto nanocomposite activated carbon nanofibers containing metal oxide nanoparticles, Sep. Purif. Technol. 114 (2013) 24–30, https://doi.org/10.1016/j.seppur.2013.04.019.
[283] R. Gil-San-Millan, P. Delgado, E. Lopez-Maya, J.D. Martin-Romera, E. Barea, J. A.R. Navarro, Layer-by-Layer Integration of Zirconium Metal−Organic Frameworks onto Activated Carbon Spheres and Fabrics with Model Nerve Agent Detoxification Properties, ACS Appl, Mater. Interfaces. (2021).
[284] X.-W. Liu, J.-L. Hu, T.-J. Sun, Y. Guo, T.D. Bennett, X.-Y. Ren, S.-D. Wang, Template-based Synthesis of a Formate Metal-Organic Framework/Activated Carbon Fiber Composite for High-performance Methane Adsorptive Separation, Chem. - Asian J. 11 (2016) 3014–3017, https://doi.org/10.1002/asia.201601134.
[285] O. Fleker, A. Borenstein, R. Lavi, L. Benisvy, S. Ruthstein, D. Aurbach, Preparation and Properties of Metal Organic Framework/Activated Carbon Composite Materials, Langmuir. 32 (2016) 4935–4944, https://doi.org/10.1021/acs.langmuir.6b00528.
[286] J.C. Muñoz-Senmache, S. Kim, R.R. Arrieta-Pérez, C.M. Park, Y. Yoon, A.J. Hernández-Maldonado, Activated Carbon-Metal Organic Framework Composite for the Adsorption of Contaminants of Emerging Concern from Water, ACS Appl. Nano Mater. 3 (2020) 2928–2940, https://doi.org/10.1021/acsanm.0c00190.
[287] L.N. McHugh, A. Terracina, P.S. Wheatley, G. Buscarino, M.W. Smith, R.E. Morris, Metal-Organic Framework-Activated Carbon Composite Materials for the Removal of Ammonia from Contaminated Airstreams, Angew. Chem. Int. Ed. 58 (2019) 11747–11751, https://doi.org/10.1002/anie.201905779.
[288] A. Soleimanpour, M. Farsi, P. Keshavarz, S. Zeinali, Modification of activated carbon by MIL-53(Al) MOF to develop a composite framework adsorbent for CO2 capturing, Environ. Sci. Pollut. Res. 28 (2021) 37929–37939, https://doi.org/10.1007/s11356-021-13382-y.
[289] M. Sathe, P.K. Sharma, V.K. Singh, N.K. Tripathi, V. Verma, S.P. Sharma, L.N.S. Tomar, A. Chaturvedi, S.S. Yadav, V.B. Thakare, J. Acharya, A.K. Gupta, K. Ganesan, Chemical Protection Studies of Activated Carbon Spheres based Permeable Protective Clothing Against Sulfur Mustard, a Chemical Warfare Agent, Def. Sci. J. 69 (2019) 577–584. 10.14429/dsj.69.13958.
[290] C.L. Mangun, Z. Yue, J. Economy, S. Maloney, P. Kemme, D. Cropek, Adsorption of Organic Contaminants from Water Using Tailored ACFs, Chem. Mater. 13 (2001) 2356–2360, https://doi.org/10.1021/cm000880g.
[291] D.A. Giannakoudakis, F. Pearsall, M. Florent, J. Lombardi, S. O'Brien, T.J. Bandosz, Barium titanate perovskite nanoparticles as a photoreactive

medium for chemical warfare agent detoxification, J. Colloid Interface Sci. 531 (2018) 233–244, https://doi.org/10.1016/j.jcis.2018.07.053.
[292] D.A. Giannakoudakis, M. Barczak, F. Pearsall, S. O'Brien, T.J. Bandosz, Composite porous carbon textile with deposited barium titanate nanospheres as wearable protection medium against toxic vapors, Chem. Eng. J. 384 (2020), https://doi.org/10.1016/j.cej.2019.123280 123280.
[293] P. Kowalczyk, P.A. Gauden, A.P. Terzyk, A.V. Neimark, Screening of carbonaceous nanoporous materials for capture of nerve agents, Phys Chem Chem Phys. 15 (2013) 291–298, https://doi.org/10.1039/C2CP43366D.
[294] F. Cataldo, Surface interaction and desorption of trimethyl phosphate from ozonized activated carbon fabric, Fuller. Nanotub. Carbon Nanostructures. 26 (2018) 379–388, https://doi.org/10.1080/1536383X.2018.1439933.
[295] G.W. Peterson, M.A. Browe, E.M. Durke, T.H. Epps, Flexible SIS/HKUST-1 Mixed Matrix Composites as Protective Barriers against Chemical Warfare Agent Simulants, ACS Appl. Mater. Interfaces. 10 (2018) 43080–43087, https://doi.org/10.1021/acsami.8b16227.
[296] N.L. Pomerantz, E.E. Anderson, N.P. Dugan, N.F. Hoffman, H.F. Barton, D.T. Lee, C.J. Oldham, G.W. Peterson, G.N. Parsons, Air, Water Vapor, and Aerosol Transport through Textiles with Surface Functional Coatings of Metal Oxides and Metal-Organic Frameworks, ACS Appl. Mater. Interfaces. 11 (2019) 24683–24690, https://doi.org/10.1021/acsami.9b04091.
[297] E. López-Maya, C. Montoro, L.M. Rodríguez-Albelo, S.D. Aznar Cervantes, A.A. Lozano-Pérez, J.L. Cenís, E. Barea, J.A.R. Navarro, Textile/Metal-Organic-Framework Composites as Self-Detoxifying Filters for Chemical-Warfare Agents, Angew. Chem. Int. Ed. 54 (2015) 6790–6794, https://doi.org/10.1002/anie.201502094.
[298] H.F. Barton, J.D. Jamir, A.K. Davis, G.W. Peterson, G.N. Parsons, Doubly-Protective MOF-Photo-Fabrics: Facile Template-Free Synthesis of PCN-222-Textiles Enables Rapid Hydrolysis, Photo-Hydrolysis and Selective Oxidation of Multiple Chemical Warfare Agents and Simulants, Chem Eur J. 26 (2020), https://doi.org/10.1002/chem.202003716.
[299] A.J. Howarth, C.T. Buru, Y. Liu, A.M. Ploskonka, K.J. Hartlieb, M. McEntee, J.J. Mahle, J.H. Buchanan, E.M. Durke, S.S. Al-Juaid, J.F. Stoddart, J.B. DeCoste, J.T. Hupp, O.K. Farha, Postsynthetic Incorporation of a Singlet Oxygen Photosensitizer in a Metal-Organic Framework for Fast and Selective Oxidative Detoxification of Sulfur Mustard, Chem. - Eur. J. 23 (2017) 214–218, https://doi.org/10.1002/chem.201604972.
[300] Y.H. Cheung, K. Ma, H.C. van Leeuwen, M.C. Wasson, X. Wang, K.B. Idrees, W. Gong, R. Cao, J.J. Mahle, T. Islamoglu, G.W. Peterson, M.C. de Koning, J.H. Xin, O. K. Farha, Immobilized regenerable active chlorine within a zirconium-based MOF textile composite to eliminate biological and chemical threats, J. Am. Chem. Soc. 143 (2021) 16777–16785, https://doi.org/10.1021/jacs.1c08576.
[301] Z. Chen, T. Islamoglu, O.K. Farha, Toward base heterogenization: A zirconium metal-organic framework/dendrimer or polymer mixture for rapid hydrolysis of a nerve-agent simulant, ACS Appl. Nano Mater. 2 (2019) 1005–1008, https://doi.org/10.1021/acsanm.8b02292.
[302] Z. Chen, K. Ma, J.J. Mahle, H. Wang, Z.H. Syed, A. Atilgan, Y. Chen, J.H. Xin, T. Islamoglu, G.W. Peterson, O.K. Farha, Integration of metal-organic frameworks on protective layers for destruction of nerve agents under relevant conditions, J. Am. Chem. Soc. 141 (2019) 20016–20021, https://doi.org/10.1021/jacs.9b11172.
[303] A.X. Lu, M. McEntee, M.A. Browe, M.G. Hall, J.B. DeCoste, G.W. Peterson, MOFabric: electrospun nanofiber mats from PVDF/UiO-66-NH $_2$ for chemical protection and decontamination, ACS Appl. Mater. Interfaces. 9 (2017) 13632–13636, https://doi.org/10.1021/acsami.7b01621.
[304] D.T. Lee, Z. Dai, G.W. Peterson, M.G. Hall, N.L. Pomerantz, N. Hoffman, G.N. Parsons, Highly breathable chemically-protective MOF-fiber catalysts, Adv. Funct. Mater. (2021) 2108004, https://doi.org/10.1002/adfm.202108004.
[305] H. Wang, J.J. Mahle, T.M. Tovar, G.W. Peterson, M.G. Hall, J.B. DeCoste, J.H. Buchanan, C.J. Karwacki, Solid-phase detoxification of chemical warfare agents using zirconium-based metal organic frameworks and the moisture effects: analyze via digestion, ACS Appl. Mater. Interfaces. 11 (2019) 21109–21116, https://doi.org/10.1021/acsami.9b04927.
[306] A. Yao, X. Jiao, D. Chen, C. Li, Photothermally enhanced detoxification of chemical warfare agent simulants using bioinspired core-shell dopamine–melanin@metal–organic frameworks and their fabrics, ACS Appl. Mater. Interfaces. 11 (2019) 7927–7935, https://doi.org/10.1021/acsami.8b19445.
[307] D.B. Dwyer, D.T. Lee, S. Boyer, W.E. Bernier, G.N. Parsons, W.E. Jones, Toxic organophosphate hydrolysis using nanofiber-templated UiO-66-NH $_2$ metal-organic framework polycrystalline cylinders, ACS Appl. Mater. Interfaces. 10 (2018) 25794–25803, https://doi.org/10.1021/acsami.8b08167.
[308] D.L. McCarthy, J. Liu, D.B. Dwyer, J.L. Troiano, S.M. Boyer, J.B. DeCoste, W.E. Bernier, W.E. Jones Jr, Electrospun metal–organic framework polymer composites for the catalytic degradation of methyl paraoxon, New J. Chem. 41 (2017) 8748–8753, https://doi.org/10.1039/C7NJ00525C.
[309] D.B. Dwyer, N. Dugan, N. Hoffman, D.J. Cooke, M.G. Hall, T.M. Tovar, W.E. Bernier, J. DeCoste, N.L. Pomerantz, W.E. Jones, Chemical protective textiles of UiO-66-integrated PVDF composite fibers with rapid heterogeneous decontamination of toxic organophosphates, ACS Appl. Mater. Interfaces. 10 (2018) 34585–34591, https://doi.org/10.1021/acsami.8b11290.
[310] M.C. de Koning, K. Ma, M. van Grol, I. Iordanov, M.J.L. Kruijne, K.B. Idrees, H. Xie, T. Islamoglu, R.P.T. Bross, O.K. Farha, Development of a Metal–Organic Framework/Textile Composite for the Rapid Degradation and Sensitive Detection of the Nerve Agent VX, Chem. Mater. (2022) acs.chemmater.1c03895. 10.1021/acs.chemmater.1c03895.
[311] S.-Y. Moon, E. Proussaloglou, G.W. Peterson, J.B. DeCoste, M.G. Hall, A.J. Howarth, J.T. Hupp, O.K. Farha, Detoxification of chemical warfare agents using a Zr6-based metal-organic framework polymer mixture, Chem Eur J. 22 (2016) 14864–14868, https://doi.org/10.1002/chem.201603976.
[312] H.-B. Luo, A.J. Castro, M.C. Wasson, W. Flores, O.K. Farha, Y. Liu, Rapid, biomimetic degradation of a nerve agent simulant byincorporating imidazole bases into a metal−organic framework, ACS Catal. 11 (2021) 1424–1429.
[313] R. Gil-San-Millan, E. López-Maya, M. Hall, N.M. Padial, G.W. Peterson, J.B. DeCoste, L.M. Rodríguez-Albelo, J.E. Oltra, E. Barea, J.A.R. Navarro, Chemical warfare agents detoxification properties of zirconium metal-organic frameworks by synergistic incorporation of nucleophilic and basic sites, ACS Appl. Mater. Interfaces. 9 (2017) 23967–23973, https://doi.org/10.1021/acsami.7b06341.
[314] Y.C. Hudiono, A.L. Miller, P.W. Gibson, A.L. LaFrate, R.D. Noble, D.L. Gin, A highly breathable organic/inorganic barrier material that blocks the passage of mustard agent simulants, Ind. Eng. Chem. Res. 51 (2012) 7453–7456, https://doi.org/10.1021/ie202977e.